VILNIUS UNIVERSITY
CENTER FOR PHYSICAL SCIENCES AND TECHNOLOGY

ELENA ADOMAITIENĖ

DEVELOPMENT OF METHODS FOR CONTROLLING EQUILIBRIUM AND SYNCHRONY OF NONLINEAR DYNAMICAL SYSTEMS

Doctoral dissertation
Physical sciences, physics (02P)

Vilnius, 2017

The dissertation was prepared at the Center for Physical Sciences and Technology from 2012 to 2017.

Scientific supervisor – dr. habil. Arūnas Vytautas Tamaševičius (Center for Physical Sciences and Technology, physical sciences, physics – 02P)

Scientific advisor – associate prof. dr. Gytis Mykolaitis (Center for Physical Sciences and Technology, physical sciences, physics – 02P)

VILNIAUS UNIVERSITETAS
FIZINIŲ IR TECHNOLOGIJOS MOKSLŲ CENTRAS

ELENA ADOMAITIENĖ

NETIESINIŲ DINAMINIŲ SISTEMŲ PUSIAUSVYROS IR SINCHRONIJOS VALDYMO METODŲ PLĖTOJIMAS

Daktaro disertacija
Fiziniai mokslai, fizika (02P)

Vilnius, 2017

Disertacija rengta 2012–2017 metais Fizinių ir technologijos mokslų centre.

Mokslinis vadovas – habil. dr. Arūnas Vytautas Tamaševičius (Fizinių ir technologijos mokslų centras, fiziniai mokslai, fizika – 02P)

Mokslinis konsultantas – doc. dr. Gytis Mykolaitis (Fizinių ir technologijos mokslų centras, fiziniai mokslai, fizika – 02P)

ACKNOWLEDGMENTS

I express my sincere gratitude to my scientific supervisor dr. habil. Arūnas Vytautas Tamaševičius for his help and guidance through the course of this work. I wish to thank my scientific advisor associate prof. dr. Gytis Mykolaitis for his warm encouragement, thoughtful guidance and the performed experiments. I am grateful to my coauthor dr. Skaidra Bumelienė for her help in graphical presentation of the results.

My sincere gratitude goes to my parents, my husband Martynas, and all my friends for their support and patience over the past years.

Elena Adomaitienė

ABBREVIATIONS

CFC – combined filter control

DFC – delayed feedback control

DH – Duffing–Holmes

FHN – FitzHugh–Nagumo

HPF – high-pass filter

IA – instrumentation amplifier

LPF – low-pass filter

OA – operational amplifier

OGY – Ott–Grebogi–Yorke

PFC – proportional feedback control

SEQ – stable equilibrium

SFC – stable filter control

UEQ – unstable equilibrium

UFC – unstable filter control

UFDC – unstable filter control combined with derivative control

CONTENTS

INTRODUCTION

Importance of the topic

Stability of any either natural or artificial system is a valuable and desired property. Stabilization in particular of unstable equilibrium (UEQ) of dynamical systems is an important problem in basic science and engineering applications, if periodic or chaotic oscillations are unacceptable behaviours. Usual control methods, based on proportional feedback control [Kuo, 1995; Ogata, 2010] require knowledge of a mathematical model of a dynamical system or at least the exact coordinates of the UEQ in the phase space for the reference point. However, in many real complex systems, especially in biology, physiology, economics, sociology, and chemistry neither the full reliable models, nor the exact coordinates of the UEQ are *a priori* known. Moreover, the position of the UEQ may change with time because of external unknown and unpredictable forces. Therefore, in these cases adaptive, i.e. model-independent and reference-free methods, automatically tracing and stabilizing unknown UEQ, can be helpful, e.g. [Rulkov *et al.*, 1994; Namajūnas *et al*., 1995b, Pyragas *et al.*, 2002].

Synchronization is a universal and very common phenomenon, widely observed in nature, science, engineering, and social life [Pikovsky *et al.*, 2003]. Coupled oscillators and their arrays, exhibiting synchrony, range from pendulum clocks to electronic oscillators, chaotic lasers, chemical systems, and various biological populations. Though in the most cases synchronization plays a positive role, sometimes it has a negative impact. Strong synchronization in the human brain is an example. It is widely believed that synchrony of spiking neurons in a neuronal population causes the symptoms of the Parkinson's disease [Rosenblum & Pikovsky, 2004]. Therefore, the development of the methods and practical techniques for controlling, more specifically, for suppressing synchrony of coupled oscillators, in general, and particularly with possible application to neuronal arrays, is of great importance [Popovych *et al.*, 2005; Pyragas *et al.*, 2007; Ratas & Pyragas, 2014; Pyragas & Tass, 2016].

Goals of the work:

1. Development of fast feedback methods using unstable filter control, stable filter control and proportional feedback control techniques for stabilizing various equilibrium states with *a priori* unknown coordinates of both weakly and strongly damped dynamical systems.
2. Development of methods for destroying synchrony or suppressing oscillations in mean-field coupled oscillators.

To achieve the scientific goals the following tasks have been assigned:

1. Design of an electronic analog of the Duffing–Holmes system.
2. Investigation of the unstable filter control technique with applications to switching between stable equilibrium and unstable equilibrium.
3. Design of an electronic analog of a conservative saddle equilibrium.
4. Creation of complex feedback techniques using:
   (a) unstable filter control and stable filter control applied in parallel,
   (b) linearly combined unstable filter control and stable filter control,
   (c) unstable filter control enhanced by a derivative control,
   (d) nonlinear feedback controller.
5. Development of the mathematical methods to estimate the uncertain (unknown) equilibrium points.
6. Design of an asymmetric version of an electronic analog of the FitzHugh–Nagumo (FHN) oscillator. Design of an electronic analog of an array of the mean-field coupled FHN oscillators.
7. Development of feedback techniques for implementing the method of repulsive coupling and the method of nullifying the mean field, both aimed to desynchronize the FHN oscillators.
8. Application of stable filter control to damping oscillations in an array of coupled FHN oscillators.

The following new scientific results have been obtained:

1. The unstable filter control technique has been demonstrated to switch from stable equilibrium to unstable equilibrium in motionless (non-oscillating and non-rotating) dynamical systems.
2. Several synergetic methods, based on combined unstable feedback control and stable filter control techniques also with an auxiliary differentiator in the feedback loop, have been shown to stabilize the saddle equilibrium.
3. The proportional feedback control for stabilizing unknown equilibrium has been developed to estimate the reference points.
4. Two-terminal feedback controllers have been demonstrated either to desynchronize or to damp array of coupled oscillators.

Main scientific statements:

1. The unstable filter inverts the stability properties of the originally stable and the originally unstable equilibrium, thus makes it possible to switch a dynamical system from an originally motionless stable equilibrium, to an *a priori* unknown unstable equilibrium.
2. Complex feedback loop, containing an unstable filter, a stable filter or a derivative unit, enable fast stabilization of saddle equilibrium in conservative and weakly damped dynamical systems.
3. Either natural or artificial stable equilibrium states allow finding unknown reference points and use them in the proportional feedback.
4. Feedback controllers, using the negative impedance converters, either desynchronize or damp oscillations in arrays of mean-field coupled FitzHugh–Nagumo oscillators.

Personal input of the author

Elena Adomaitienė (guided by the scientific supervisor) derived differential equations and performed mathematical stability analysis of equilibrium. Author obtained numerical results using the package MATHEMATICA. In addition, some of the simulations she performed using the circuit simulator ELECTRONICS WORKBENCH PROFESSIONAL.

LIST OF AUTHOR'S PAPERS INCLUDED IN THE DISSERTATION

I. Articles recorded in the *Clarivate Analytics* database *Web of Science*

[1] Tamaševičiūtė E., Tamaševičius A., Mykolaitis G., Bumelienė S., Lindberg E., Analogue electrical circuit for simulation of the Duffing–Holmes equation, ***Nonlinear Analysis: Modelling and Control***, 2008, V.13, No.2, pp.241–252. ISSN 1392–5113. IF – n/a, Q – n/a.

[2] Tamaševičius A., Tamaševičiūtė E., Mykolaitis G., Bumelienė S., Switching from stable to unknown unstable steady states of dynamical systems, ***Physical Review E***, 2008, V.78, No.2, 026205. ISSN 1539–3755. IF=2.508, Q1.

[3] Tamaševičius A., Tamaševičiūtė E., Mykolaitis G., Bumelienė S., Kirvaitis R., Stoop R. Neural spike suppression by adaptive control of an unknown steady state, ***Lecture Notes in Computer Science***, 2009, V.5768, part I, pp.618–627. ISSN 0302–9743. IF – n/a, Q – n/a.

[4] Tamaševičius A., Tamaševičiūtė E., Mykolaitis G., Bumelienė S., Kirvaitis R. Stabilization of saddle steady states of conservative and weakly damped dissipative dynamical systems, ***Physical Review E***, 2010, V.82, No.2, 026205. ISSN 1539–3755. IF=2.352, Q1.

[5] Tamaševičiūtė E., Mykolaitis G., Tamaševičius A. Analogue modelling an array of the FitzHugh–Nagumo oscillators, ***Nonlinear Analysis: Modelling and Control***, 2012, V.17, No.1, pp.118–125. ISSN 1392–5113. IF=0.861, Q2.

[6] Tamaševičius A., Tamaševičiūtė E., Mykolaitis G. Feedback controller for destroying synchrony in an array of the FitzHugh–Nagumo oscillators, ***Applied Physics Letters***, 2012, V.101, No.22, 223703. ISSN 1077–3118. IF=3.794, Q1.

[7] Tamaševičiūtė E., Tamaševičius A., Stabilizing uncertain steady states of some dynamical systems by means of proportional feedback, ***Nonlinear Analysis: Modelling and Control***, 2013, V.18, No.1, pp.86–98. ISSN 1392–5113. IF=0.914, Q2.

[8] Tamaševičius A., Tamaševičiūtė E., Mykolaitis G., Bumelienė S. Enhanced control of saddle steady states of dynamical systems, ***Physical Review E***, 2013, V.88, No.3, 032904. ISSN 1539–3755. IF=2.326, Q1.

[9] Tamaševičiūtė E., Mykolaitis G., Bumelienė S., Tamaševičius A., Stabilizing saddles, ***Physical Review E*** (*Rapid Communication*), 2013, V.88, No.6, 060901. ISSN 1539–3755. IF=2.326, Q1.

[10] Tamaševičiūtė E., Tamaševičius A., Mykolaitis G., Bumelienė S., Tracking and controlling unstable steady states of dynamical systems, ***Communications in Nonlinear Science and Numerical Simulation***, 2014, V.19, No.3, pp.649–655. ISSN 1007–5704. IF=2.866, Q1.

[11] Tamaševičius A., Mykolaitis G., Tamaševičiūtė E., Bumelienė S., Two-terminal feedback circuit for suppressing synchrony of the FitzHugh–Nagumo oscillators, ***Nonlinear Dynamics***, 2015, V.81, No.1–2, pp.783–788. ISSN 0924–090X. IF=3.000, Q1.

[12] Adomaitienė E., Mykolaitis G., Bumelienė S., Tamaševičius A., Adaptive nonlinear controller for stabilizing steady states of dynamical systems, ***Nonlinear Dynamics***, 2015, V.82, No.4, pp.1743–1753. ISSN 0924–090X. IF=3.000, Q1.

[13] Adomaitienė E., Mykolaitis G., Bumelienė S., Tamaševičius A., Suppresing activity of an array of coupled Fitzhugh–Nagumo oscillators, ***Acta Physica Polonica A***, 2016, V.129, No.4, pp.562–564. ISSN 0587–4246. IF=0.469, Q4.

[14] Adomaitienė E., Mykolaitis G., Bumelienė S., Tamaševičius A., Inhibition of spikes in an array of coupled FitzHugh–Nagumo oscillators by external periodic forcing, ***Nonlinear Analysis: Modelling and Control***, 2017, V.22, No.3, pp.421–429. ISSN 1392–5113. IF=0.952, Q2 (JCR'2016).

[15] Adomaitienė E., Bumelienė S., Mykolaitis G., Tamaševičius A., Stabilization of a network of the FitzHugh–Nagumo oscillators by means of a single capacitor based RC filter feedback technique, ***Complexity***, 2017, V.2017, 324879. ISSN 1099–0526. IF=4.621, Q1 (JCR'2016).

II. Papers in conference proceedings

[16] Tamaševičiūtė E., Mykolaitis G., Stabilization of unknown steady states in Duffing–Holmes type system by means of unstable controller, ***Proc. 11th Conf. of Young Lithuanian Scientists "Science – Future of Lithuania"*** (*Bioengineering and Bioinformatics; Physics and Physical Computer Science*), Apr3–4, 2008, Vilnius, Lithuania, pp.48–55 (in Lithuanian). ISBN 978-9955-28-301-0.

[17] Tamaševičiūtė E., Mykolaitis G., Bumelienė S., Tamaševičius A., Adaptive control of steady states and slowly varying states in the Duffing–Holmes type system with unstable high-pass filter, ***Proc. 2008 Int. Symp. Nonlinear Theory and its Applications, NOLTA'2008***, Sep7–10, 2008, Budapest, Hungary, pp.309–312. ISBN 978-4-88552-234-5 C3055.

[18] Tamaševičius A., Bumelienė S., Tamaševičiūtė E., Mykolaitis G., Kirvaitis R., Lindberg E. Controlling unknown saddle type steady states of dynamical systems with latency in the feedback loop, ***Proc. 2009 Int. Symp. Nonlinear Theory and its Applications, NOLTA'2009***, Oct18–21, 2009, Sapporo, Japan, pp.70–73. ISBN 978-4-88552-241-3 C3055.

[19] Tamaševičiūtė E., Mykolaitis G., Bumelienė S., Tamaševičius A., Adaptive stabilization of a saddle steady state of a conservative dynamical system: a spacecraft at the Lagrange point L2 of the Sun–Earth system, ***Proc. 2010 Int. Symp. Nonlinear Theory and its Applications, NOLTA'2010***, Sep5–9, 2010, Krakow, Poland, pp.442–445. ISBN 978-4-88552-251-2 C3055.

[20] Tamaševičiūtė E., Mykolaitis G., Bumelienė S., Tamaševičius A., 'Three-shot' technique for stabilizing unknown saddle steady states of dynamical systems, ***Proc. 2014 Int. Symp. Nonlinear Theory and its Applications, NOLTA'2014***, Sep14–18, 2014, Lucerne, Switzerland, pp.842–845.

[21] Adomaitienė E., Mykolaitis G., Bumelienė S., Tamaševičius A., Feedback controller for damping oscillations in arrays of coupled neurons, ***Proc. 18th Int. Conf. Biomedical Engineering 2014***, V.18, No.1, Nov27–28, 2014, Kaunas, Lithuania, pp.51–54. ISSN 2029–3380.

[22] Tamaševičius A., Adomaitienė E., Bumelienė S., Mykolaitis G., Lindberg E., Negative resistance circuit for damping an array of coupled FitzHugh–Nagumo oscillators, ***Proc. 22nd Eur. Conf. Circuit Theory and Design, ECCTD'2015***, Aug24–26, 2015, Trondheim, Norway, ISBN: 978-1-4799-9877-7. DOI: 10.1109/ECCTD.2015.7300082.

LIST OF CONFERENCES

(International conferences [C1–C20] and National conferences [C21–C28])

C1. 10th Experimental Chaos Conf., ECC'10, June 3–6, 2008, Catania, Italy (poster).

C2. 2008 Int. Symposium Nonlinear Theory and its Applications, NOLTA' 2008, September 7–10, Budapest, Hungary (oral*).

C3. 17th Int. Workshop Nonlinear Dynamics of Electronic Systems, NDES' 2009, June 21–24, Rapperswil, Switzerland (oral*).

C4. 19th Int. Conf. Artificial Neural Networks, ICANN'2009, September 14–17, Limassol, Cyprus (oral).

C5. 2009 Int. Symposium Nonlinear Theory and its Applications, NOLTA' 2009, October 18–21, Sapporo, Japan (oral).

C6. 18th Int. Workshop Nonlinear Dynamics of Electronic Systems, NDES' 2010, May 26–28, Dresden, Germany (oral).

C7. 2010 Int. Symposium Nonlinear Theory and its Applications, NOLTA' 2010, September 5–9, Krakow, Poland (oral*).

C8. 15th World Multi–Conference on Systemics, Cybernetics and Informatics, WMSCI'2011, July 19–22, Orlando, USA (oral).

C9. 5th Int. Scientific Conf. Physics and Control, PhysCon'2011, September 5–8, Leon, Spain (poster*).

C10. 2013 IEEE 4th Latin American Symposium Circuits and Systems, LASCAS' 2013, February 27 – March 1, Cusco, Peru (oral).

C11. 21st Int. Conf. Nonlinear Dynamics of Electronic Systems, NDES'2013, July 10–12, Bari, Italy (oral & oral*).

C12. Experimental Chaos and Complexity Conf. 2014, ECC'2014, August 25–28, Aberdeen, UK (poster & poster).

C13. 2014 Int. Symposium Nonlinear Theory and its Applications, NOLTA' 2014, September 14–18, 2014, Lucerne, Switzerland (oral*).

C14. 18th Int. Conf. Biomedical Engineering, November 27–28, 2014, Kaunas, Lithuania (oral*).

C15. 5th Int. Congress 'Advances in Applied Physics and Materials Science', APMAS'2015, April 16–19, Oludeniz, Turkey (oral*).

C16. Eur. Conf. Circuit Theory and Design, ECCTD'2015, August 24–26, Trondheim, Norway (oral).

C17. 23rd Int. Conf. Nonlinear Dynamics of Electronic Systems, NDES' 2015, September 7–11, Como, Italy (oral).

C18. 2016 Int. Conf. Systems, Control, Signal Processing and Informatics, May 28–30, Riga, Latvia (oral).

C19. Int. Conf. 'Perspectives in Nonlinear Dynamics', PNLD'2016, July 24–29, Berlin, Germany (poster).

C20. 25th Int. Workshop Nonlinear Dynamics of Electronic Systems, NDES' 2017, June 5–7, Zernez, Switzerland (oral).

C21. 10th Conf. of Young Lithuanian Scientists "Science – Future of Lithuania" (Bioengineering and Bioinformatics; Physics and Physical Computer Science), April 5–6, 2007, Vilnius, Lithuania (oral*).

C22. 37th Lithuanian Conf. on Physics, June 11–13, 2007, Vilnius, Lithuania (poster*).

C23. 11th Conf. of Young Lithuanian Scientists "Science – Future of Lithuania" (Bioengineering and Bioinformatics; Physics and Physical Computer Science), April 3–4, 2008, Vilnius, Lithuania (oral*).

C24. 38th Lithuanian Conf. on Physics, June 8–10, 2009, Vilnius, Lithuania (poster* & poster*).

C25. 39th Lithuanian Conf. on Physics, October 6–8, 2011, Vilnius, Lithuania (poster* & poster*).

C26. 4th Conf. of Young Scientists ‘Interdisciplinary Research in Physical Sciences and Technology’, February 11, 2014, Vilnius, Lithuania (oral*).

C27. 57th Scientific Conf. for Young Students of Physics and Natural Sciences, Open Readings’2014, March 19–21, Vilnius, Lithuania (oral*).

C28. 5th Conf. of Young Scientists ‘Interdisciplinary Research in Physical Sciences and Technology’, February 10, 2015, Vilnius, Lithuania (oral*).

*) papers presented personally by E. Adomaitienė (Tamaševičiūtė); 8 papers at the International conferences and 10 papers at the National conferences.

CHAPTER 1

CONTROLLING EQUILIBRIUM AND SYNCHRONY OF DYNAMICAL SYSTEMS (*review*)

1.1. Methods for controlling unstable equilibrium

Control of dynamical systems is one of the most important fields in applied nonlinear science. Although engineers and applied mathematicians have solved many basic problems a long time ago, the pioneering idea of "controlling chaos" introduced by Ott, Grebogi, and Yorke (OGY) [Ott *et al*., 1990] inspired many physicists worldwide to develop new techniques for controlling chaos, e.g., [Pyragas, 1992; Pyragas & Tamaševičius, 1993; Schöll & Schuster, 2008; Lenci & Rega, 2006; Ahlborn & Parlitz, 2006; Tamaševičius *et al*., 2009b; Olyaei & Wu, 2015, Pyragas & Pyragas, 2015]. The OGY method and new approaches are based on the fact that a chaotic attractor embeds an infinite number of unstable periodic orbits (UPOs) which can be stabilized only through tiny, carefully chosen perturbations.

Stabilization of unstable equilibrium[1] (UEQ) of dynamical systems is also an important problem in basic science and engineering applications, when neither chaotic nor periodic oscillations are desirable behaviours.

Let us consider time continuous n-dimensional autonomous nonlinear dynamical system with at least one accessible output to observe (to measure) the state of the system and with at least one accessible input to apply a control signal, given by a set of ordinary differential equations

$$\begin{aligned} \dot{\mathbf{x}} &= \mathbf{F}(\mathbf{x}(t), y(t)), \\ \dot{y} &= f(\mathbf{x}(t), y(t)) \end{aligned} \tag{1.1}$$

with the initial conditions $\mathbf{x}(0)$ and $y(0)$. In Eq. (1.1) $\mathbf{x}(t)$ is the $(n-1)$-dimensional vector variable, the $y(t)$ is a scalar variable, the $\mathbf{F}(\ldots)$ and the $f(\ldots)$ is a vector and a scalar nonlinear function, respectively. We assume that an

[1] 'Equilibrium' is also called either 'steady state' (to characterize a physical state) or 'fixed point' (to present the state as a geometrical image in phase space).

autonomous system has at least one equilibrium. Its coordinates ($\mathbf{x}_0$,y_0) are found from the algebraic equations

$$\begin{aligned} \mathbf{F}(\mathbf{x}_0, y_0) &= 0, \\ f(\mathbf{x}_0, y_0) &= 0. \end{aligned} \tag{1.2}$$

If the ($\mathbf{x}_0$,y_0) is a stable equilibrium (SEQ), then the system (1.1) converges to the SEQ, ($\mathbf{x}(t)\to x_0$, $y(t)\to y_0$) with $t\to\infty$. At the beginning stage ($t \geq 0$) starting from $\mathbf{x}(0)$ and $y(0)$ the system exhibits transient, either damped oscillations (stable spirals) or relaxation behaviour (stable nodes). An exception is rare case when the initial conditions either intentionally or accidentally are set on the SEQ, $\mathbf{x}(0)=\mathbf{x}_0$ and $y(0)=y_0$.

If the ($\mathbf{x}_0$,y_0) is an unstable equilibrium (UEQ), the system (1.1) either escapes from it to some SEQ ($\mathbf{x}_{SEQ}$,y_{SEQ}), coexisting with the UEQ due to the nonlinearity, or exhibits periodic/chaotic oscillations. If these cases are undesirable behaviours, one should apply a proper stabilization technique, which makes the initially unstable equilibrium to become stable, without changing its original coordinates ($\mathbf{x}_0$,y_0). Here, in Sec.1.1 we will consider the feedback algorithms only (non-feedback technique will be briefly discussed in Sec.5.4).

There are number of methods developed so far for stabilizing the UEQ in system (1.1). The general form of the scalar feedback methods can be presented in the following way

$$\begin{aligned} \dot{\mathbf{x}} &= \mathbf{F}(\mathbf{x}(t), y(t)), \\ \dot{y} &= f(\mathbf{x}(t), y(t)) + \Phi(r, y(t)). \end{aligned} \tag{1.3}$$

Here r is the reference coordinate, depending on a specific control method is either a constant value r_0 or a scalar variable $r(t)$. In general, the feedback function $\Phi(r,y(t))$ should be designed so that it should vanish when the desirable SEQ is achieved:

$$\Phi(r, y(t)) \to 0, \text{ if } \mathbf{x}(t) \to x_0 \text{ and } y(t) \to y_0. \tag{1.4}$$

This requirement guarantees that the coordinates of the initial UEQ ($\mathbf{x}_0$,y_0) are not changed. The form of Φ for different control techniques is discussed below. In some specific cases the "diagonal" scalar variable $y(t)$ in $\Phi(r,y(t))$ should be

replaced with an appropriate measurable scalar component $x_i(t)$, where $1 \le i \le n-1$, of the vector variable $\mathbf{x}(t)$.

Proportional feedback control (PFC). Conventional control methods, based on proportional feedback [Kuo, 1995; Ogata, 2010], require knowledge either of a full mathematical model of a system or at least the exact coordinates of the UEQ.

$$\begin{aligned} \dot{\mathbf{x}} &= \mathbf{F}(\mathbf{x}, y), \\ \dot{y} &= f(\mathbf{x}, y) + k(y_0 - y). \end{aligned} \tag{1.5}$$

Here and elsewhere time t is omitted for simplicity. Evidently, $k(y_0-y)\to 0$, when $y \to y_0$. In Eq. (1.5) and elsewhere k is the feedback coefficient (feedback gain). Its threshold value k_{th} in most cases can be derived analytically (if the dynamics is known), else it is an empirically adjusted parameter.

However, in many real systems, especially in biology, physiology, economics, sociology, chemistry, neither the reliable models are available nor the exact locations of the UEQ are *a priori* known. Moreover, the position of the UEQ may slowly vary with time because of external unknown and unpredictable forces. Therefore, adaptive methods, automatically tracing and stabilizing unknown UEQ, are needed.

Derivative control. The simplest adaptive technique for stabilizing UEQ is based on the derivative controller.

$$\begin{aligned} \dot{\mathbf{x}} &= \mathbf{F}(\mathbf{x}, y), \\ \dot{y} &= f(\mathbf{x}, y) - k\dot{x}_i. \end{aligned} \tag{1.6}$$

Evidently the derivative $\dot{x}_i$ becomes zero, when all variables $\mathbf{x}$,y become constant. Control term $k\dot{x}_i$ does not change the original system, since it vanishes when the variable $x_i(t)$ approaches the stabilized equilibrium. This technique works well for originally oscillating systems [Bielawski *et al*., 1993; Johnston & Hunt, 1993, Parmananda *et al*., 1994].

Stable filter control (SFC). Another adaptive method for stabilizing UEQ employs either low-pass filter (LPF) in the feedback loop [Rulkov *et al*., 1994; Namajūnas *et al*., 1995b, 1997; Schenk zu Schweinsberg & Dressler, 2001;

Huijberts, 2006], or high-pass filter (HPF) [Ciofini *et al.*, 1999]. Provided the cut-off frequency of the filter is low enough, the filtered image $v(t)$ of the observable $y(t)$ or $x_i(t)$ asymptotically approaches the UEQ and therefore can be used as a reference point in the proportional feedback. This method has been successfully applied to several experimental systems, including electronic circuits [Rulkov *et al.*, 1994; Namajūnas *et al.*, 1995b, 1997] and lasers [Ciofini *et al.*, 1999; Schenk zu Schweinsberg & Dressler, 2001].

The system (1.3) is supplemented with an auxiliary equation, describing the first order stable filter (its variable $v(t)$)

$$\begin{aligned} \dot{\mathbf{x}} &= \mathbf{F}(\mathbf{x}, y), \\ \dot{y} &= f(\mathbf{x}, y) + k(v - y), \\ \dot{v} &= \omega_{\mathrm{f}}(y - v). \end{aligned} \tag{1.7}$$

Here ω_{f} is the cut-off frequency of the filter (commonly $\omega_{\mathrm{f}} \ll 1$). When the equilibrium of the overall system (1.7) is stabilized, the $v_0=y_0$. Consequently, the control term $k(v_0-y_0)$ in Eq. (1.7) vanishes, as required.

Delayed feedback control (DFC). This method [Pyragas, 1992] is originally designed to control chaos that is to stabilize UPOs. Under appropriate setting of parameters, it can stabilize UEQ as well [Pyragas, 1995; Chang *et al.*, 1998; Hövel & Schöll, 2005; Yanchuk *et al.*, 2006; Hövel, 2010; Ding *et al.*, 2010; Rezaie & Motlagh, 2011; Gjurchinovski *et al.*, 2013; Zhou & Yang, 2013]. The DFC can be presented by:

$$\begin{aligned} \dot{\mathbf{x}} &= \mathbf{F}(\mathbf{x}, y), \\ \dot{y} &= f(\mathbf{x}, y) + k(y_\tau - y). \end{aligned} \tag{1.8}$$

Here y_τ is a time delayed version of the original variable $y(t)$: $y_\tau \equiv y(t-\tau)$. Evidently, when $y(t)\to y_0$, the $y(t-\tau)\to y_0$ as well. Therefore, the control term in Eq. (1.8) vanishes.

Notch filter control (NFC). Similarly to the DFC, the NFC has been originally to stabilize UPOs [Ahlborn & Parlitz, 2006; Tamaševičius *et al.*, 2007a; Tamaševičius *et al.*, 2009b]. The technique employs either single Wien-bridge filter [Ahlborn & Parlitz, 2006], or single LC filter [Tamaševičius *et al.*, 2007a],

or several LC filters coupled in series [Tamaševičius *et al*., 2009b]. To stabilize UEQ two notch filters with incommensurate cut-off frequencies ω_1 and ω_2 should be applied [Ahlborn & Parlitz, 2006]. The method is given by the set:

$$\begin{aligned}
\dot{\mathbf{x}} &= \mathbf{F}(\mathbf{x}, y), \\
\dot{y} &= f(\mathbf{x}, y) + k(v_1 + v_2 - y), \\
\dot{v}_1 &= \omega_1^2 (w_1 + k_1 (y - v_1 - v_2)), \\
\dot{w}_1 &= -v_1 - b_1 w_1, \\
\dot{v}_2 &= \omega_2^2 (w_2 + k_2 (y - v_1 - v_2)), \\
\dot{w}_2 &= -v_2 - b_2 w_2 .
\end{aligned} \tag{1.9}$$

Unstable filter control (UFC). However, it turns out that for a wide class of dynamical systems the developed methods [Pyragas, 1992; Pyragas & Tamaševičius, 1993; Schöll & Schuster, 2008; Ahlborn & Parlitz, 2006; Rulkov *et al*., 1994; Namajūnas *et al*., 1995b; Ciofini *et al*., 1999; Schenk zu Schweinsberg & Dressler, 2001] do not work. If an unstable state, say an UPO, is a torsion-free orbit (or in mathematical language an orbit with an odd number of real positive Floquet exponents), more sophisticated controllers should be used. The idea of using an auxiliary unstable degree of freedom in the feedback loop was introduced in [Pyragas, 2001] and has been experimentally verified for stabilizing torsion-free UPOs of autonomous the van der Pol oscillator [Höhne *et al*., 2007] and nonautonomous the Duffing–Holmes oscillator [Tamaševičius *et al*., 2007b] dynamical systems.

To solve the problem of the odd number limitation of the methods for stabilizing UEQ Pyragas *et al*. [Pyragas *et al*., 2002] proposed to use an unstable filter that is an elegant idea to fight one instability with another instability. The method has been demonstrated to stabilize saddles in a variety of mathematical models [Pyragas *et al*., 2002; 2004; Braun, 2008] also in the experiments with an electrochemical oscillator [Pyragas *et al*., 2002; 2004; Pyragas, 2007].

In contrast to the SFC, described by Eq. (1.7), the UFC employs an inherently unstable filter (the auxiliary equation for variable u):

$$\begin{aligned} \dot{\mathbf{x}} &= \mathbf{F}(\mathbf{x}, y), \\ \dot{y} &= f(\mathbf{x}, y) + k(u - x_i), \\ \dot{u} &= \omega_{\mathrm{f}}(u - x_i). \end{aligned} \tag{1.10}$$

Note the positive sign of the variable u on the right hand side in the equation for u, in contrast to the negative sign of the variable v on the right hand side in the equation for v in Eq. (1.7). Similarly to the case of SFC, the control term $k(u–x_i)\to 0$, since $u\to u_0 = x_{i0}$ and $x_i \to x_{i0}$. The method has a limitation concerning the damping coefficient of the system under control. Let us illustrate this point with a simple 2nd order linear (linearized around the saddle) dynamical system as an example:

$$\begin{aligned} \dot{x} &= y, \\ \dot{y} &= x - by + k(u - x), \\ \dot{u} &= \omega_{\mathrm{f}}(u - x). \end{aligned} \tag{1.11}$$

This advanced method is limited, however, to dissipative dynamical systems only. It is not applicable to conservative systems. The limitation of the unstable filter method can be proved analytically using the Routh–Hurwitz stability criterion. The necessary condition for stabilizing a saddle UEQ is that the cut-off frequency ω_{f} of the unstable filter is lower than the damping coefficient b of the system [Pyragas *et al*., 2004; Braun, 2008].

$$\omega_{\mathrm{f}} < b. \tag{1.12}$$

In conservative systems, damping b is zero by definition. Formally, the cut-off frequency could be set negative. However, this would mean that the unstable filter should become a stable one and, therefore, inappropriate to stabilize a saddle UEQ. Detailed mathematical proof of (1.12) is presented in Sec.3.3 using the Routh–Hurwitz criterion. The inequality (1.12) holds for diverse systems, including the mechanical pendulum, the Duffing–Holmes oscillator, a body at the Lagrange points of the Sun–Earth system, the Lorenz system [Lorenz, 1963], the Duffing– Lindberg autonomous chaotic electronic oscillator [Lindberg *et al*., 2009; Tamaševičius *et al*., 2009a].

The above control techniques deal with single oscillators. In a very recent paper [Zou *et al*., 2017] coupled dynamical networks have been considered.

1.2. Methods for controlling synchrony of coupled oscillators

Synchronization is a universal and very common phenomenon, widely observed in nature, science, engineering, and social life [Pikovsky *et al*. 2003]. Coupled oscillators and their arrays, exhibiting synchrony, range from pendulum clocks to electronic oscillators, chaotic lasers, chemical systems, and various biological populations [Pikovsky *et al*. 2003; Rosenblum & Pikovsky, 2003; Luo, 2009]. Though in the most cases synchronization plays a positive role, sometimes it has a negative impact. Strong synchronization in the human brain is an example. It is widely believed that synchrony of spiking neurons in a large neuronal population causes the symptoms of the essential tremor and the Parkinson's disease [Rosenblum & Pikovsky, 2004]. Therefore, development of the methods and practical techniques for controlling, more specifically, for suppressing synchrony of coupled oscillators, in general, and particularly with possible application to neuronal arrays, is of great importance [Rosenblum & Pikovsky, 2004; Popovych *et al*., 2005; Pyragas *et al*., 2007]. Seeking to destroy synchrony, the feedback methods, e.g. based on the inversion of the mean field [Tsimring *et al*., 2005; Hong & Srogatz, 2011], might be promising.

Let us consider an array of N nonidentical 2nd order oscillators, given by the 2N-dimensional system

$$\begin{aligned} \dot{x}_i &= f_i(x_i, y_i), \\ \dot{y}_i &= g_i(x_i, y_i), \quad i = 1, 2, ...N. \end{aligned} \tag{1.13}$$

In Eq. (1.13) the individual oscillators are not coupled and each of them oscillates at its own frequency and its own phase. Evidently, they behave in a nonsynchronous way[2]. To make the oscillators synchronous some coupling between them should be introduced. There are several different architectures of coupling, e.g. each-to-each coupling, mean-field coupling, the nearest-neighbours coupling. To be specific, we illustrate the synchronous and nonsynchronous behaviours with the example of the mean-field coupling

[2] Synchronous behaviour of ideally identical oscillators, i.e. $f_i(x_i,y_i) = f(x_i,y_i)$ and $g_i(x_i,y_i) = g(x_i,y_i)$ for all indexes i, is a formal and impractical exception.

$$\begin{aligned} \dot{x}_i &= f_i(x_i, y_i) + k(\langle x \rangle - x_i), \\ \dot{y}_i &= g_i(x_i, y_i), \quad i = 1, 2, ...N, \end{aligned} \tag{1.14}$$

where $\langle x \rangle$ is the mean value of the variables x_i

$$\langle x \rangle = \frac{1}{N} \sum_{i=1}^{N} x_i \, . \tag{1.15}$$

The specific phase portraits and waveforms are presented in Fig. 1.1 and Fig. 1.2, respectively for the array of 30 mean-field coupled FitzHugh–Nagumo (FHN) oscillators, given by the 60-dimensional system

$$\begin{aligned} \dot{x}_i &= x_i - x_i^3 / 3 - y_i + c_i + k(\langle x \rangle - x_i), \\ \dot{y}_i &= \varepsilon(x_i - b y_i), \quad i = 1, 2, ...30. \end{aligned} \tag{1.16}$$

Here

$$\langle x \rangle = \frac{1}{30} \sum_{i=1}^{30} x_i \, . \tag{1.17}$$

The oscillators in Eq. (1.16) are all different due to different bias terms c_i. Note in Fig. 1.1a that there is a finite width loop in the phase portrait. This means that it is not a complete synchronization, $x_j(t)=x_i(t)$, but is the so-called phase synchronization, $x_j(t+\Delta\varphi_j)=x_i(t)$. All units oscillate at the same frequency and have stable phase differences $\Delta\varphi_j$, which are not necessarily zero.

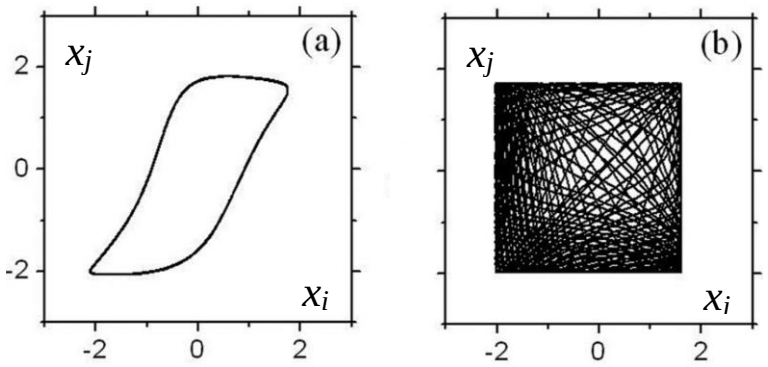

FIG. 1.1. Phase portraits, x_j *vs.* x_i, $j \neq i$ for the FHN oscillators. (a) coupled ($k \neq 0$; therefore synchronized; Eq. (1.16)), (b) either uncoupled ($k = 0$; therefore nonsynchronized; Eq. (1.16)), or coupled ($k \neq 0$; but desynchronized; Eq. (1.19)). $\varepsilon = 0.3$, $b = 0.1$, $c_{i+1} = c_i + 0.05$, $c_1 = -5$.

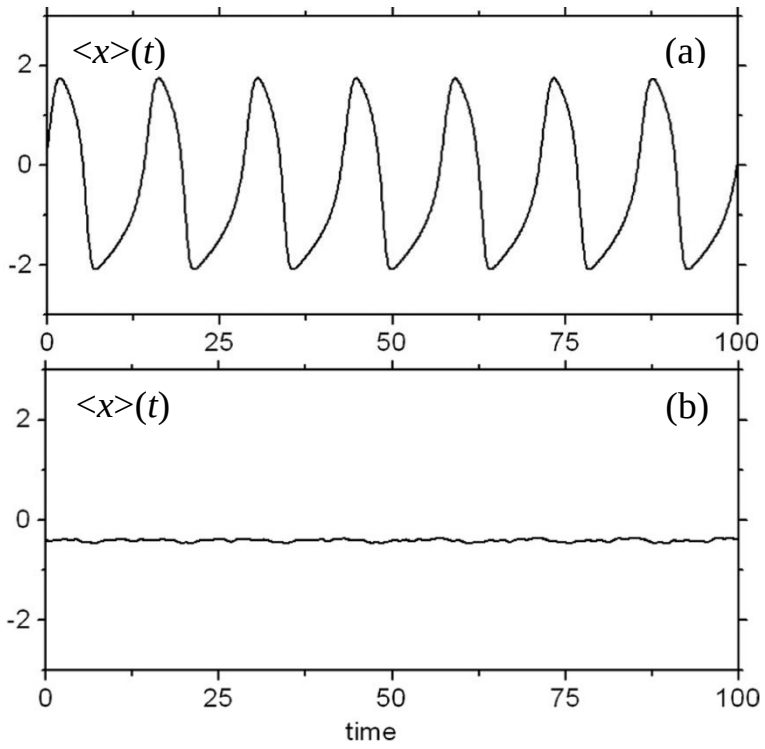

FIG. 1.2. Waveforms of the mean-field variable <*x*> for the FHN oscillators. (a) coupled ($k \neq 0$; therefore synchronized; Eq. (1.16)), (b) either uncoupled ($k = 0$; therefore nonsynchronized; Eq. (1.16)), or coupled ($k \neq 0$; but desynchronized; Eq. (1.19)). $\varepsilon = 0.3$, $b = 0.1$, $c_{i+1} = c_i + 0.05$, $c_1 = -5$.

To avoid synchrony, if it is not a desirable, but a harmful state, a number of non-feedback and feedback methods have been developed so far. The most popular of the non-feedback methods is the external periodic forcing

$$\begin{aligned} \dot{x}_i &= f_i(x_i, y_i) + k(\langle x \rangle - x_i) + A\sin \omega t, \\ \dot{y}_i &= g_i(x_i, y_i), \quad i = 1, 2, ...N, \end{aligned} \tag{1.18}$$

where the external frequency should be much higher than the natural frequencies of the oscillators ($\omega >> \omega_0$). Above some threshold amplitude A_{th} the inherent oscillations, e.g. spikes in neuronal models, are totally inhibited. This is not a desynchronization in its genuine sense. We simply get around the problem of synchrony by a straightforward damping of the oscillators. On one hand, the effect can be considered as a dynamical stabilization of the UEQ of the oscillators [Thomsen, 2003; Pyragas *et al.*, 2007; Pyragas & Tass, 2016]. On the other hand, some residual (response) oscillations (about 10 to 20 % of the original amplitude) in the individual oscillators $x_i(t)$ and in their mean-field

variable $\langle x\rangle(t)$ at the external drive frequency ω are still observed. Therefore, the effect can be interpreted as the synchronization of the array of the oscillators to the high frequency external driving force, whereas with an essentially lower response amplitude compared to the original natural oscillations.

The external periodic forcing is conventionally used as a therapy for patients with the Parkinson's disease. In medicine, it is called 'deep brain stimulation' (DBS). Strong relatively high frequency (100 to 200 Hz) periodic pulse trains are applied to the appropriate regions of the brain. Unfortunately, this treatment is often accompanied with side effects.

A large number of feedback techniques to avoid synchronization of interacting oscillators in general and more specifically with the possible application to neuronal arrays have been described in the literature, e.g. [Rosenblum & Pikovsky, 2004; Popovych *et al*., 2005; 2006; Tsimring *et al*., 2005; Tass, 2007; Tukhlina *et al*., 2007; Pyragas *et al*., 2007; Luo & Xu, 2011; Hong & Strogatz, 2011; Sheeba *et al*., 2011; Franci *et al*., 2012].

Extremely small mean field values (Fig. 1.2b) can be achieved by the feedback techniques, for example by the so-called 'repulsive coupling' or 'repulsive synchronization' method [Tsimring *et al*., 2005][3], where the $\langle x\rangle$ is fed back into the array with an inverted sign:

$$\begin{aligned} \dot{x}_i &= f_i(x_i, y_i) + k(-\langle x\rangle - x_i), \\ \dot{y}_i &= g_i(x_i, y_i), \quad i = 1, 2, ...N. \end{aligned} \tag{1.19}$$

Note the minus sign in front of $\langle x\rangle$. The physical mechanism behind the 'repulsive synchronization' has a simple intuitive explanation. Once $+\langle x\rangle$ in Eq. (1.14) means 'attractive coupling' and provides synchronous states, the $-\langle x\rangle$ in Eq. (1.19), in contrast, means 'repulsive coupling' and yields nonsynchronous states. In mathematics, it is easy to replace '+' with '–'. However, in practical implementations it is a nontrivial problem.

[3] Tsimring *et al.* considered an array of simple 1-dimensional phase oscillators (the Kuramoto model), in contrast to the 2-dimensional (2nd order) oscillators in Eq. (1.19).

CHAPTER 2

PYRAGAS' UNSTABLE FILTER METHOD FOR CONTROLLING SADDLE EQUILIBRIUM

2.1. Switching from stable states to unknown saddle states [2]

***Proportional feedback control* (*PFC*) *and stable filter control* (*SFC*).** A dynamical system given by

$$\dot{x} = a(x - x^*)$$

with $a > 0$ has an unstable equilibrium (UEQ) point $x_0 = x^*$. If the value of x^* is known, the point x_0 can be easily stabilized by means of a PFC:

$$\dot{x} = a(x - x^*) + k(x^* - x) \equiv (a - k)(x - x^*).$$

The equilibrium point of the controlled system is $x_0 = x^*$, i.e., exactly the same as that of the free-flowing system. The PFC does not change the location of the equilibrium, but makes it stable if $k > a$.

If the equilibrium point is unknown, one can think of the conventional SFC used to stabilize UEQ in chaotically oscillating systems [Rulkov *et al.*, 1994, Namajūnas *et al.*, 1995b, Ciofini *et al.*, 1999]. Let us try to apply such a filter to the unstable system:

$$\dot{x} = a(x - \xi) + k(v - x),$$
$$\dot{v} = \omega_f (x - v).$$

Here ξ is an unknown parameter, k is the control gain, v is the variable of the stable filter control (SFC), and ω_f is its cut-off frequency. However, by means of simple stability analysis one can show that the new point $(x_0, v_0) = (\xi, \xi)$ is a saddle, i.e., the SFC fails to stabilize UEQ of this type for any set of the parameters a, k, and ω_f.

Unstable filter control (UFC). Let us consider a simple one-dimensional nonlinear example

$$\dot{x} - x + x^2 = \xi.$$

For $\xi < 0.25$ the system has two equilibrium points $x_{01,02} = -0.5 \pm \sqrt{0.25 - \xi}$. The first one, x_{01} is a stable equilibrium (SEQ) and the second one an UEQ. If

the value of the parameter ξ is either unknown for some reasons or ξ is not a constant, but slowly varies with time, the locations of both equilibrium points become unspecified.

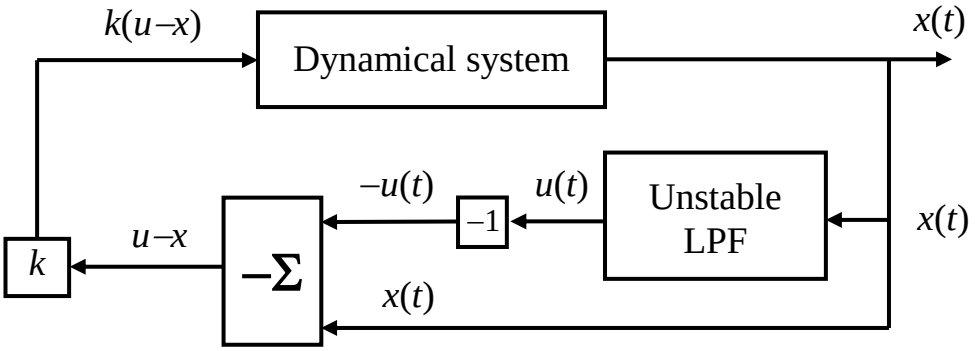

FIG. 2.1. Block diagram of controlling unknown equilibrium of a dynamical system by means of an UFC.

Now we supplement the system with an auxiliary degree of freedom implemented by an *unstable filter* [Pyragas *et al.*, 2002] (Fig. 2.1):

$$\dot{x} = x + x^2 + \xi + k(u - x),$$
$$\dot{u} = \omega_f (u - x).$$

Here u is the variable of the filter. The equilibrium points of the closed-loop system (x,u) are $(x_{01,02},x_{01,02})$, i.e., their x components are exactly the same as those of the free-flowing systems. Their stability properties can be easily checked using standard analysis method. The parameter matrices of the linearized equations are

$$A_{1,2} = \begin{pmatrix} 1 + 2x_{01,02} - k & k \\ -\omega_f & \omega_f \end{pmatrix}.$$

The corresponding traces $\sigma_{1,2}$ and the determinants $\Delta_{1,2}$ of the matrices $A_{1,2}$ are

$$\sigma_{1,2} = \mathrm{Tr}(A_{1,2}) = 1 + 2x_{01,02} - k + \omega_f,$$
$$\Delta_{1,2} = \det(A_{1,2}) = (1 + 2x_{01,02})\omega_f.$$

Since $\Delta_1 < 0$, the first fixed point x_{01}, originally a SEQ point, becomes a saddle, i.e., an UEQ point. The eigenvalues of the characteristic equation

$$\lambda^2 - \sigma_1 \lambda + \Delta_1 = 0$$

are both real and have opposite signs. Instability of the fixed point depends neither on the parameter ξ nor on the value of the control gain $k > 0$.

Since $\Delta_2 < 0$, the second, originally UEQ point x_{02} becomes a SEQ point if $\sigma_2 < 0$. Its stability does not depend on ξ, similarly to the first fixed point, but here the trace σ_2 should be negative, that is, the control gain k should exceed some threshold value $(k > k_{th} = 1 + 2x_0 + \omega_f)$. The eigenvalues $\lambda_{1,2}$ of the corresponding characteristic equation

$$\lambda^2 - \sigma_2 \lambda + \Delta_2 = 0$$

either are both real and negative or $\mathrm{Re}\lambda_{1,2}<0$. The stabilized point is either a stable node, if $\sigma_2^2 > 4\Delta_2$, or a stable spiral, if $\sigma_2^2 < 4\Delta_2$. The fastest control is achieved when both negative eigenvalues are equal: $\lambda_1 = \lambda_2 = \sigma_2 / 2 < 0$. This is satisfied if the discriminant $D \equiv \sigma_2^2 - 4\Delta_2 = 0$, yielding $k_{opt} = k_{th} + 2\sqrt{\Delta_2}$.

In summary, the UFC inverts the stability properties of the two equilibrium points. The originally SEQ point loses its stability, while the originally UEQ (a saddle) gains stability.

***Switching the states of a mechanical pendulum*.** As a simple second-order nonlinear example, we consider a mechanical pendulum

$$\ddot{\varphi} + \beta\dot{\varphi} + \sin\varphi = \xi . \qquad (2.1)$$

Here φ is the angle between the downward vertical and the pendulum, β is a damping parameter, and ξ is a constant or slowly varying torque. There are two equilibrium points: $[\varphi_{01}, \dot{\varphi}_{01}] = [\arcsin\xi, 0]$, $[\varphi_{02}, \dot{\varphi}_{02}] = [\pi - \arcsin\xi, 0]$. The first one is a SEQ point, either a spiral or a node, depending on the damping parameter β. The second one is an UEQ point (a saddle). We present Eq. (2.1) in a form of two 1st-order equations and add an equation for the unstable filter (variable u) also a feedback term in the equation for the angular velocity ω:

$$\begin{aligned} \dot{\varphi} &= \omega, \\ \dot{\omega} &= -\beta\omega - \sin\varphi + \xi + k(u - \varphi), \\ \dot{u} &= \omega_f (u - \varphi). \end{aligned} \qquad (2.2)$$

Switching from the originally SEQ to the originally UEQ, including the transient process, is shown in Fig. 2.2 for two different values of the damping parameter β. To achieve stability the cut-off frequency of the filter ω_f should be set sufficiently low ($\omega_f < \beta$) [Pyragas *et al.*, 2004]. For small β this leads to a very slow transient. For larger β, the ω_f can be increased and the transient becomes shorter.

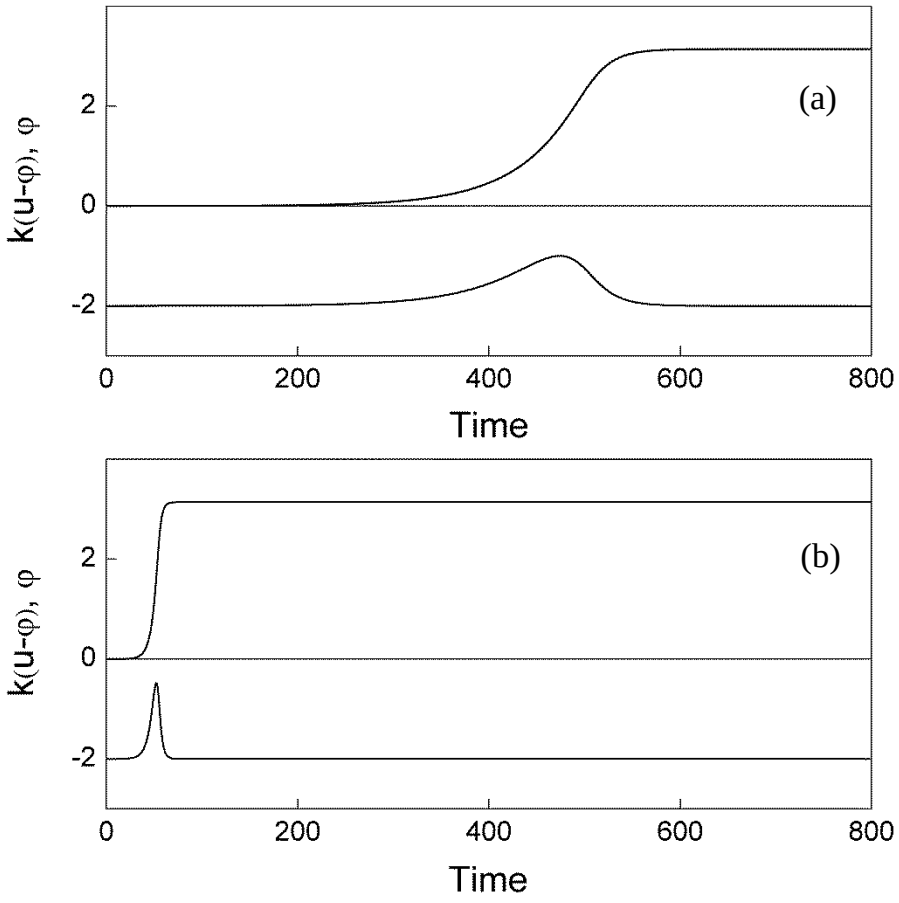

FIG. 2.2. Switching from the SEQ to the UEQ of the pendulum from Eq. (2.2) with $\xi = 0$ ($\varphi_{01} = 0, \varphi_{02} = \pi$). (a) $\beta = 0.1, k = 2.1, \omega_f = 0.05$. (b) $\beta = 2, k = 6, \omega_f = 1$. Upper traces in the top and bottom plots are the angles φ, lower traces (shifted down by 2 for clarity) are the control terms $k(u - \varphi)$. Control is turned on at $t = 0$.

Switching the states of the Duffing–Holmes (DH) system. The second example is the DH oscillator. We consider it without external periodic drive but with a constant external force ξ:

$$\ddot{x} + b\dot{x} - x + x^3 = \xi. \tag{2.3}$$

Here b is the damping coefficient. In the case, when the force ξ is not too large ($|\xi| < 2/\sqrt{27}$), Eq. (2.3) has three real equilibrium points $(x_{01,02,03},0)$. Their x-projections are found from a cubic algebraic equation $x_0^3 - x_0 - \xi = 0$:

$$x_{01,02} = -h\cos\frac{\pi \mp \theta}{3}, \quad x_{03} = h\cos\frac{\theta}{3},$$

with $h = 2/\sqrt{3}$ and $\theta = \arccos(3\xi/h)$. In the limit case of zero force (ξ=0), the auxiliary angle $\theta = \pi/2$. Then $x_{01}^* = -1, x_{02}^* = 0, x_{03}^* = 1$, as expected, and correspond to the symmetric double-well potential of the DH system. Two of the points $(x_{01},0)$ and $(x_{03},0)$ are SEQ points, while the middle point $(x_{02},0)$ is a saddle. We rewrite Eq. (2.3) in a more convenient form and add a feedback term that combines the observable $x(t)$ and the output of the filter $u(t)$:

$$\begin{aligned} \dot{x} &= y, \\ \dot{y} &= -by + x - x^3 + \xi + k(u - x), \\ \dot{u} &= \omega_f (u - x). \end{aligned} \tag{2.4}$$

Let us consider the equilibrium points and their stability properties for $k > 0$. The x_0 and the y_0 projections remain unchanged, while the u_0 projection coincides with the x_0 projection. This means that control does not influence the location of the equilibrium points. However, the originally UEQ $(x_{02},0)$ under certain conditions can become a SEQ $(x_{02},0,x_{02})$. In order to check the stability of the system, we linearize Eq. (2.4) around this point:

$$\begin{aligned} \dot{x} &= y, \\ \dot{y} &= -by - (k - 1 + 3x_{02}^2)x + ku, \\ \dot{u} &= \omega_f (u - x) \end{aligned} \tag{2.5}$$

and analyse its characteristic equation

$$\lambda^3 + (b - \omega_f)\lambda^2 + (k - 1 + 3x_{02}^2 - b\omega_f)\lambda + \omega_f = 0. \tag{2.6}$$

The system is stable, if the real parts of all three eigenvalues of Eq. (2.6) are negative. The necessary and sufficient conditions can be found using the Routh–Hurwitz matrix

$$H = \begin{pmatrix} b-\omega_f & \omega_f & 0 \\ 1 & k-1-b\omega_f+3x_{02}^2 & 0 \\ 0 & b-\omega_f & \omega_f \end{pmatrix}.$$

The eigenvalues $\mathrm{Re}\lambda_{1,2,3}$ are all negative if all diagonal minors of the *H* matrix are positive:

$$\begin{aligned} &\Delta_1 = b-\omega_f > 0, \\ &\Delta_2 = (b-\omega_f)(k-1-b\omega_f+3x_{02}^2)-\omega_f > 0, \\ &\Delta_3 = \omega_f\Delta_2 > 0. \end{aligned} \qquad (2.7)$$

These inequalities are satisfied if

$$0<\omega_f<b, \quad k>k_{th}=\frac{b}{b-\omega_f}+b\omega_f-3x_{02}^2. \qquad (2.8)$$

For small b and ξ the threshold gain $k_{th}\approx b/(b-\omega_f)$. For example, at $b=0.1, \omega_f=0.03, \xi=0$, the gain $k_{th}\approx 1.43$. In order to find the optimal value of the gain corresponding to the maximum convergence rate we have solved Eq. (2.6) numerically (Fig. 2.3). $\mathrm{Re}\lambda<0$ and $|\mathrm{Re}\lambda|$ have maximal values at $k_{opt}\approx 2.3$. We note that in Fig. 2.3 two originally positive λ become negative at $k\approx 1.43$, coinciding with the k_{th} found from the Routh–Hurwitz criterion.

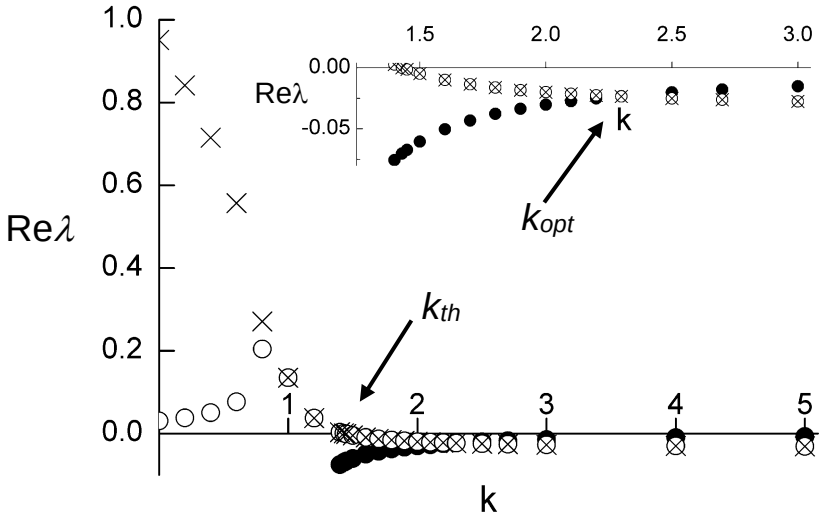

FIG. 2.3. Dependence of the real parts of the eigenvalues $\mathrm{Re}\lambda$ on the control gain *k* from Eq. (2.6). $\xi=0, b=0.1, \omega_f=0.03$.

Numerical results obtained by integrating Eq. (2.4) are presented in Fig. 2.4. The lengths of transient processes in the DH system, as in the pendulum, are different for weak and strong damping.

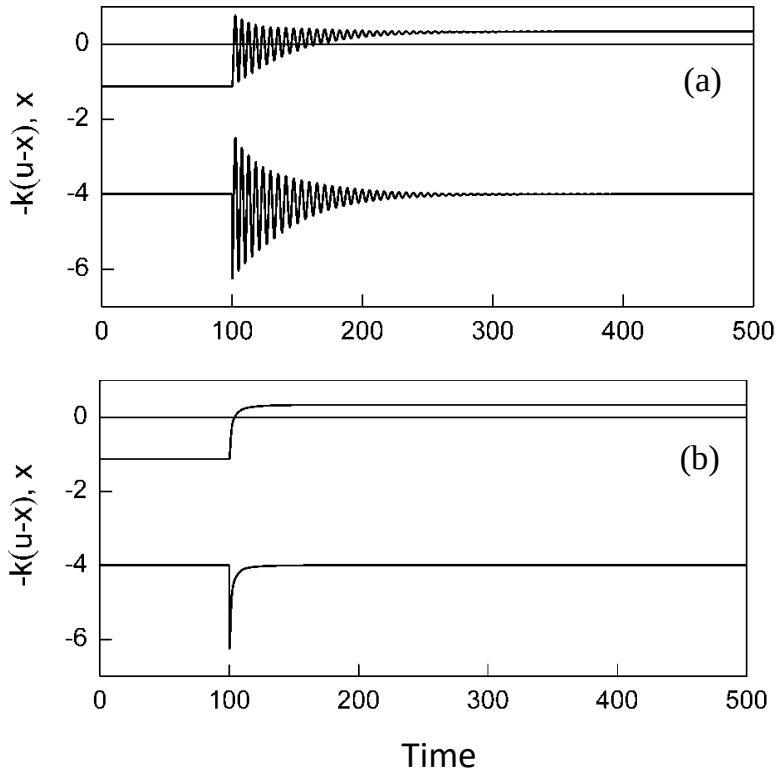

FIG. 2.4. Switching from the SEQ to the UEQ of the DH oscillator from Eq. (2.4) with $k = 2$ and $\xi = -0.3$. (a) $b = 0.1, \omega_f = 0.03$. (b) $b = 2, \omega_f = 0.1$. Upper traces in the top and bottom plots are observables x; lower traces (shifted down by 4 for clarity) are the control terms $k(u–x)$. Control is turned on at $t = 100$.

Experiment. Experimental results are presented in Fig. 2.5. An electronic circuit, imitating dynamics of the DH oscillator is given in *Appendix* 1, the circuit implementing the UFC is referred in *Appendix* 5.

The main difference between the results in Figs. 2.2, 2.4, and 2.5 and the investigations in [Pyragas *et al.*, 2002, 2004] lies in the following. The electrochemical oscillator [Pyragas *et al.*, 2002], the pendulum, and the Lorenz system [Pyragas *et al.*, 2004] are all in the oscillating regimes before the control is turned on. In contrast, the control in Figs. 2.2, 2.4, and 2.5 is

activated when the systems are in the SEQ (either stable spirals or stable nodes). Although it is stated nowhere in the text of [Pyragas *et al*., 2002, 2004], the presented illustrations of originally oscillating and rotating systems give an inadequate impression that a saddle point can be stabilized only if it is surrounded or approached by the trajectories of the limit cycles and chaotic attractors. In our case the original SEQ and UEQ points are fixed and rather remote objects in the phase space. In addition, the examples of overdamped systems (bottom plots in Figs. 2.2, 2.4, and 2.5) show that in order to switch from a SEQ to a saddle it is not necessary (even for the transient trajectories) to oscillate around the saddle. In contrast, the target can be reached point blank.

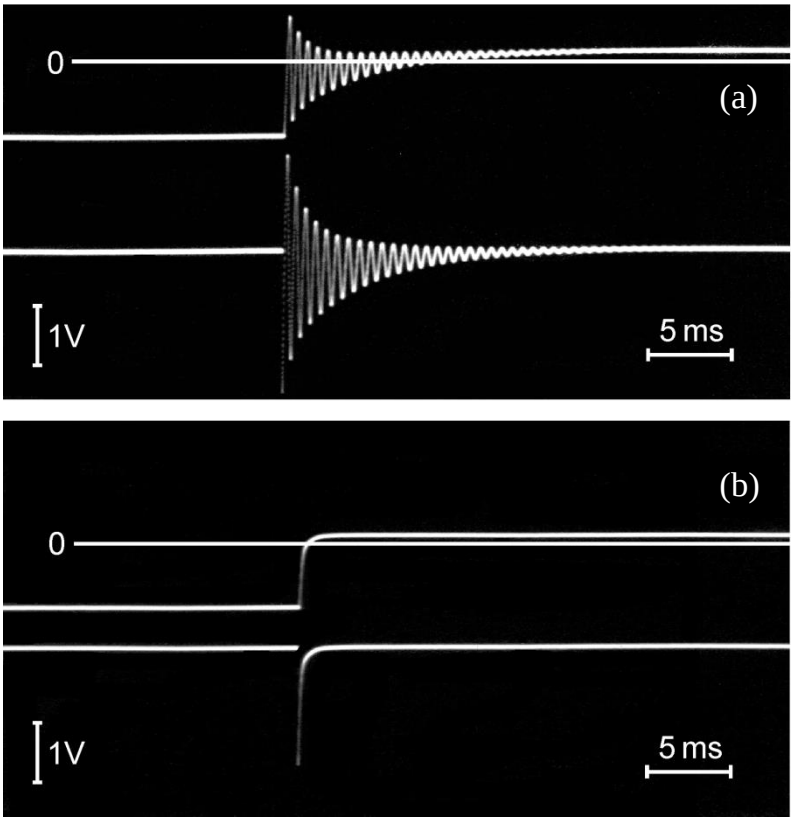

FIG. 2.5. Experimental control of the equilibrium of the DH electrical circuit with R_{11}=5 kΩ (k = 2), V^*=30 V (V_0=−300 mV). (a) R=20 Ω (b = 0.1), C_1=330 nF (ω_f = 0.03). (b) R=400 Ω (b = 2), C_1=100 nF (ω_f = 0.1). Upper traces in the top and bottom photos are the signals $V_C \propto x$; the lower traces are the control signals $V_{\text{contr}} \propto -k(u-x)$.

2.2. Controlling slowly varying equilibrium by means of unstable high-pass filter (HPF) [17]

The saddle equilibrium also can be controlled by means of the unstable HPF (Fig 2.6 and Fig. 2.7), which allows much simpler practical implementation.

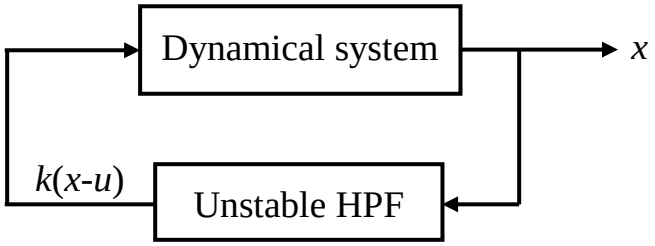

FIG. 2.6. Block diagram of controlling unknown equilibrium of a dynamical system by means of an unstable HPF.

In addition, the saddles can be slowly varying states. The corresponding equations are exactly the same as Eq. (2.4), except the unknown force ξ which is considered here to be time-dependent term: $\xi(t) = \xi_0 + \xi_1 \sin(\Omega_1 t)$, $\Omega_1 \ll 1$.

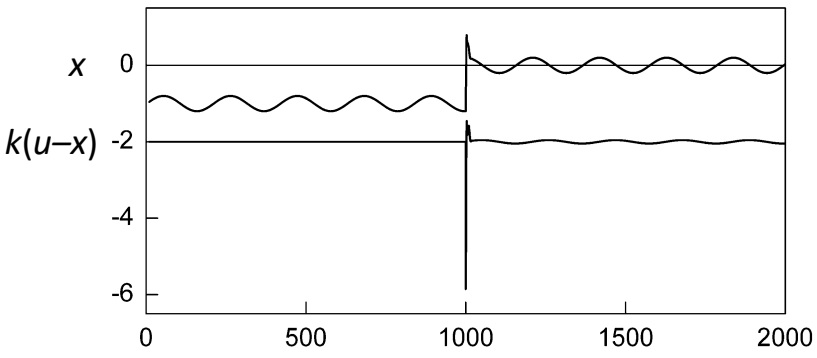

FIG. 2.7. Switching from slowly varying spiral to slowly varying saddle of the DH oscillator from Eq. (2.4) with $k = 3$, $\xi_0 = 0$, $\xi_1 = 0.2$, $\Omega_1 = 0.03$. $b = 2$, $\omega_f = 0.4$. Lower trace (control term $k(u-x)$) is shifted down by 2 for clarity. Control is turned on at $t = 1000$.

Experiment. A photo taken from the screen of a multichannel oscilloscope is presented in Fig. 2.8. Experimental results are in a good agreement with the numerical simulations.

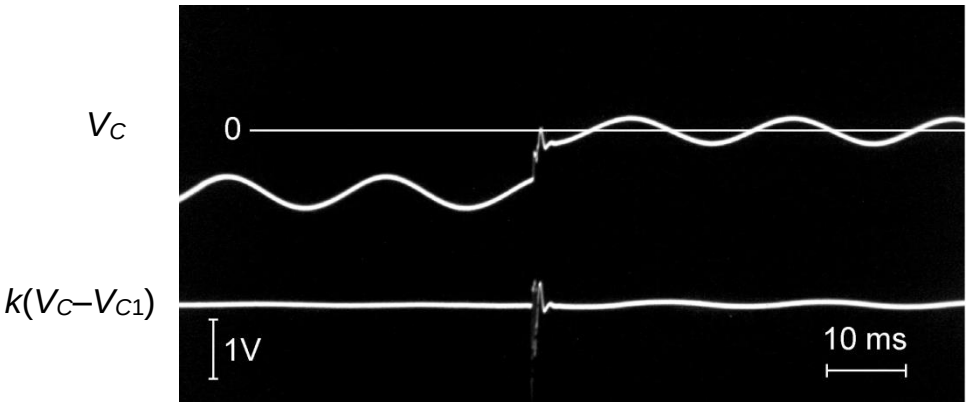

FIG. 2.8. Control of slowly varying saddle state of the DH electrical circuit (*Appendix* 1) with R_7=R_8=20 kΩ (k = 3), V_0=0, V_1=2 V, f_1=50 Hz (Ω_1= 0.03). R=400 Ω (b = 2), R_f=−20 kΩ, C_1=13 nF (ω_f = 0.4); Upper trace is the main signal $V_C \propto x$, lower trace is the control signal $V_{contr} \propto -k(u-x)$.

2.3. Analogue controller with the instrumentation amplifiers (IA) for stabilizing saddles, spirals and nodes [10]

The diagram of controller is shown Fig. 2.9. The dynamical system is supposed to have an inverting input, as the physical examples provided below. Otherwise a signal inverter should be inserted between the controller and the system. In the case the inherent gain of the controller (k_0 = 2) is insufficient, an additional amplifier, either inverting or non-inverting unit, should be used.

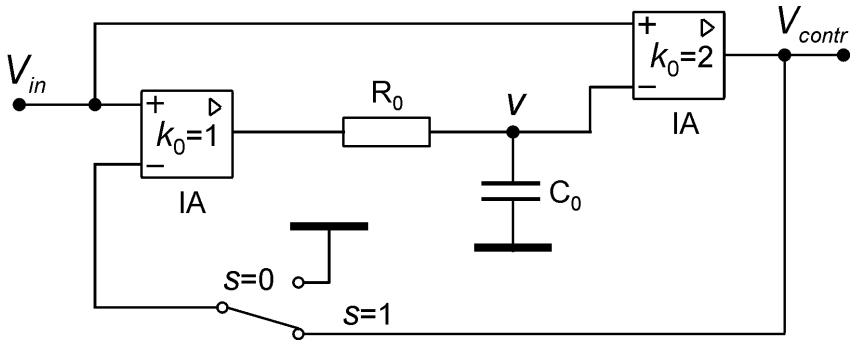

FIG. 2.9. Circuit diagram of the controller. We use rectangular boxes with small triangles inside as the symbols of IA to avoid confusion with the standard operational amplifier (OA).

The electronic controller in Fig. 2.9 is an extremely simple device. It includes four units only: two IAs, a stable RC filter, and a switch. The latter allows to choose between stabilizing the spirals/nodes (s = 0) and the saddles (s = 1). The IAs are the AD620 or similar type devices. The controller itself

has an internal positive feedback loop (when $s = 1$), which makes a stable RC filter to behave as an unstable one. The output voltage v of the RC LPF is given by the first order differential equation

$$\dot{v} = \Omega_f [V_{in} - v - 2s(V_{in} - v)].$$

Here $\Omega_f = (R_0 C_0)^{-1}$ is the cut-off frequency of the filter, V_{in} is the input signal of the controller, v is the output signal of the filter. In the case $s = 0$ the RC circuit is a simple stable filter

$$\dot{v} = \Omega_f (V_{in} - v),$$

applicable for stabilizing spirals and nodes. Whereas, if $s = 1$, it becomes an unstable unit

$$\dot{v} = \Omega_f (v - V_{in}),$$

suitable to stabilize saddles. The output signal of the controller in both cases has the same form, $V_{contr} = 2(V_{in} - v)$.

We demonstrate the performance of the controller for two autonomous nonlinear dynamical systems, namely the damped DH oscillator and the chaotic Lorenz oscillator, having *a priori* unknown equilibrium states.

DH oscillator. The oscillator and the controller with s=1 are described by

$$\begin{aligned} \dot{x} &= y, \\ \dot{y} &= x - x^3 - by + k(v - x) + p, \\ \dot{v} &= \omega_f (v - x). \end{aligned} \tag{2.9}$$

Here b is the damping parameter, k is the control gain (without an additional amplifier $k = 2$), p is an unknown external force, ω_f is the dimensionless cut-off frequency of the RC filter. Uncontrolled DH system has three real equilibrium points: two stable spirals (x_{01},0), (x_{03},0) and one UEQ point (x_{02},0), which is a saddle. However, the x–coordinates are unknown because of the *a priori* unknown force p. When $p = 0$, the $x_{01} = -1$, $x_{02} = 0$, $x_{03} = +1$, as expected for the symmetric double–well potential of the DH system [Moon *et al.*, 1987]. For small p, the $x_{02} \approx -p$. When the control is applied ($k > k_{th}$) the two SEQ points (the spirals) lose their stability, whereas the originally UEQ (the saddle) gains stability. We demonstrate that once the saddle point is stabilized, $x \to x_{02} = f(p)$

the adaptive controller independently on the value of the unknown force p and/or on the function $f(p)$ quickly tracks the changes of x_{02} and keeps the saddle point stable with only minor applied feedback force $k(v–x)$. We note that p should not be too large: $|p| < 2/\sqrt{27} \approx 0.38$. Otherwise the double–well potential is bent so much that the saddle point does not longer exist. Numerical results are presented in Fig. 2.10a and Fig. 2.10b for fast and slow changes of the unknown force p, respectively.

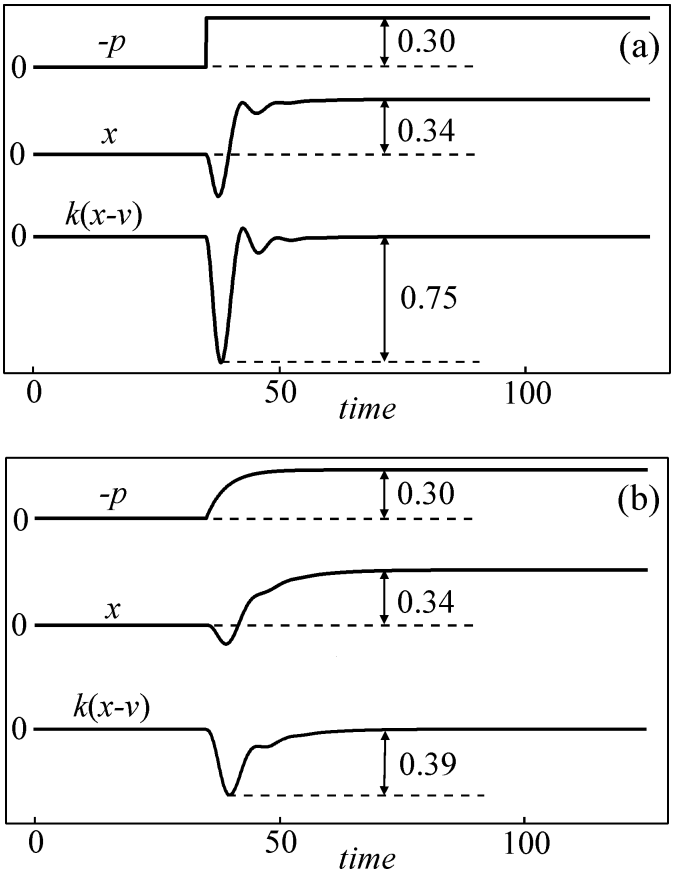

FIG. 2.10. Numerical integration of Eq. (2.9), b =1, ω_f = 0.22, k = 2, p_0 jumps from 0 to –0.3. (a) Fast change of $p = p_0$. (b) Slow change of perturbation: $\dot{p} = \varepsilon(p_0 - p)$ with ε = 0.25.

Experiment. The experiment has been carried out with an electronic circuit, imitating the DH system (*Appendix* 1). The results are presented in Fig. 2.11.

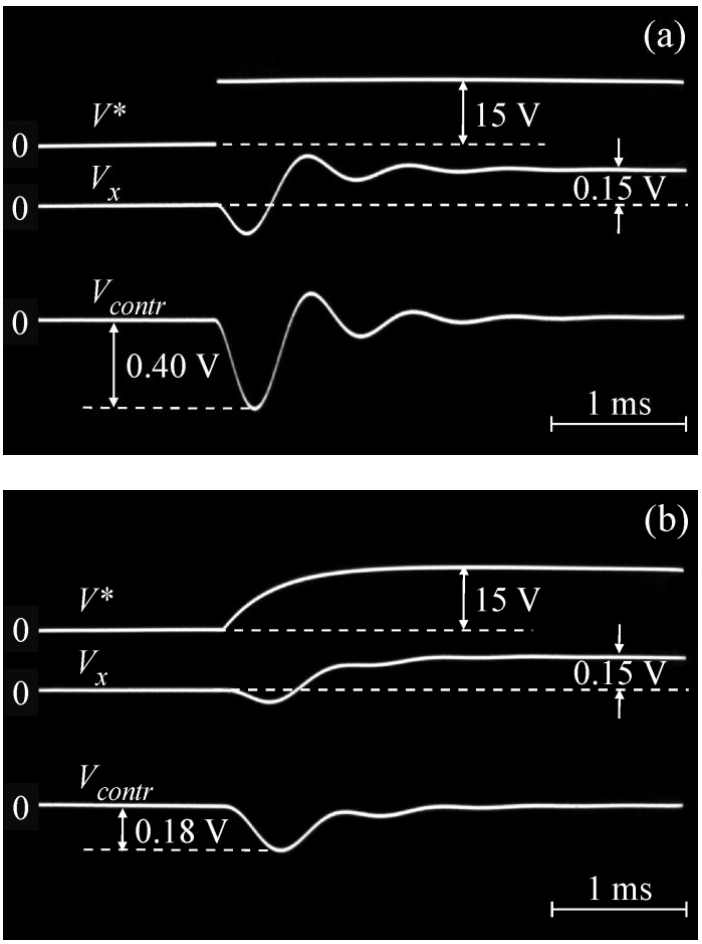

FIG. 2.11. (a) Fast change of dc bias. (b) Slow change of dc bias, using an auxiliary integrating circuit $R'C' \approx 0.38$ ms (dimensionless parameter $\varepsilon = R'C'/\sqrt{LC} \approx 4$). R_0=9.1 kΩ, C_0=47 nF ($\omega_f = \sqrt{LC}/R_0C_0 \approx 0.22$), k = 2. $V_p = -V^*/100$ changes from 0 to –0.15 V (dimensionless force $p = V_p/V_b$ changes from 0 to –0.3). New saddle coordinate $V_x \approx -V_p = +0.15$ V.

The Lorenz system. The second example is the famous Lorenz system, exhibiting chaotic oscillations [Lorenz, 1963; Moon *et al.*, 1987]. The equations of the Lorenz system combined with the equation for the adaptive controller read

$$\begin{aligned} \dot{x} &= -\sigma x + \sigma y, \\ \dot{y} &= -xz + rx - y + k(v - y), \\ \dot{z} &= xy - bz + p, \\ \dot{v} &= \omega_f [y - v - 2s(y - v)]. \end{aligned} \tag{2.10}$$

Here the σ, r and b are fixed parameters. The k and p are the same notations as in Eq. (2.9). In contrast to the previous example, we employ in the controller

the variable y instead of x. Though the controller also works with x, but it shows faster convergence to the equilibrium state, if y is used.

The uncontrolled ($k = 0$) and unforced ($p = 0$) Lorenz system at $r > 1$ has three equilibrium states, a saddle at the origin and two stable symmetrical spirals:

$$(0,0,0),\ \left(\pm\sqrt{b(r-1)},\pm\sqrt{b(r-1)},r-1\right). \tag{2.11}$$

For $r > r_{th}$, where

$$r_{th} = \sigma\frac{\sigma+b+3}{\sigma-b-1}, \tag{2.12}$$

the spirals become unstable giving rise to chaotic oscillations. For standard parameter values $\sigma = 10$ and $b = 8/3$ the $r_{th} \approx 24.74$.

The force p changes the position of the equilibrium points and the threshold value r_{th} in the following way:

$$(0,0,p/b),\ \left(\pm\sqrt{b(r-1)-p},\pm\sqrt{b(r-1)-p},r-1-p/b\right), \tag{2.13}$$

$$r_{th} = \sigma\frac{\sigma+b+3}{\sigma-b-1} + \frac{p}{b}. \tag{2.14}$$

Therefore, to sustain chaos either the p should not be too large or r should be increased (see caption to Fig. 2.12, where $r = 38$ instead of classical value $r = 28$). We checked stabilization of spirals and saddles for various values of p (positive and negative). Some of the results are shown in Fig. 2.12. Even though it may seem surprising that the control term $k(v–y)$ (Fig. 2.12c) is zero during the change of p and z (in contrast to the DH system), it can be easily explained. Such a behaviour is a special feature of the Lorenz system, in which independently on p the saddle equilibrium x_0– and y_0–coordinates are zeros (formula 2.13) Therefore, once the saddle is stabilized for a specific p, e. g. for $p = 0$, the all values, y, v, and $k(v–y)$ remain zeros.

In addition, the product xy in Eq. (2.10) in the equilibrium state is nullified and the reaction of z–coordinate to the changes of p is simply given by an isolated relaxation equation (2.15).

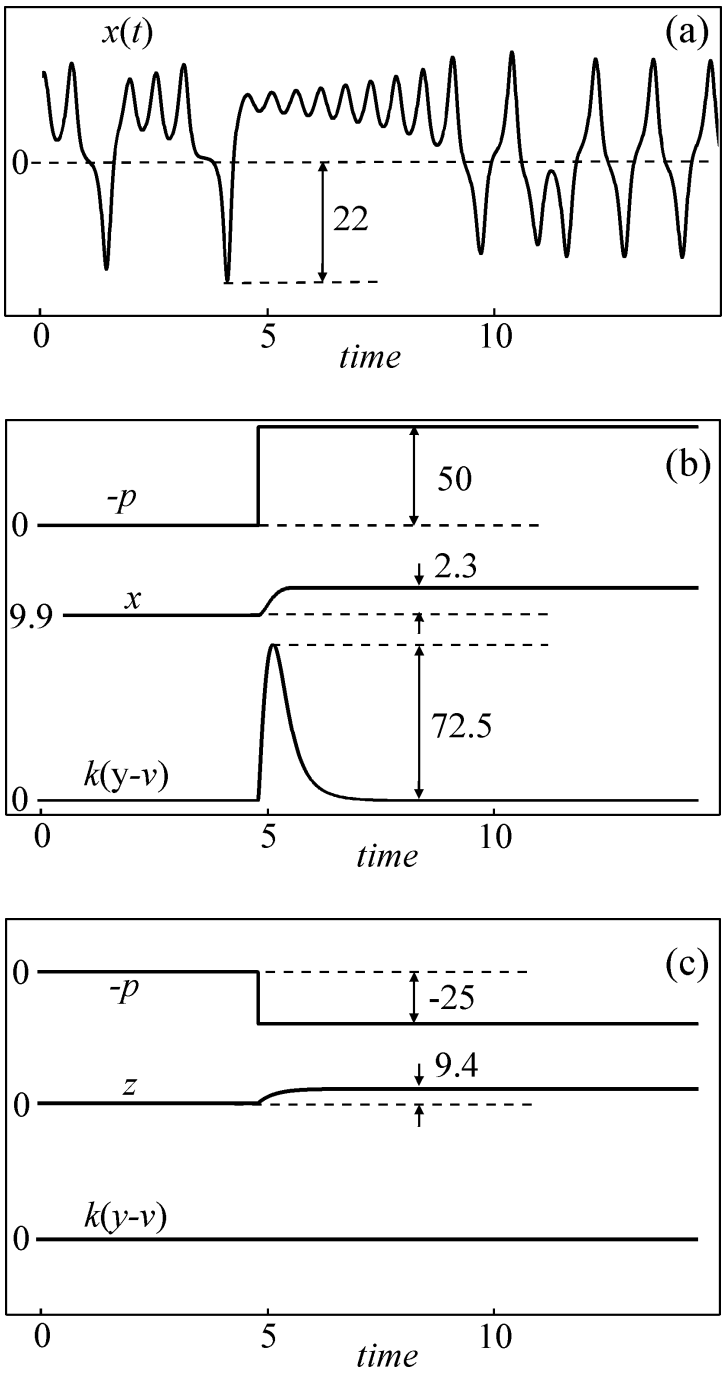

FIG. 2.12. Numerical integration of Eq. (2.10), $\sigma = 10$, $r = 38$, $b = 8/3$. (a) Chaotic solution, $k = p = 0$. (b) Tracking the spiral, $s = 0$, p changes from 0 to –50. (c) Tracking the saddle, $s = 1$, p changes from 0 to +25. In (b) and (c) $k = 60$, $\omega_f = 2.6$.

$$\dot{z} = p - bz\,. \tag{2.15}$$

The rate of convergence from $z = 0$ to $z = p/b$ does not depend on the cut-off frequency of the filter ω_f, but depends on b only.

The controller has been also tested experimentally using a hardware electronic analogue of the Lorenz system. First of all, to meet the limited dynamical range of the op–amps and the in–amps (±15 V) we apply linear transformations to the variables and parameter *p*:

$$x = 10X,\ y = 10Y,\ z = 10Z,\ p = 10P.$$

Then the Lorenz equations read:

$$\begin{aligned} \dot{X} &= -\sigma X + \sigma Y, \\ \dot{Y} &= -10XZ + rX - Y + k(V - Y), \\ \dot{Z} &= 10XY - bZ + P, \\ \dot{V} &= \omega_f [Y - V - 2s(Y - V)]. \end{aligned} \tag{2.16}$$

Note, that parameters σ, *r*, *b*, and *k* are still the same as in Eq. (2.10).

Furthermore, to avoid large values of the parameters inconvenient for electronic implementation, we divide all lines of Eq. (2.16) by a factor of 10, scaling the time $10t \to t$ and introducing the new parameters:

$$\tilde{\sigma} = \sigma / 10 = 1,\ \tilde{r} = r / 10,\ \tilde{b} = b / 10,$$
$$\tilde{k} = k / 10,\ \tilde{p} = P / 10 = p / 100,\ \tilde{\omega}_f = \omega_f / 10.$$

Finally, we obtain a compact set of differential equations suitable for building its electronic analog (*Appendix* 2)

$$\begin{aligned} \dot{X} &= -X + Y, \\ \dot{Y} &= -XZ + \tilde{r}X - 0.1Y + \tilde{k}(V - Y), \\ \dot{Z} &= XY - \tilde{b}Z + \tilde{p}, \\ \dot{V} &= \tilde{\omega}_f [Y - V - 2s(Y - V)]. \end{aligned} \tag{2.17}$$

Experiment. The experimental results are shown in Fig. 2.13. They agree very well with the numerical results in Fig. 2.12.

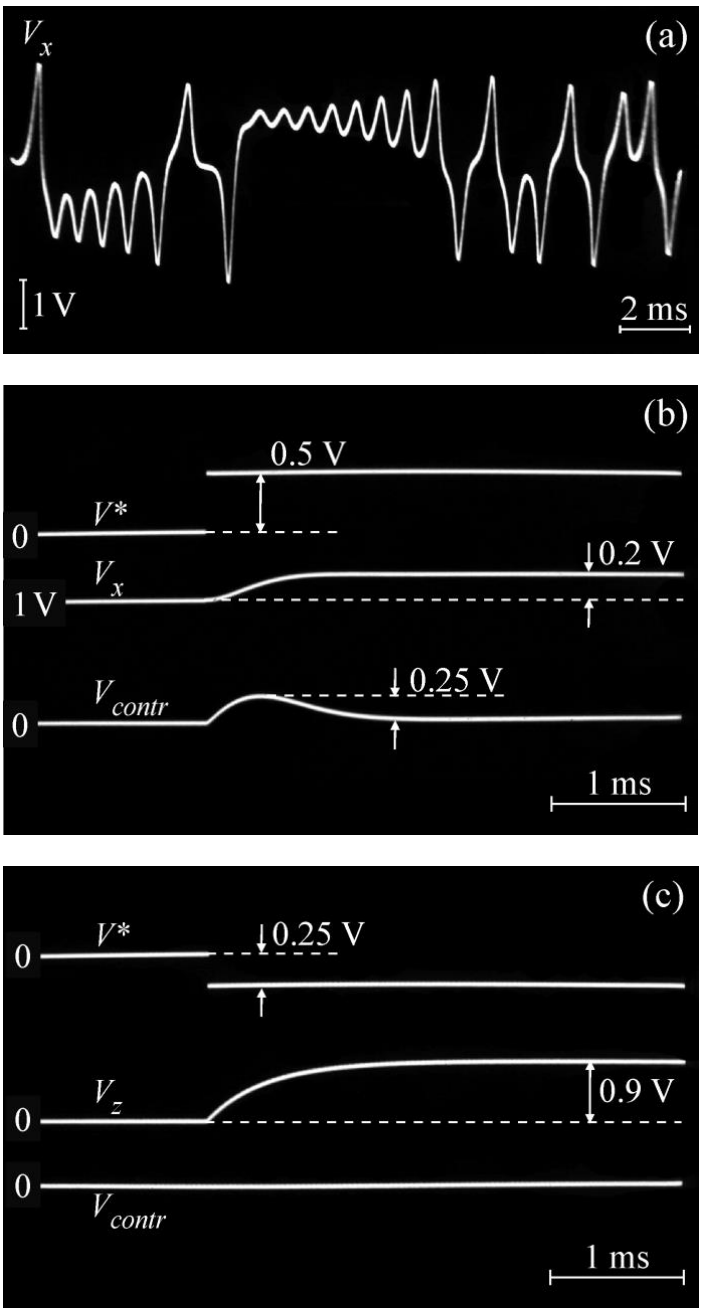

FIG. 2.13. (a) Chaotic oscillation from the Lorenz system. (b) Controlling the spiral ($s = 0$), $V_p = -V^*$ changes from 0 to –0.5 V. (c) Controlling the saddle, ($s = 1$), $V_p = -V^*$ changes from 0 to +0.25 V. In (b) and (c) R_0=9.1 kΩ, C_0=47 nF ($\omega_f = RC/R_0C_0 = 0.26$), $k = 6$. New saddle coordinate $V_z = V_pR_2/R$ = +0.9 V.

CHAPTER 3

SYNERGETIC FEEDBACK METHODS FOR STABILIZING SADDLE EQUILIBRIUM

3.1. Stabilizing saddles of conservative and weakly damped systems by means of unstable and stable filters coupled in parallel [4,19]

The advanced method described in Chapter 2 is limited to dissipative dynamical systems only. It is not applicable to conservative systems. The situation is somewhat similar to the famous Ott–Grebogi–Yorke (OGY) method [Ott *et al.,* 1990], in the sense that it does not work in the Hamiltonian systems [Lai *et al.*, 1993]. The limitation of the Pyragas' unstable filter method can be proved analytically using the well-known Hurwitz stability criterion. According to this criterion, the necessary condition for stabilizing saddle equilibrium is that the cut-off frequency of the unstable filter is lower than the damping coefficient of the system under control. In the conservative systems damping is zero under definition. Formally, to fulfil the stability criterion, the cut-off frequency could be set negative. However, this would mean that the unstable filter should become a stable one and, therefore, inappropriate to stabilize a saddle equilibrium. In this section, to break the vicious circle in the problem of stabilizing conservative saddles we suggest using synergetic technique that involves both, unstable filter control (UFC) and stable filter control (SFC).

Lagrange point L2. To be specific, we consider dynamics of a body of mass μ along the Sun–Earth line (Fig. 3.1). Taking into account the centrifugal forces and forces of gravity the dynamics is given by

$$\mu\ddot{R} + B\dot{R} - \mu\Omega^2(R_0 + R) + \frac{\gamma\mu M}{(R_0 + R)^2} + \frac{\gamma\mu m}{R^2} = P. \qquad (3.1)$$

Here B is the coefficient of friction ($B \to 0$), γ is the gravitational constant; M and m are the masses of the Sun and the Earth, respectively, R_0 is the distance of the Earth from the Sun, R is the distance of the L2 point from the Earth, P is an unknown external force, either constant or slowly varying in time.

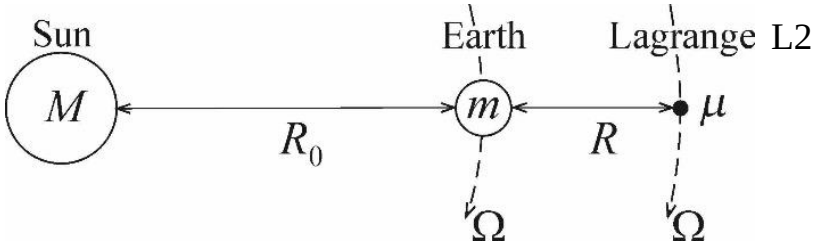

FIG. 3.1. The Lagrange point L2 of the Sun–Earth system (the Sun diameter, the Earth diameter, the distances R_0, and R are not in scale).

Since L2 lies on the same line as the Sun and the Earth, the angular velocity Ω in the centrifugal force of the body at the L2 is just the same as that of the Earth: $\Omega^2 = \gamma M / R_0^3$. By introducing the dimensionless quantities $r = R / R_0$, $\varepsilon = m / M \approx 3\times10^{-6}$ and $\xi = P / \mu R_0 \Omega^2$ Eq. (3.1) can be presented as

$$\begin{aligned} &\ddot{r} - \Omega^2 F(r,\xi) = 0, \\ &F(r,\xi) = 1 + r - \frac{1}{(1+r)^2} - \frac{\varepsilon}{r^2} + \xi. \end{aligned} \tag{3.2}$$

The nonlinear function $F(r,\xi)$ is depicted in Fig. 3.2. The equilibrium state of the system r_0 can be found from an algebraic equation $F(r_0,\xi) = 0$. The equilibrium point can be estimated from a simple formula: $r_0 \approx (\varepsilon/3)^{1/3}$, which is valid for $(r_0, \xi) << 1$.

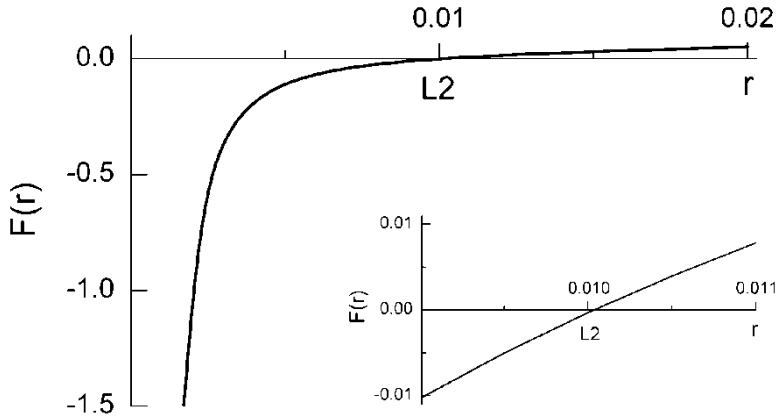

FIG. 3.2. Nonlinear function $F(r)$ from Eq. (3.2) with $\varepsilon = 3\times10^{-6}$ and $\xi = 0$.

Because of the unknown parameter ξ exact position of the equilibrium r_0 is not defined. We note that for further analysis it is not necessary to know exactly the nonlinear function $F(r,\xi)$. The only required knowledge is that its derivative with respect to r is positive, i.e. $F'(r_0,\xi) > 0$. The positive sign of the derivative is evident from Fig 3.2, independently on the vertical shift ξ. In this case the equilibrium is a saddle UEQ.

Purely conservative system. First of all we apply the UFC [Pyragas *et al*., 2002; 2004] trying to stabilize the saddle UEQ:

$$\begin{aligned} &\ddot{r} - \Omega^2 F(r,\xi) = K_1(u-r), \\ &\dot{u} = \Omega_1(u-r). \end{aligned} \tag{3.3}$$

Here, K_1 is the feedback coefficient and Ω_1 is the cut-off frequency of the unstable filter. It is evident that the equilibrium of the unstable filter u_0 is the same as that of the main system, i.e., $u_0 = r_0$. To check the stability of the equilibrium with the controller we linearize the equations around the r_0. If $|r-r_0| = |r_1| << 1, |u-u_0| = |u_1| << 1$, then $F(r,\xi) = F(r_0,\xi) + F'(r_0,\xi)r_1$ and

$$\begin{aligned} &\ddot{r}_1 - \Lambda^2 r_1 = K_1(u_1 - r_1), \\ &\dot{u} = \Omega_1(u_1 - r_1). \end{aligned} \tag{3.4}$$

The characteristic runaway time from L2, $\tau_L = \Lambda^{-1} = \Omega^{-1}/\sqrt{F'(r_0,\xi)} \approx Y_E/6\pi$, where Y_E is the orbital period of the Earth rotating around the Sun, i.e. the Earth year; thus, $\tau_L \approx 19$ days. After introducing dimensionless parameters $\tau_L\Lambda = \theta$, and $K_1/\Lambda^2 = k_1, \Omega_1/\Lambda = \omega_1$ the linearized equations read

$$\begin{aligned} &\ddot{r}_1 - r_1 = k_1(u_1 - r_1), \\ &\dot{u}_1 = \omega_1(u_1 - r_1). \end{aligned} \tag{3.5}$$

The corresponding characteristic equation is

$$\lambda^3 - \omega_1\lambda^2 + (k_1 - 1)\lambda + \omega_1 = 0. \tag{3.6}$$

There is a considerable drop of the largest $\mathrm{Re}\lambda$ with k_1; however, it remains positive indicating instability of the closed loop (Fig. 3.4a).

Although the SFC is not expected to stabilize saddle equilibrium, we consider it here for comparison:

$$\begin{aligned} \ddot{r} - \Omega F(r,\xi) &= K_2(v-r), \\ \dot{v} &= \Omega_2(r-v). \end{aligned} \tag{3.7}$$

Here, K_2 is the feedback coefficient and Ω_2 is the cut-off frequency of the stable filter. Similarly to the previous case the equilibrium state of the stable filter v_0 is the same as that of the main system, i.e., $v_0=r_0$. The linearized equations have the following form:

$$\begin{aligned} \ddot{r}_1 - \Lambda^2 r_1 &= K_2(v_1 - r_1), \\ \dot{v}_1 &= \Omega_1(r_1 - v_1). \end{aligned} \tag{3.8}$$

or

$$\begin{aligned} \ddot{r}_1 - r_1 &= k_2(v_1 - r_1), \\ \dot{v}_1 &= \omega_2(r_1 - v_1), \end{aligned} \tag{3.9}$$

where $k_2 = K^2/\Omega^2$ and $\omega_2 = \Omega_2 / \Lambda$. From the characteristic equation

$$\lambda^3 + \omega_2\lambda^2 + (k_2 - 1)\lambda - \omega_2 = 0 \tag{3.10}$$

one can make sure that the result for the SFC is practically the same (Fig. 3.4b) as for the UFC (Fig. 3.4a). The controller fails to stabilize the saddle.

However, when the UFC and the SFC are applied in parallel (UFC||SFC), as shown in Fig. 3.3 and presented by Eq. (3.11) the two control techniques working in parallel give excellent synergetic result.

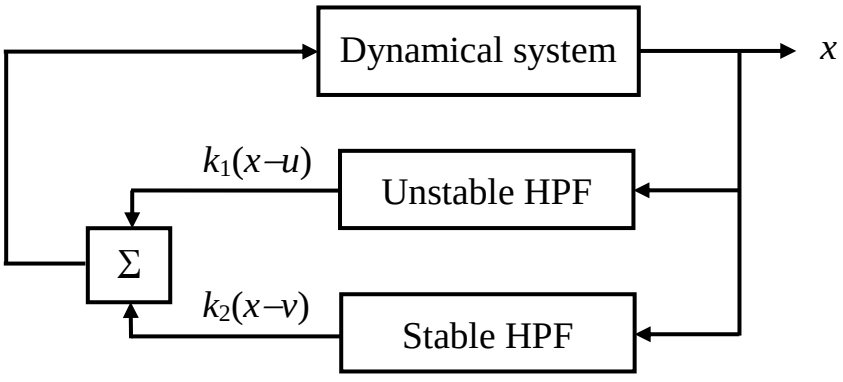

FIG. 3.3. Block diagram of controlling unknown equilibrium of a dynamical system by means of the UFC||SFC.

$$\begin{aligned} &\ddot{r} - \Omega^2 F(r,\xi) = K_1(u-r) + K_2(v-r), \\ &\dot{u} = \Omega_1(u-r), \\ &\dot{v} = \Omega_2(r-v). \end{aligned} \tag{3.11}$$

It is evidenced in Fig. 3.4c, obtained from the linearized equations (3.12) and the corresponding characteristic equation (3.13). Indeed, the largest eigenvalue crosses zero at a certain value of the feedback coefficient $k_1 \approx 1.8$ (Fig. 3.4c).

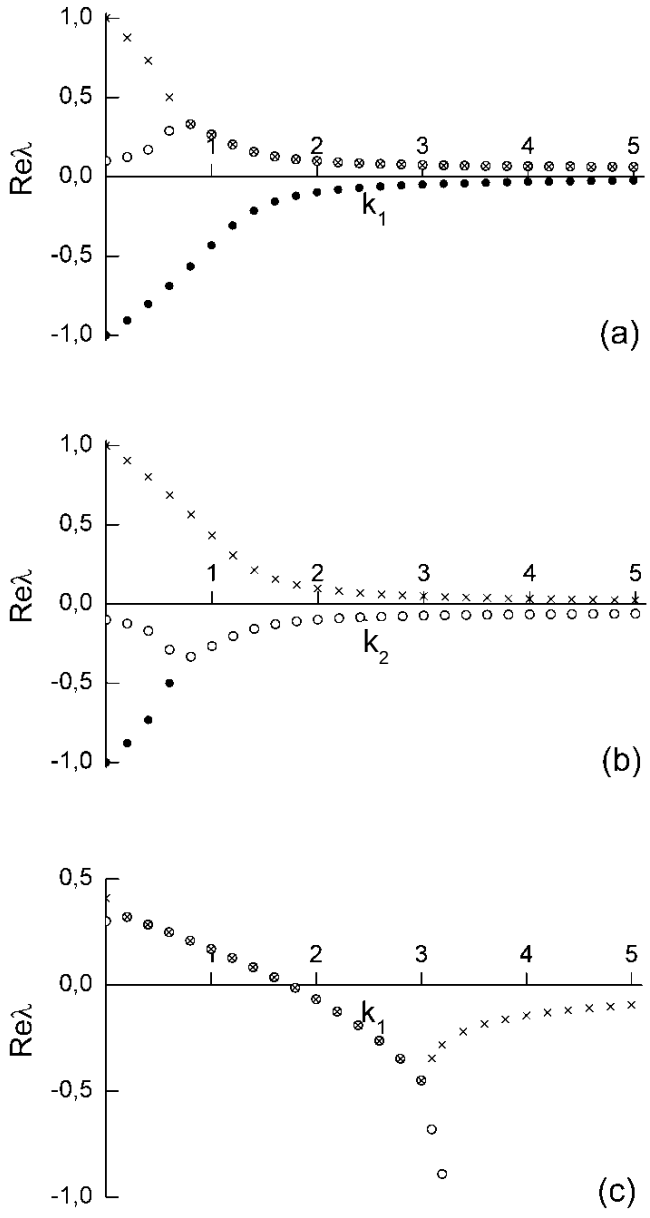

FIG. 3.4. Dependence of the real part of the eigenvalues Reλ on the control gains k_i. (a) UFC only with $\omega_1 = 0.1$. (b) SFC only with $\omega_2 = 0.1$. (c) UFC||SFC with $\omega_1 = 0.3$, $\omega_2 = 7$, and $k_2 = 15$.

The linearized equations read

$$\begin{aligned} &\dot{r}_1 - r_1 = k_1(u_1 - r_1) + k_2(v_1 - r_1), \\ &\dot{u}_1 = \omega_1(u_1 - r_1), \\ &\dot{v}_1 = \omega_2(r_1 - v_1). \end{aligned} \tag{3.12}$$

The corresponding characteristic equation is

$$\lambda^4 + (\omega_2 - \omega_1)\lambda^3 + (k_1 + k_2 - 1 - \omega_1\omega_2)\lambda^2 + [(k_1 - 1)\omega_2 - (k_2 - 1)\omega_1)]\lambda + \omega_1\omega_2 = 0. \tag{3.13}$$

The stability can be also checked using the Hurwitz criterion. The Hurwitz matrix of Eq. (3.13) is

$$H_4 = \begin{pmatrix} a_1 & a_3 & 0 & 0 \\ 1 & a_2 & a_4 & 0 \\ 0 & a_1 & a_3 & 0 \\ 0 & 1 & a_2 & a_4 \end{pmatrix}.$$

In the above H_4 matrix the elements are the following:

$$\begin{aligned} a_1 &= \omega_2 - \omega_1, \\ a_2 &= k_1 + k_2 - 1 - \omega_1\omega_2, \\ a_3 &= (k_1 - 1)\omega_2 - (k_2 - 1)\omega_1, \\ a_4 &= \omega_1\omega_2. \end{aligned}$$

The eigenvalues Reλ of Eq. (3.13) are all negative if the diagonal minors of the H_4 matrix are all positive:

$$\begin{aligned} &\Delta_1 = a_1 = \omega_2 - \omega_1 > 0, \\ &\Delta_2 = a_1a_2 - a_3 = \omega_2k_2 - \omega_1k_1 - (\omega_2 - \omega_1)\omega_1\omega_2 > 0, \\ &\Delta_3 = a_1a_2a_3 - a_1^2a_4 - a_3^2 = a_3\Delta_2 - a_1^2a_4 > 0, \\ &\Delta_4 = a_4\Delta_3 > 0. \end{aligned} \tag{3.15}$$

It follows from Δ_1 that the necessary condition is

$$\omega_2 > \omega_1, \tag{3.16}$$

i.e., the cut-off frequency of the stable filter should be higher than that of the unstable filter. In general, the explicit form of Δ_2 is rather cumbersome. Assuming for simplicity $\omega_2 >> \omega_1$, we can roughly estimate the gain k_2 from Δ_2:

$$k_2 > \omega_1\omega_2, \tag{3.17}$$

and the gain k_1 from Δ_3:

$$k_1 > 1 + k_2 \frac{\omega_1}{\omega_2} + \frac{\omega_1 \omega_2}{k_2 - \omega_1 \omega_2}. \tag{3.18}$$

Finally, in Eq. (3.15) $\Delta_4 > 0$ if $\Delta_3 > 0$ since $a_4 > 0$. Using the parameter values as in Fig. 3.4, $\omega_1 = 0.3, \omega_2 = 7$ ($\omega_2 >> \omega_1$), $k_2 = 15$ ($k_2 > \omega_1 \omega_2 = 2.1$), we find from inequality (3.18) that $k_1 > 1.8$, which is in a good agreement with the threshold value of k_1 from the numerical results presented in Fig. 3.4c.

Weakly dissipative system. One can think that the UFC||SFC method works for the ideal conservative systems only and that even small dissipation can destroy the algorithm. Therefore, we introduce in Eq. (3.11) finite damping term $B\dot{r}$:

$$\begin{aligned} &\ddot{r} - B\dot{r} - \Omega^2 F(r, \xi) = K_1(u - r) + K_2(v - r), \\ &\dot{u} = \Omega_1(u - r), \\ &\dot{v} = \Omega_2(r - v). \end{aligned} \tag{3.19}$$

The linearized equations read

$$\begin{aligned} &\ddot{r}_1 - b\dot{r}_1 - r_1 = k_1(u_1 - r_1) + k_2(v_1 - r_1), \\ &\dot{u}_1 = \omega_1(u_1 - r_1), \\ &\dot{v}_1 = \omega_2(r_1 - v_1). \end{aligned} \tag{3.20}$$

Here, $b = B/\Lambda$. Then the corresponding characteristic equation is

$$\begin{aligned} &\lambda^4 + (\omega_2 - \omega_1 + b)\lambda^3 + [k_1 + k_2 - 1 - \omega_1 \omega_2 + b(\omega_2 - \omega_1)]\lambda^2 \\ &+ [(k_1 - 1)\omega_2 - (k_2 - 1)\omega_1 - b\omega_2 \omega_1]\lambda + \omega_1 \omega_2 = 0 \end{aligned}, \tag{3.21}$$

which for $b = 0$ coincides with Eq. (3.13), as expected. Evidently, the Hurwitz matrix for Eq. (3.21) has the same form as H_4 for the conservative system:

$$H_4^* = \begin{pmatrix} c_1 & c_3 & 0 & 0 \\ 1 & c_2 & c_4 & 0 \\ 0 & c_1 & c_3 & 0 \\ 0 & 1 & c_2 & c_4 \end{pmatrix},$$

with the modified elements c_i:

$$\begin{aligned} &c_1 = \omega_2 - \omega_1 + b, \\ &c_2 = k_1 + k_2 - 1 - \omega_1 \omega_2 + b(\omega_2 - \omega_1), \\ &c_3 = (k_1 - 1)\omega_2 - (k_2 - 1)\omega_1 - b\omega_1 \omega_2, \\ &c_4 = \omega_1 \omega_2. \end{aligned} \tag{3.22}$$

In the limit case of $b = 0, c_i = a_i$. The diagonal minors of the H_4^* matrix are the following:

$$\begin{aligned}
&\Delta_1^* = c_1 = \omega_2 - \omega_1 > 0,\\
&\Delta_2^* = c_1c_2 - c_3 = \omega_2 k_2 - \omega_1 k_1 - (\omega_2 - \omega_1)\omega_1\omega_2 + b(\omega_2 - \omega_1)^2\\
&+ b^2(\omega_2 - \omega_1) + b(k_1 + k_2 - 1) > 0,\\
&\Delta_3^* = c_1c_2c_3 - c_1^2c_4 - c_3^2 = c_3\Delta_4^* - c_1^2c_4 > 0,\\
&\Delta_4^* = c_4\Delta_3^* > 0.
\end{aligned} \tag{3.23}$$

The first inequality in (3.23) is satisfied if

$$\omega_2 > \omega_1 - b \approx \omega_1. \tag{3.24}$$

It means that the nonzero value of *b* is not a problem to set the first minor $\Delta_1^* > 0$. For $\omega_2 >> \omega_1$ and *b* <<1, the second inequality in (3.23) is satisfied if

$$k_2 > (\omega_1 - b)\omega_2 \approx \omega_1\omega_2. \tag{3.25}$$

So, there is no problem to set the second minor $\Delta_2^* > 0$ for small *b*. Meanwhile, for stronger dissipation there is no need to use the UFC||SFC since the Pyragas' method [Pyragas *et al*., 2002; 2004] works well. The gain k_1 can be estimated from the third inequality in (3.23):

$$k_1 > 1 + k_2\frac{\omega_1}{\omega_2} + \frac{\omega_1\omega_2 + 2b\omega_1}{k_2 - \omega_1\omega_2 + b\omega_2}. \tag{3.26}$$

The threshold value of k_1 is practically insensitive to the friction coefficient up to *b* = 0.2 and is about 1.8 for the given parameters $\omega_1 = 0.3, \omega_2 = 7,$ and $k_1 = 15$. Thus, the conclusion of this subsection is that weak dissipation does not destroy the control algorithm. Moreover, the required control parameters are nearly the same like in the conservative system.

Analogue simulation. Analogue circuit, imitating dynamics of a system with a saddle UEQ is shown in *Appendix* 3, an electronic controller implementing the UFC||SFC is referred in *Appendix* 5. The experimental nonlinear function *F*(*r*) is presented in Fig. 3.5 and is very similar to that given in Fig. 3.2. The analogue simulation results, photos taken from the screen of a multichannel (Ch1…Ch4) oscilloscope are presented in Fig. 3.6.

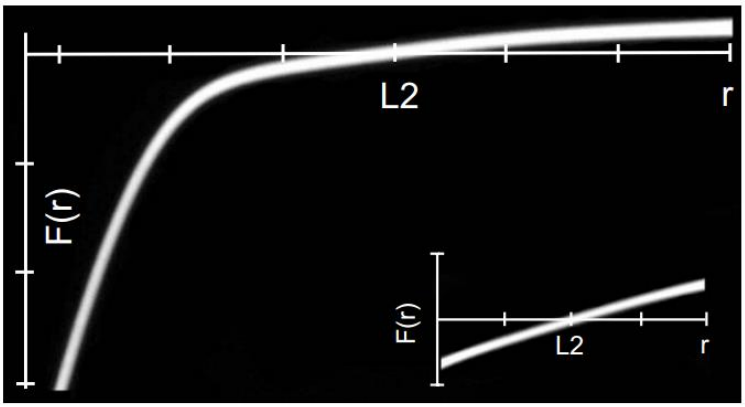

FIG. 3.5. Nonlinear function $F(r)$ from the analogue circuit. Horizontal scale: 0.1 V/div.; vertical scale: 1 V/div (in the main photo). Horizontal scale: 50 mV/div.; vertical scale: 200 mV/div. (in the insert).

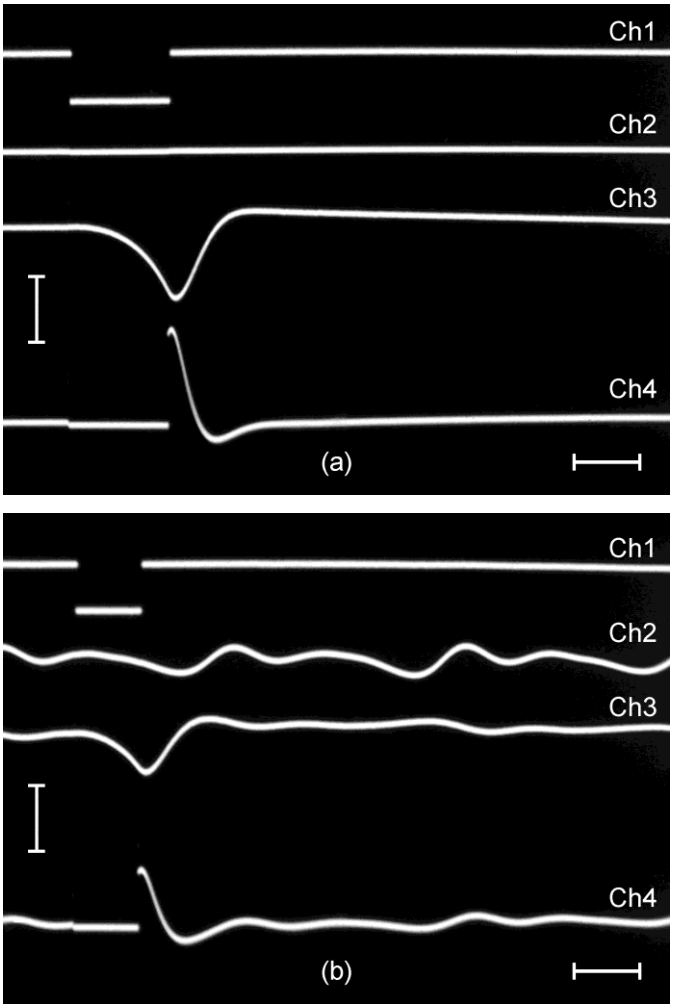

FIG. 3.6. Stabilization of the saddle UEQ. Ch1: control status (high level control is on; low level control is off), Ch2: perturbation, Ch3: voltage across the capacitor *C*, Ch4: feedback signal. (a) Control is off for 3 ms, no external perturbation. (b) Control is off for 2 ms, chaotic perturbation.
Horizontal scale: 2 ms, vertical scale: 100 mV (Ch1…Ch3), 500 mV (Ch4).

3.2. Stabilizing saddles under influence of inertia of control [18]

Mathematical model and its analysis. Let us consider a dynamical system given by

$$\ddot{x} + b\dot{x} + F(x) = 0 \tag{3.27}$$

or in a more convenient form

$$\begin{aligned} \dot{x} &= y, \\ \dot{y} &= -F(x) - by. \end{aligned} \tag{3.28}$$

Here b is the damping coefficient, $F(x)$ is a nonlinear function (in general unknown). We assume that the system has at least one equilibrium point $(x_0, y_0) = (x_0, 0)$. Here x_0 is found from an algebraic equation $F(x_0) = 0$. If

$$F'(x)\big|_{x0} < 0,$$

then the equilibrium point $(x_0,0)$ is a saddle. Let us apply the UFC, taking into account possible inertia in the feedback loop:

$$\begin{aligned} \dot{x} &= y, \\ \dot{y} &= -F(x) - by + z, \\ \dot{u} &= \omega_1(u - x), \\ \tau\dot{z} &= k(u - x) - z. \end{aligned} \tag{3.29}$$

Here k is the control gain, ω_1 is the cut-off frequency of the unstable filter. The fourth equation in Eq. (3.29) represents inertia with normalized time constant τ. To check the stability properties we linearize Eq. (3.29) around the equilibrium point:

$$\begin{aligned} \dot{x} &= y, \\ \dot{y} &= -F'(x)\big|_{x0}\, x - by + z, \\ \dot{u} &= \omega_1(-x + u), \\ \tau\dot{z} &= k(-x + u) - z \end{aligned} \tag{3.30}$$

and analyse its characteristic equation. If the inertia is neglected ($\tau = 0$) the characteristic equation reads:

$$\lambda^3 + (b - \omega_1)\lambda^2 + (k - 1 - b\omega_1)\lambda + \omega_1 = 0. \tag{3.31}$$

In (3.30) and further we assume for simplicity $F'(x)\big|_{x0} = -1$ to avoid cumbersome coefficients. For the Duffing–Holmes oscillator the nonlinear

function $F(x) = -x + x^3$, the central equilibrium point $x_0 = 0$; the $F'(x)\big|_{x0} = -1$ is an exact value.

For $\tau > 0$ the characteristic equation becomes more complicated:

$$\begin{aligned}&\lambda^4 + (b + 1/\tau - \omega_1)\lambda^3 + (b/\tau - 1 - b\omega_1 - \omega_1/\tau)\lambda^2 \\ &+ (k/\tau - 1/\tau - \omega_1 - b\omega_1/\tau)\lambda + \omega_1/\tau = 0.\end{aligned} \tag{3.32}$$

In order to find the threshold k_{th} and the optimal k_{opt} control gains we have solved Eq. (3.31) and Eq. (3.32) numerically (Fig. 3.7). General view of (a) and (b) plots looks very alike, however detailed inserts reveal quite different features. In plot (a) for $k > k_{th} \approx 1.1$ all the Reλ are negative indicating stabilization of the saddle point. The optimal feedback gain providing the fastest control is $k_{opt} \approx 1.3$. However, the convergence is very slow, given by Re$\lambda \approx -0.003$. While in plot (b) the largest Reλ is positive. Thus, even small inertia of only $\tau = 0.007 << 1$ destroys the stability.

Now we apply the UFC||SFC technique:

$$\begin{aligned}\dot{x} &= y, \\ \dot{y} &= -F(x) - by + z, \\ \dot{u} &= \omega_1(u - x), \\ \dot{v} &= \omega_2(x - v), \\ \tau\dot{z} &= k_1(u - x) - k_2(v - x) - z.\end{aligned} \tag{3.33}$$

Here v is the dynamical variable of the stable filter, ω_2 is its cut-off frequency. Linearization about the initially UEQ point yields:

$$\begin{aligned}\dot{x} &= y, \\ \dot{y} &= -F'(x_0)x - by + z, \\ \dot{u} &= \omega_1(-x + u), \\ \dot{v} &= \omega_2(x + u), \\ \tau\dot{z} &= -(k_1 + k_2)x + k_1u + k_2v - z.\end{aligned} \tag{3.34}$$

The corresponding characteristic equation with the same assumption of $F'(x_0) = -1$ for $\tau = 0$ reads

$$\begin{aligned}&\lambda^4 + (b + \Delta\omega)\lambda^3 + (b\Delta\omega - \omega_1\omega_2 + k - 1)\lambda - (-\Delta\omega - b\omega_1\omega_2 + \omega_2k_1 - \omega_1k_2) = 0, \\ &\Delta\omega = \omega_2 - \omega_1,\ k = k_1 + k.\end{aligned} \tag{3.35}$$

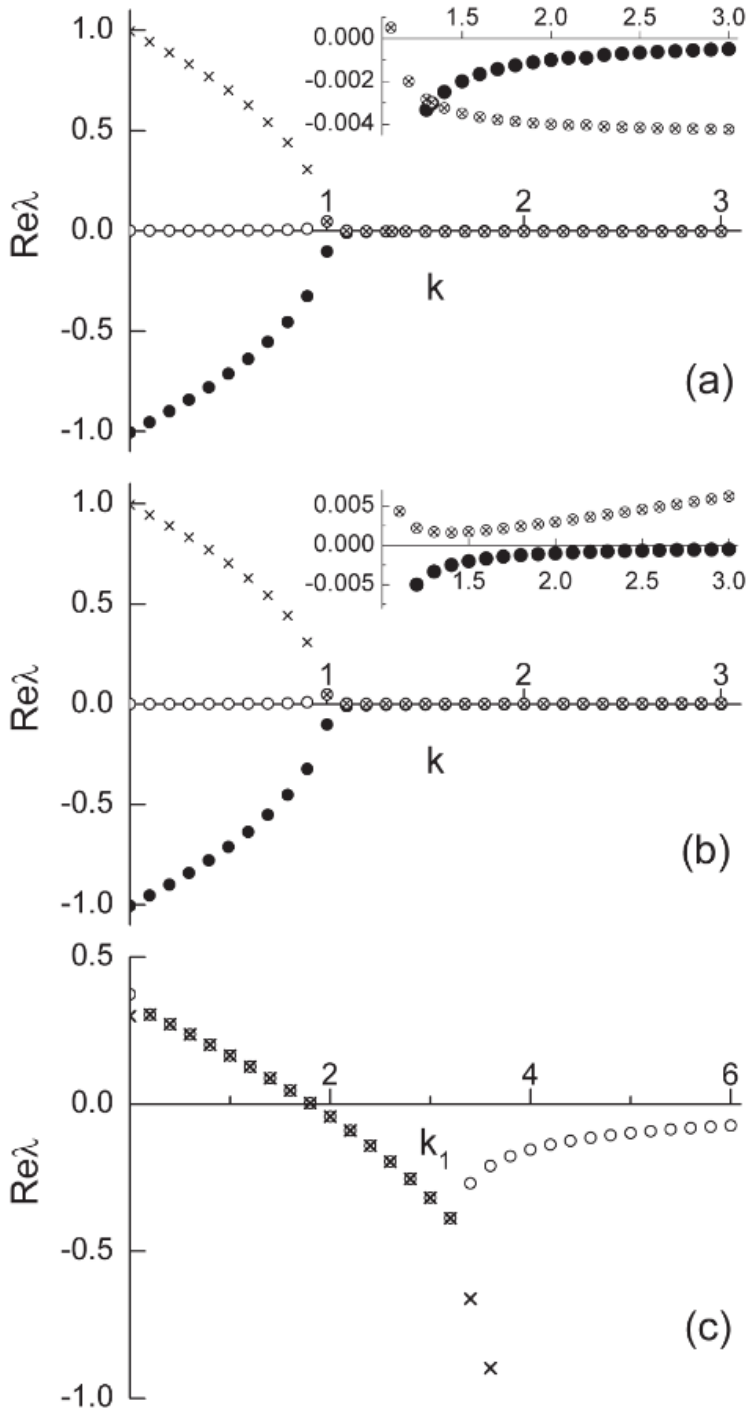

FIG. 3.7. Real parts of the largest eigenvalues versus the control gain k_1 for b = 0.01. (a) from Eq. (3.31) with $\omega_1 = 0.001$, (b) from Eq. (3.32) with $\omega_1 = 0.001$, $\tau = 0.007$, (c) from Eq. (3.36) with $\omega_1 = 0.3$, $\tau = 0.007$, $\omega_2 = 7$, $k_2 = 17$. The set of the control parameters, ω_1, ω_2, and k_2 is somewhat arbitrary and empirical.

For $\tau > 0$ the characteristic equation becomes the 5[th]-power algebraic equation:

$$\begin{aligned}&\lambda^5 + (1/\tau + b - \Delta\omega)\lambda^4 \\ &+ [b/\tau + 1/\tau + b)\Delta\omega - \omega_1\omega_2 - 1]\lambda^3 \\ &+ [b/\tau - 1)\Delta\omega - (1/\tau + b)\omega_1\omega_2 - (k-1)/\tau]\lambda^2 \\ &+ [1 - b/\tau)\omega_1\omega_2 - (\omega_2 k_1 - \omega_1 k_2 - \Delta\omega)/\tau]\lambda \\ &+ \omega_1\omega_2/\tau = 0.\end{aligned} \tag{3.36}$$

Numerical solution of Eq. (3.36) is presented in Fig. 3.7c. In contrast to the plots (a) and (b), the plot (c) clearly exhibits deep negative Reλ above threshold gain $k_{th} \approx 1.8$. The optimal gain value $k_{opt} \approx 3.2$ provides Re$\lambda \approx -0.4$. We intentionally do not present here the result for zero inertia from Eq. (3.35), since the results coincide with the plot (c) within 0.5%.

Experimental results. The UFC (Fig. 3.8a) fails to stabilize the UEQ. Instead, it gives rise to periodic oscillations as predicted by Re$\lambda > 0$. Whereas the UFC||SFC (Fig. 3.8b) demonstrates very good performance.

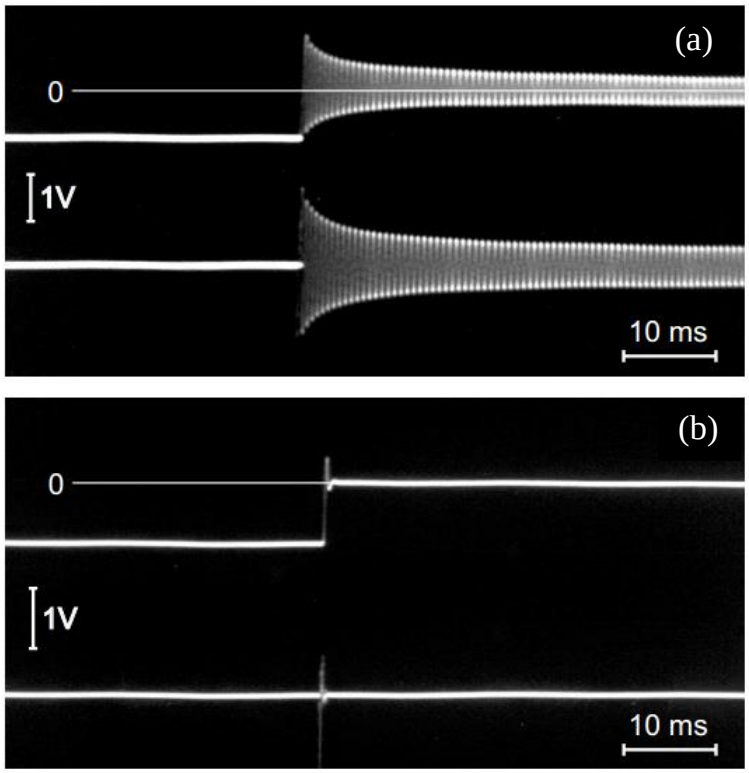

FIG. 3.8. Experimental control of the Duffing–Holmes oscillator. (a) UFC only; (b) UFC||SFC. Upper traces in both photos is the output of the oscillator, lower traces are the control signals.

We note, that double filter technique for stabilizing equilibrium states has been described in [Ahlborn *et al*., 2006], where the both filters are the 2nd order Wien-bridge circuits. Thus, the overall controller is a 4th order system. Moreover, the filters in [Ahlborn *et al*., 2006], are stable ones, therefore are not applicable to stabilize saddles.

3.3. Stabilizing saddles by means of combined filter control (CFC) [8]

Examples. We consider saddle equilibrium states of five different physical systems. The 1st example is a mechanical pendulum given by

$$\ddot{\varphi} + \beta\dot{\varphi} + \sin\varphi = 0. \tag{3.37}$$

Here, φ is the angle between the downward vertical and the rod, and β is the damping parameter. Pendulum has two equilibrium states $(\varphi_0, \dot{\varphi}_0)$: a stable spiral or a node (depending on β) at (0,0) and a saddle at (π,0).

The 2nd example is the Duffing–Holmes damped oscillator [Ott, 1993]:

$$\ddot{x} + b\dot{x} + x^3 - x = 0. \tag{3.38}$$

Here, b is the damping coefficient. The oscillator has three equilibrium states $(x_0, \dot{x})$, two symmetrical stable spirals or nodes (depending on b) at (±1,0) and a saddle at (0,0).

The 3rd example is a conservative system, namely a body at the Lagrange point L2 of the Sun–Earth system, considered in details in Section 3.1:

$$\ddot{r} - \Omega^2 F(r,\xi) = 0, \quad F(r,\xi) = 1 + r - \frac{1}{(1+r)^2} - \frac{\varepsilon}{r^2} + \xi. \tag{3.39}$$

The system has a single equilibrium $[r_0, \dot{r}] = [(\varepsilon/3)^{1/3}, 0]$, which is a saddle.

The 4th example is the chaotic Lorenz system [Lorenz, 1963]

$$\begin{aligned} \dot{x} &= -\sigma x + \sigma y, \\ \dot{y} &= -xz + rx - y, \\ \dot{z} &= xy - bz. \end{aligned} \tag{3.40}$$

Here σ, r, and b are fixed positive parameters. The Lorenz system at $r > 1$ has three equilibrium states, a saddle at the origin (0,0,0) and two stable spirals

$(\pm\sqrt{b(r-1)}, \pm\sqrt{b(r-1)}, r-1)$. For $r > r_{th} = \sigma(\sigma+b+3)/(\sigma-b-1)$, the spirals become unstable giving rise to chaotic oscillations. For common parameter values $\sigma = 10$ and $b = 8/3$ the $r_{\text{th}} \approx 24.7$.

Finally, the 5th example is the Lindberg oscillator [Lindberg *et al*., 2009; Tamaševičius *et al*., 2009a]:

$$\begin{aligned} &\ddot{x} - b\dot{x} + x^3 - x + cz = 0, \\ &\dot{z} = \omega_c(\dot{x} - z). \end{aligned} \tag{3.41}$$

In contrast to the Duffing–Holmes damped oscillator, the Lindberg oscillator has a negative damping term $-b\dot{x}$, which makes it oscillating. In Eq. (3.41), the $c \approx 1$ and $\omega_c < 1$ [Lindberg *et al*., 2009]. The Lindberg oscillator has three equilibrium states $(x_0, \dot{x}_0, z_0)$: two symmetrical unstable spirals or nodes (depending on b) (±1,0,0) and a saddle at the origin (0,0,0).

Common form. When linearized around the saddle equilibrium states, all the above systems have a simple common form:

$$\begin{aligned} &\dot{Q} = P, \\ &\dot{P} = aQ - bP, \end{aligned} \tag{3.42}$$

with the generalized variables Q, P and parameters a, b presented in Table 1.

TABLE 1. Variables Q, P and parameters a, b of Eq. (3.42).

System	***Q***	***P***	***a***	***b***
Pendulum	φ	$\dot{\varphi}$	1	$\beta > 0$
Duffing–Holmes	x	$\dot{x}$	1	$b > 0$
Lagrange L2	r	$\dot{r}$	$\Omega^2 F'(r)\big\|_{r0} > 0$	0
Lorenz	x	$-x + y$	$(r-1)/\sigma > 0$	$(\sigma+1)/\sigma$
Lindberg	x	$\dot{x}$	$1 - c\omega_c > 0$	$-b < 0$

Though the Lorenz system is a set of three equations, when linearized around the saddle (0,0,0) equations become partially decoupled:

$$\begin{aligned} \dot{x} &= -\sigma x + \sigma y, \\ \dot{y} &= rx - y, \\ \dot{z} &= -bz, \end{aligned} \tag{3.43}$$

i.e. the equation for z contains neither x nor y. Consequently, dynamics of the Lorenz system near the saddle point can be described by the 2nd order linear system. Note, that to obtain the common form of Eq. (3.42) the following linear transformations $\sigma t \to t$ and $P = (-x + y)$ have been applied to the linearized Lorenz equations. Therefore, the new variable P and parameters a, b in Table 1 for the Lorenz system are combinations of the original variables x, y and r, σ , respectively.

Somewhat different situation is with the Lindberg oscillator at the origin (0,0,0). In this case, the equation for z remains coupled via the $\dot{x}$ variable. However, because of $\omega_c < 1$ dynamics of the z variable is relatively slow and the second equation in Eq. (3.41) can be reduced to $\dot{z} \approx \omega_c \dot{x}$ and $z \approx \omega_c x$. Then the dynamics of the Lindberg oscillator near the saddle point can be approximated by Eq. (3.42) with an effective parameter $a \approx 1 - c\omega_c$.

Unstable filter control (UFC). In this subsection, we demonstrate the limitations of the UFC used to stabilize saddle equilibrium. Eq. (3.42) with the control term $k(u-Q)$ and the additional equation of the unstable filter for variable u read

$$\begin{aligned} \dot{Q} &= P, \\ \dot{P} &= aQ - bP + k(u - Q), \\ \dot{u} &= \omega(u - Q). \end{aligned} \tag{3.44}$$

The corresponding characteristic equation is

$$\lambda^3 + (b - \omega)\lambda^2 + (k - a - \omega b)\lambda + a\omega = 0. \tag{3.45}$$

The overall system is stable if the real parts of all three eigenvalues of Eq. (3.45) are negative. The necessary and sufficient conditions can be found from the Hurwitz matrix:

$$H_3 = \begin{pmatrix} b-\omega & \omega & 0 \\ 1 & k-a-b\omega & 0 \\ 0 & b-\omega & a\omega \end{pmatrix}.$$

The eigenvalues $\mathrm{Re}\lambda_{1,2,3}$ are all negative if the diagonal minors of the H_3 matrix are all positive:

$$\Delta_1 = b-\omega > 0,$$
$$\Delta_2 = (b-\omega)(k-a-b\omega) - \omega > 0,$$
$$\Delta_3 = a\omega\Delta_2 > 0.$$

These inequalities are satisfied if

$$\omega < b, \quad k > k_{th} = a + \frac{\omega}{b-\omega} + b\omega. \tag{3.46}$$

For example, at $a = 1$, $b = 0.1$, and $\omega = 0.02$ the $k_{\mathrm{th}} = 1.252$. On one hand, according to the first inequality, the ω could be only slightly less than b. On the other hand, ω should not be too close to b, because small value of the denominator $(b-\omega)$ in the second inequality would heavily increase the stabilization threshold k_{th}. Numerical solution of the characteristic equation is plotted in Fig. 3.9.

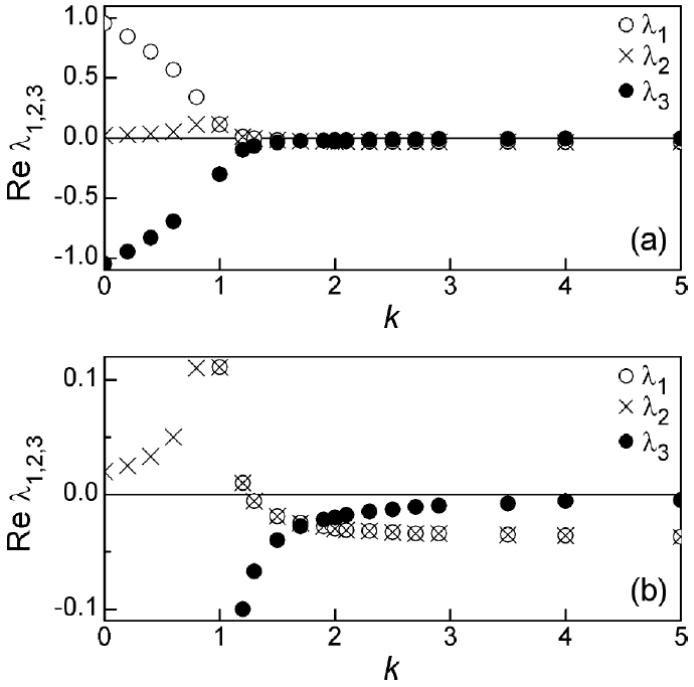

FIG. 3.9. Real parts of the eigenvalues *vs*. the control gain k from Eq. (3.45) with $a = 1$, $b = 0.1$, $\omega = 0.02$. (a) Full scale. (b) Vertically zoomed in scale.

The largest eigenvalues $\mathrm{Re}\lambda_1 = \mathrm{Re}\lambda_2$ cross zero axis at $k \approx 1.25$ in a good agreement with the analytical result. We note very small absolute values of the largest $\mathrm{Re}\lambda_{max}$ at $k > k_{th}$. However, even at $k = k_{opt} = 1.7$ the $|\mathrm{Re}\lambda_{max}| = 0.025$. Such a low value, related to small parameters b and ω, results in slow convergence (long transients) to the equilibrium. This is a serious shortcoming of the UFC, especially if applied to weakly damped ($b < 0.1$).

Now we present numerical results (Fig. 3.10) of the control dynamics under the influence of an *a priori* unknown external constant force p, which changes the position of the saddle equilibrium state. To be specific, we consider the DH nonlinear system, Eq. (3.38) given in the following form:

$$\begin{aligned} \dot{x} &= y, \\ \dot{y} &= x - x^3 - by + k(u - x) + p, \\ \dot{u} &= \omega(u - x). \end{aligned} \tag{3.47}$$

At $t < 50$ the saddle equilibrium state (0, 0) is stabilized. The external force $p = -0.3$ applied at $t \geq 50$ changes the coordinates of the equilibrium state from (0, 0) to (0.34, 0). After some transient process, the controller stabilizes the new equilibrium state. The transients are sufficiently short for large b (Fig. 3.10a). However, for smaller b they become extremely long (Fig. 3.10c). Moreover, before settling on the new equilibrium state (+0.34), the x variable, even for heavy damping ($b = 1$), exhibits undesirably deep negative drop (-0.3), for weak damping ($b = 0.1$) the drop is even deeper (-0.5).

Combined filter control (CFC). We suggest the following modification of the UFC to improve its performance:

$$\begin{aligned} \dot{Q} &= P, \\ \dot{P} &= aQ - bP + k_1(u - Q) + k_2(v - Q), \\ \dot{u} &= \omega_1[(u - Q) + k_2(v - Q)], \\ \dot{v} &= \omega_2(Q - v). \end{aligned} \tag{3.48}$$

Here, the unstable filter (variable u) is combined with a stable one (variable v), whereas the feedback force in Eq. (3.48) consists of two terms, $k_1(u-Q)$ and $k_2(v-Q)$. The corresponding block diagram of the CFC is presented in Fig. 3.11.

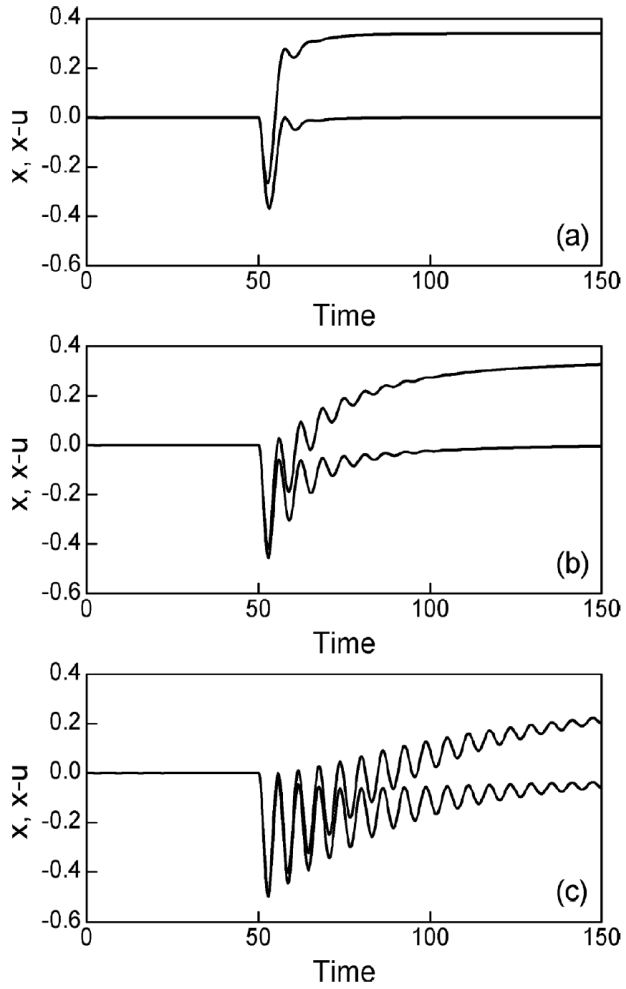

FIG. 3.10. Controlling the saddle in the DH system from Eq. (3.47). $k = 2$. (a) $b = 1$, $\omega = 0.2$. (b) $b = 0.3$, $\omega = 0.06$. (c) $b = 0.1$, $\omega = 0.02$. Upper traces, variable x; lower traces, inverted control term $-k(u-x)/2 = (x-u)$.

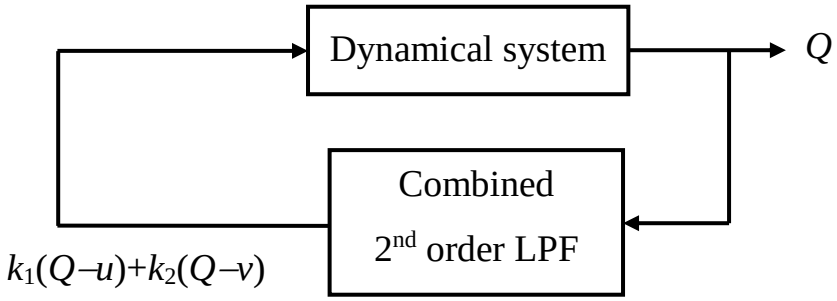

FIG. 3.11. Block diagram of controlling unknown equilibrium of a dynamical system by means of the CFC.

The characteristic equation is

$$\lambda^4 + (\omega_2 - \omega_1 + b)\lambda^3 + [k_1 + k_2 - a - \omega_1\omega_2 + b(\omega_2 - \omega_1)]\lambda^2 + [(k_1 - a)\omega_2 - (k_2 - a)\omega_1 - b\omega_1\omega_2 + k_1k_2\omega_1]\lambda + a\omega_1\omega_2 = 0. \quad (3.49)$$

The Hurwitz matrix is

$$H_4 = \begin{pmatrix} a_1 & a_3 & 0 & 0 \\ 1 & a_2 & a_4 & 0 \\ 0 & a_1 & a_3 & 0 \\ 0 & 1 & a_2 & a_4 \end{pmatrix}, \tag{3.50}$$

$$\begin{aligned} a_1 &= \omega_2 - \omega_1 + b, \\ a_2 &= k_1 + k_2 - a - \omega_1\omega_2 + b(\omega_2 - \omega_1), \\ a_3 &= (k_1 - a)\omega_2 - (k_2 - a)\omega_1 - b\omega_1\omega_2 + k_1k_2\omega_1, \\ a_4 &= a\omega_1\omega_2. \end{aligned}$$

The diagonal minors of the H_4 matrix are the following:

$$\begin{aligned} &\Delta_1 = a_1 = \omega_2 - \omega_1 + b > 0, \\ &\Delta_2 = a_1a_2 - a_3 = \omega_2k_2 - \omega_1k_1 - (\omega_2 - \omega_1)\omega_1\omega_2 + b(\omega_2 - \omega_1)^2 \\ &+ b^2(\omega_2 - \omega_1) + b(k_1 + k_2 - a) - k_1k_2\omega_1 > 0, \\ &\Delta_3 = a_3\Delta_2 - a_1^2a_4 > 0, \quad \Delta_4 = a_4\Delta_3 > 0. \end{aligned} \tag{3.51}$$

The first inequality in (3.51) is satisfied if

$$\omega_2 > \omega_1 - b\,. \tag{3.52}$$

For small b, inequality Eq. (3.52) reads $\omega_2 > \omega_1$. It means that, in contrast to the simple UFC, the stability criterion of the CFC does not depend on the system parameters, but can be fully satisfied by the controller parameters.

For $\omega_2 >> \omega_1$ and $0 < b << 1$, the threshold gain k_{2th} can be roughly estimated from the second inequality in (3.51):

$$k_{2th} \approx \frac{\omega_1\omega_2^2}{\omega_2 - k_1\omega_1}. \tag{3.53}$$

For example, at $k_1 = 2$, $\omega_1 = 1$, and $\omega_2 = 5$ the $k_{2\text{th}} \approx 8.3$. In (3.51), $\Delta_4 > 0$, if $\Delta_3 > 0$, since $a_4 > 0$. However, analysis of the third diagonal minor Δ_3 is very complicated. Therefore, we solve Eq. (3.49) numerically. Results are presented in Fig. 3.12. Note deeply negative values of Reλ.

Similarly to the previous subsection, describing the UFC, here we consider the CFC, using the example of the DH system with the external perturbation p:

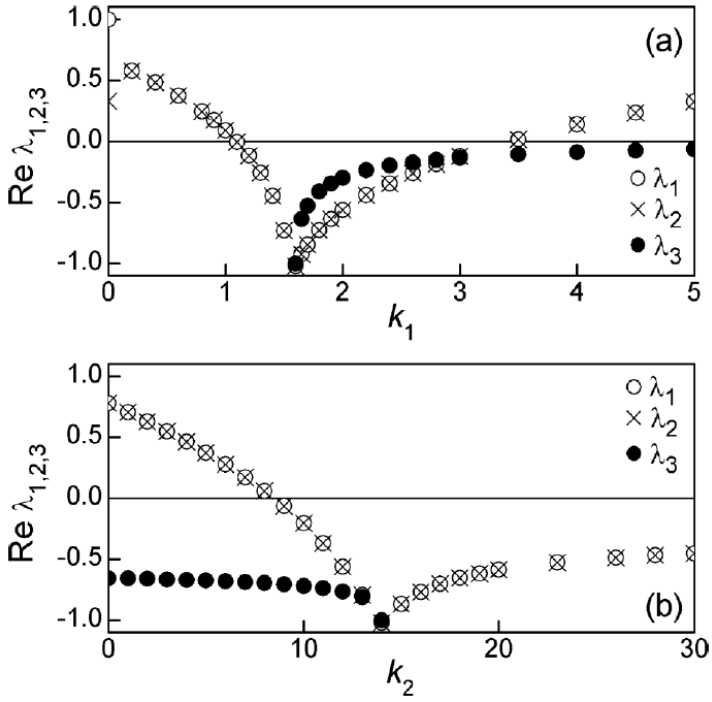

FIG. 3.12. Real parts of the eigenvalues *vs*. the control gains k_1 and k_2 from Eq. (3.49) for the CFC. $a = 1$, $b = 0.1$, $\omega_1 = 1$, $\omega_2 = 5$. (a) $k_2 = 14$. (b) $k_1 = 1.6$. The eigenvalues $\mathrm{Re}\lambda_4 < -1$ are not plotted.

$$\begin{aligned} \dot{x} &= y, \\ \dot{y} &= x - x^3 - by + k_1(u - x) + k_2(v - x) + p, \\ \dot{u} &= \omega_1[(u - x) + k_2(v - x)], \\ \dot{v} &= \omega_2(x - v). \end{aligned} \tag{3.54}$$

The numerical results are shown in Fig. 3.13. The external perturbation $p = -0.3$ (the same as in Fig. 3.10) is applied at $t \geq 50$. There are two main differences of the CFC in comparison with the simple UFC (Fig. 3.10). Firstly, the transients in the case of the CFC are essentially shorter. Secondly, the negative drop of the x variable is only -0.04, which is more than 10 times smaller than in the case of the simple UFC. In addition, the CFC is capable of stabilizing saddle equilibrium states in conservative systems ($b = 0$) and active oscillators with negative damping ($b < 0$).

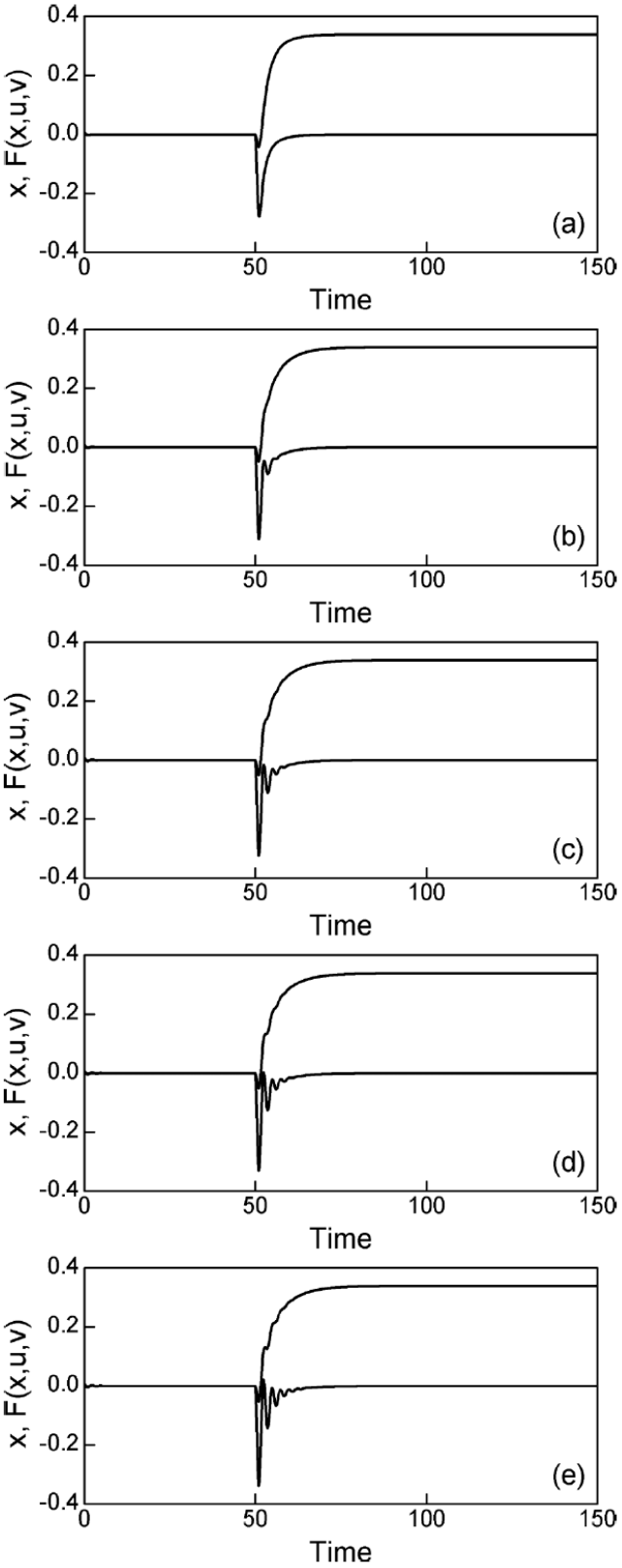

FIG. 3.13. Controlling the saddle in the DH system from Eq. (3.48). $k_1 = 2$, $k_2 = 14$, $\omega_1 = 1$, $\omega_2 = 5$. (a) $b = 1$. (b) $b = 0.3$. (c) $b = 0.1$. (d) $b = 0$. (e) $b = -0.1$. Upper traces: variable x; lower traces: inverted control term $F(x,u,v) = -[k_1(u-x) + k_2(v-x)]/2$.

Experimental results. Circuit diagram of the DH oscillator is shown in *Appendix* 1. Experimental results, presented in Fig. 3.14 and Fig. 3.15 coincide very well with the numerical simulations shown in Fig. 3.10 and Fig. 3.13, respectively.

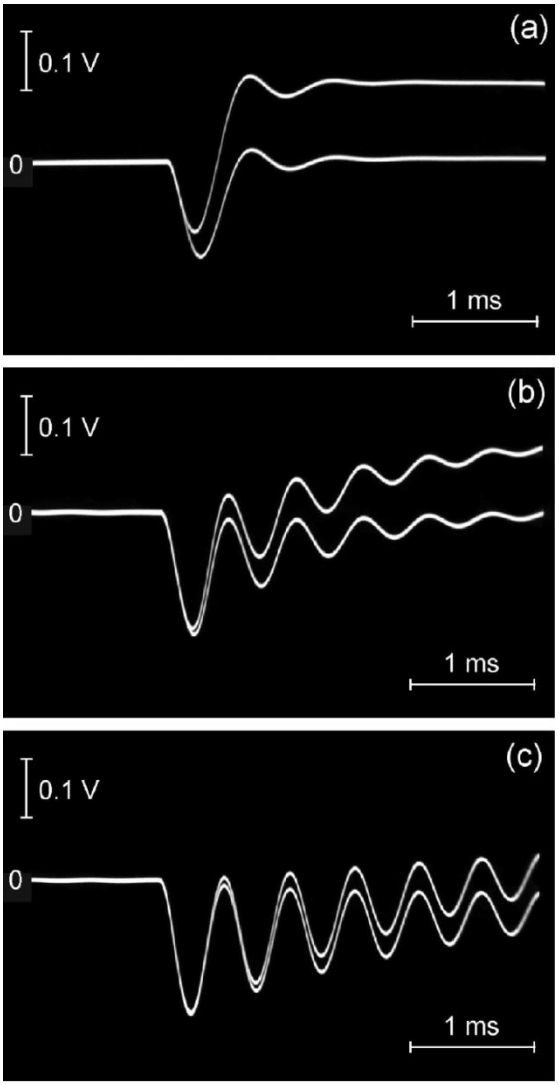

FIG. 3.14. Controlling the saddle in the DH oscillator. External perturbation V^*= 15 V. (a) R = 200 Ω (b = 1), C_1 = 51 nF (ω = 0.2). (b) R = 60 Ω (b = 0.3), C_1 = 175 nF (ω = 0.06). (c) R = 20 Ω (b = 0.1), C_1 = 510 nF (ω = 0.02). Upper traces, output signal of the oscillator V_x; lower traces, control signal V_{contr} / 2.

To implement "zero" damping ($b \approx 0$) in Fig. 3.15d we have removed the series resistor R in the circuit of the DH oscillator; the remaining resistance is r = 2 Ω only, where r is the internal resistance of the inductive coil L.

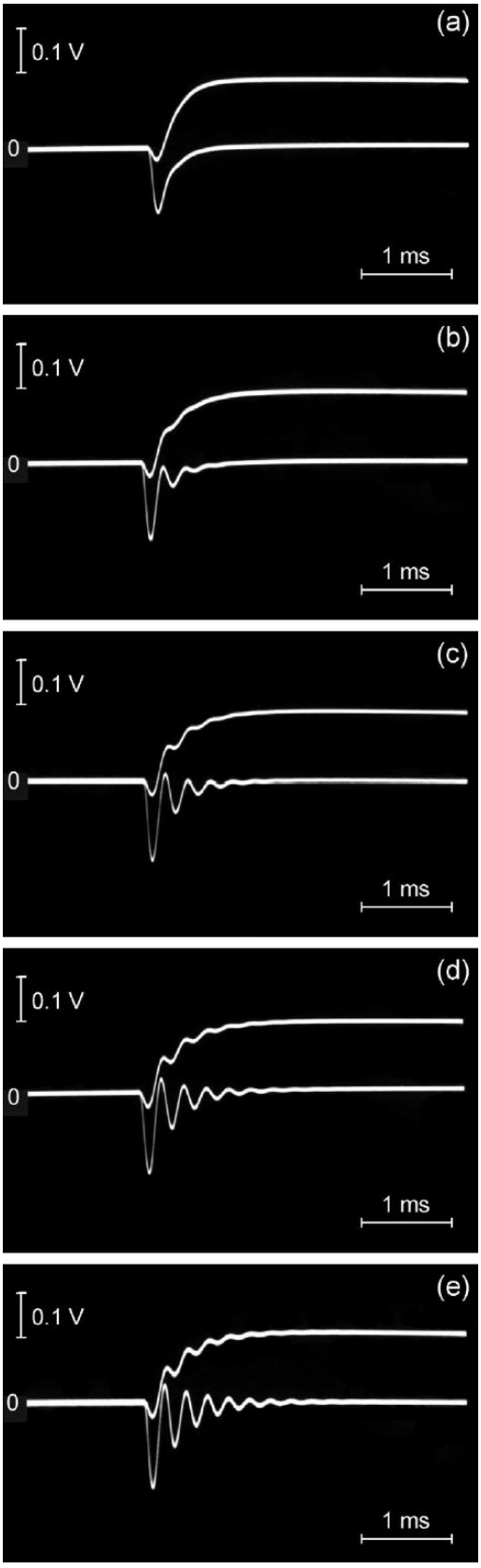

FIG. 3.15. Controlling saddle in the DH oscillator. External perturbation V^*= 15 V. (a) R = 200 Ω (b = 1). (b) R = 60 Ω (b = 0.3). (c) R = 20 Ω (b = 0.1). (d) r = 2 Ω (b = 0.01 ≈ 0). (e) R_{eff} = −20 Ω (b = −0.1). Upper traces, output signal of the oscillator V_x; lower traces, control signal V_{contr} / 2.

Negative damping in Fig. 3.15e is introduced in the system with moderate positive damping ($R = 20\ \Omega$, like in Fig. 3.15c) by means of additional coupling a negative resistance $R_N = -1\ \text{k}\Omega$ in parallel to the capacitor C. This is not a full circuit of the Lindberg oscillator [Lindberg *et al.*, 2009], since it lacks the inertial sub-circuit. However, it reflects the properties of a saddle equilibrium in a system with a negative damping.

3.4. Stabilizing saddles by means of unstable filter supported by derivative control [9]

We suggest an efficient synergetic method, which combines the UFC and the derivative control (we abbreviate it as UFDC), for stabilizing saddle equilibrium and inspect the response of the overall system to the external a priori unknown force.

We consider the DH autonomous damped oscillator as an example:

$$\ddot{x} + b\dot{x} - x + x^3 = 0. \tag{3.55}$$

Here b is the damping coefficient. The oscillator has three equilibrium states $(x_0, \dot{x}_0)$: two symmetrical stable spirals or nodes (depending on b) at $(\pm 1,0)$ and a saddle at $(0,0)$.

To stabilize the saddle we apply two methods for comparison, namely, the simple UFC method [Pyragas *et al.*, 2002, 2004] and the synergetic UFDC method (Fig. 3.16).

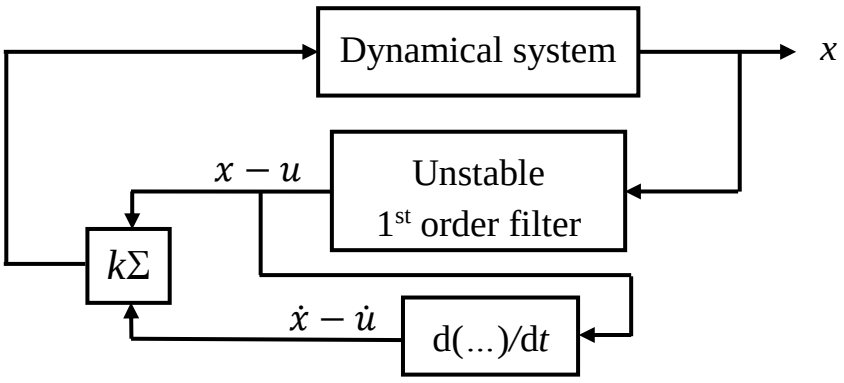

FIG. 3.16. Block diagram of stabilizing saddle state of a dynamical system by means of the UFDC.

The UFC and UFDC are described by Eq. (3.56) and Eq. (3.57), respectively

$$\begin{aligned} \dot{x} &= y, \\ \dot{y} &= x - x^3 - by + k(u - x) + p, \\ \dot{u} &= \omega(u - x). \end{aligned} \tag{3.56}$$

$$\begin{aligned} \dot{x} &= y, \\ \dot{y} &= x - x^3 - by + k(u + \dot{u} - x - \dot{x}) + p, \\ \dot{u} &= \omega(k - 1)(u - x). \end{aligned} \tag{3.57}$$

In Eq. (3.56) and Eq. (3.57) p is a perturbation. Note that set of equations similar to Eq. (3.57) can be obtained from Eq. (3.54) in the limit $\omega_2 \to \infty$:

$$\begin{aligned} \dot{x} &= y, \\ \dot{y} &= x - x^3 - by + k(u - x) - \frac{k_2}{\omega_2}\dot{x} + p, \\ \dot{u} &= \omega(k - 1)(u - x) \end{aligned}$$

or in case $k_2/\omega_2 = k$:

$$\begin{aligned} \dot{x} &= y, \\ \dot{y} &= x - x^3 - by + k(u - x - \dot{x}) + p, \\ \dot{u} &= \omega(k - 1)(u - x), \end{aligned}$$

which in comparison with Eq. (3.57) lacks term $\dot{u}$. When linearized around the saddle equilibrium point Eq. (3.56) and Eq. (3.57) read

$$\begin{aligned} \dot{x} &= y, \\ \dot{y} &= x - by + k(u - x), \\ \dot{u} &= \omega(u - x), \end{aligned} \tag{3.58}$$

$$\begin{aligned} \dot{x} &= y, \\ \dot{y} &= x - by + k(u + \dot{u} - x - \dot{x}), \\ \dot{u} &= \omega^*(u - x), \end{aligned} \tag{3.59}$$

respectively, with $\omega^* = (k-1)\omega$ and $k > 1$. Here we assumed $p = 0$ for simplicity without loss of generality. The corresponding characteristic equations are

$$\begin{aligned} &\lambda^3 + (b - \omega)\lambda^2 + (k - 1 - \omega b)\lambda + \omega = 0, \\ &\lambda^3 + (b + k - \omega^*)\lambda^2 + (k - 1 - \omega^* b)\lambda + \omega^* = 0. \end{aligned} \tag{3.60}$$

Numerical solutions of Eq. (3.60) for the UFC and the UFDC are presented in Fig. 3.17 and Fig. 3.18, respectively.

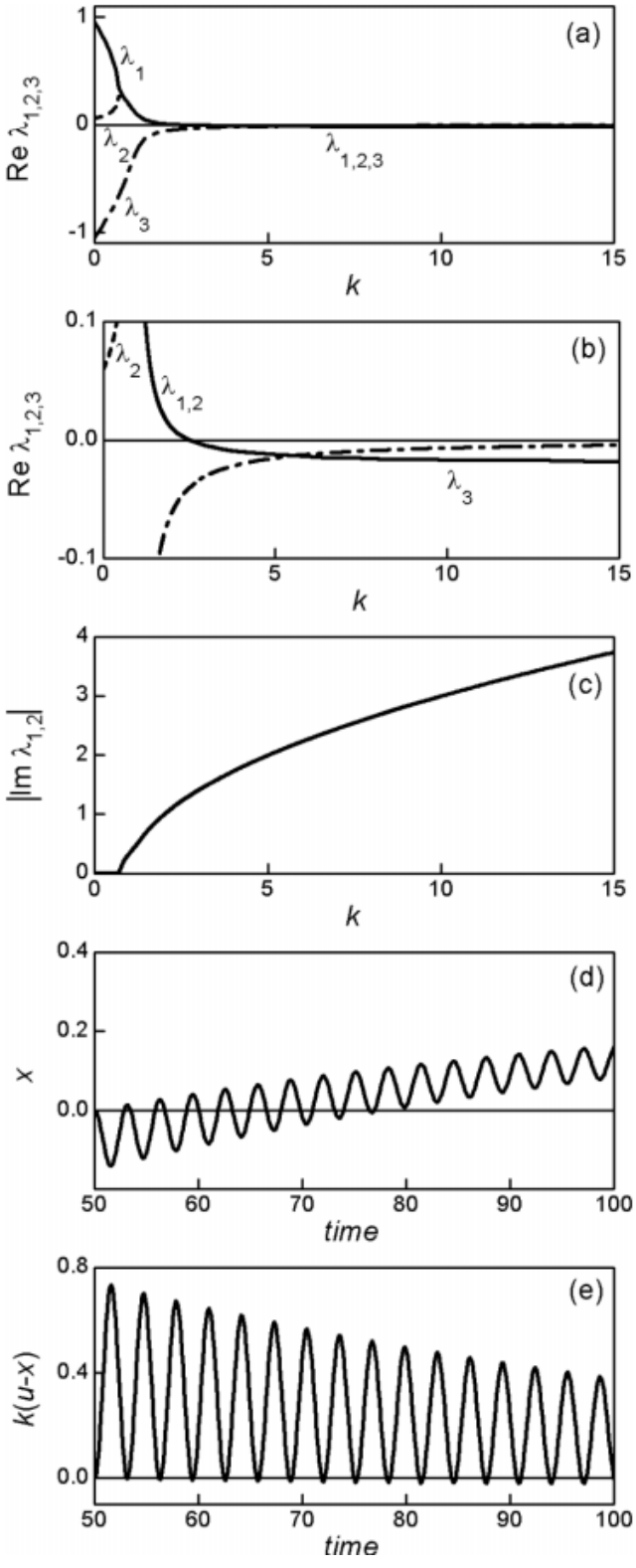

FIG. 3.17. Stabilizing the saddle by means of simple UFC, $b = 0.1$, $\omega = 0.06$ ($\omega < b$). (a) Real parts of the eigenvalues $\mathrm{Re}\lambda_{1,2,3}$ versus the control gain k from Eq. (3.60). (b) Same as (a), but the vertical scale is zoomed by a factor of 10. (c) Imaginary parts of the eigenvalues $\mathrm{Im}\lambda_{1,2}$ versus the control gain k from Eq. (3.60).(d) Variable x from Eq. (3.56). (e) Control term $k(u-x)$ from Eq. (3.56). In (d) and (e) $k = 5$, perturbation $p = -0.3$ is applied at $t = 50$.

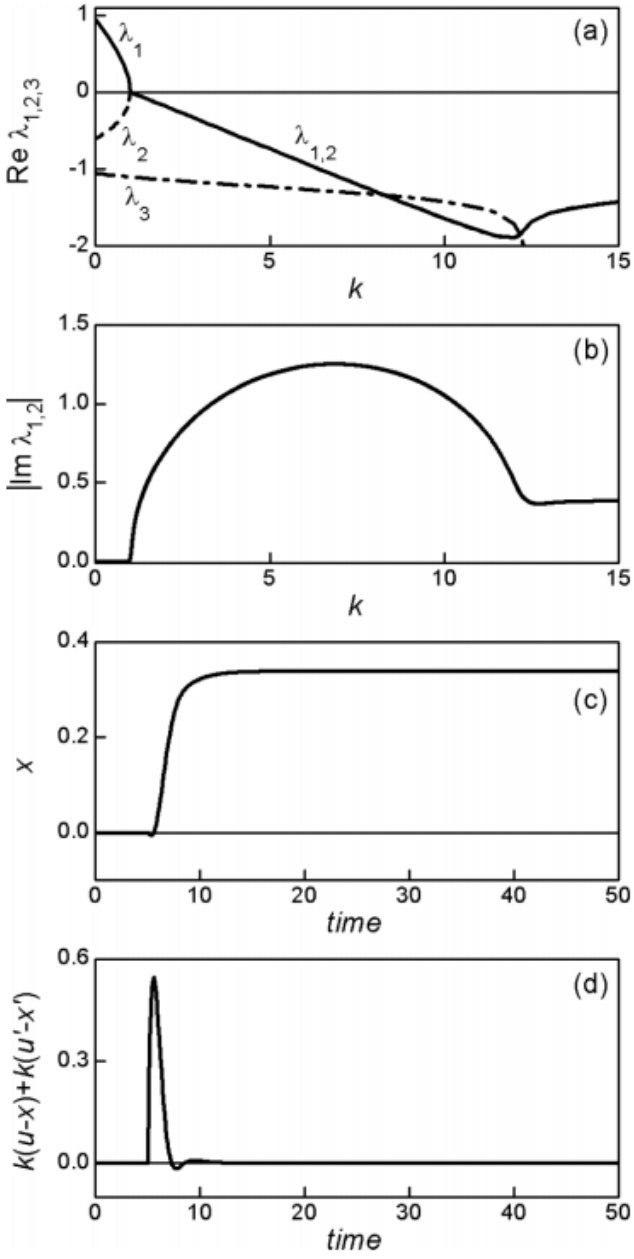

FIG. 3.18. Stabilizing the saddle by means of the synergetic UFDC method, $b = 0.1$, $\omega = 0.6$. (a) Real parts of the eigenvalues $\mathrm{Re}\lambda_{1,2,3}$ versus the control gain k from Eq. (3.60). (b) Imaginary parts of the eigenvalues $\mathrm{Im}\lambda_{1,2}$ versus the control gain k from Eq. (3.60). (c) Variable x from Eq. (3.57). (d) Control term from Eq. (3.57). In (c) and (d) $k = 10$, perturbation $p = -0.3$ is applied at $t = 5$.

The overall system is stable, if the real parts of all three eigenvalues are negative. The necessary and sufficient conditions can be found analytically from the Hurwitz matrices

$$H = \begin{pmatrix} b-\omega & \omega & 0 \\ 1 & k-1-\omega b & 0 \\ 0 & b-\omega & \omega \end{pmatrix}, \tag{3.61}$$

$$H^* = \begin{pmatrix} b+k-\omega^* & \omega^* & 0 \\ 1 & k-1-\omega^* b & 0 \\ 0 & b+k-\omega^* & \omega^* \end{pmatrix}. \tag{3.62}$$

The eigenvalues $\mathrm{Re}\lambda_{1,2,3}$ are all negative if the diagonal minors of the H and H^* matrices are all positive. For the matrix H the diagonal minors are

$$\begin{aligned} &\Delta_1 = b-\omega > 0, \\ &\Delta_2 = (b-\omega)(k-1-\omega b) - \omega > 0, \\ &\Delta_3 = \omega\Delta_2 > 0. \end{aligned} \tag{3.63}$$

These inequalities are satisfied if

$$\omega < b, \quad k > k_{th} = \frac{b}{b-\omega} + \omega b. \tag{3.64}$$

For example, at $b = 0.1$ and $\omega = 0.06$ the $k_{th} \approx 2.5$. On one hand, the ω could be only slightly less than b. On the other hand, it should not be too close to b, because small value of the denominator $b-\omega$ would heavily increase the stabilization threshold k_{th}.

The largest eigenvalues $\mathrm{Re}\lambda_1=\mathrm{Re}\lambda_2$ in Fig. 3.17 cross zero axis at $k \approx 2.5$ in a good agreement with the analytical result. We note very small absolute values of the largest $\mathrm{Re}\lambda_{\max}$ at $k > k_{th}$. In the full scale (Fig. 3.17a) the curve lays almost on the abscissa. Only the zoomed in plot (Fig. 3.17b) reveals the negative values. However, even at $k = k_{\mathrm{opt}} = 5$ the $|\mathrm{Re}\lambda_{\max}| = 0.01$. Such a low value, related to small parameters b and ω, results in slow convergence to the equilibrium. This is a serious shortcoming of the UFC method, especially if applied to weakly damped ($b \le 0.1$) and Hamiltonian dynamical systems. Numerical results of the control dynamics under the influence of an *a priori* unknown external constant force p, which changes the position of the saddle state, are shown in Fig. 3.17d and Fig. 3.17e.

The diagonal minors of the matrix H^* are

$$\Delta_1^* = b + k - \omega^* > 0,$$
$$\Delta_2^* = (b + k - \omega^*)(k - 1 - \omega^* b) - \omega^* > 0, \qquad (3.65)$$
$$\Delta_3^* = \omega^* \Delta_2^* > 0.$$

Inequalities (3.65) provide the following stability criterion:

$$\omega < \frac{k+b}{k-1}, \quad k > k_{th} \approx 1. \qquad (3.66)$$

For large k the required cut-off frequency of the unstable filter $\omega < 1$ and in contrast to the UFC method does not depend on b. In (3.66) k_{th} is derived for weak damping ($b < 0.1$); the value $k_{th} \approx 1$ is in good agreement with the numerical results (Fig.3.18a).

Experimental results. The results for the both methods, the UFC and the UFDC, taken from the analogue circuits, are shown in Fig. 3.19.

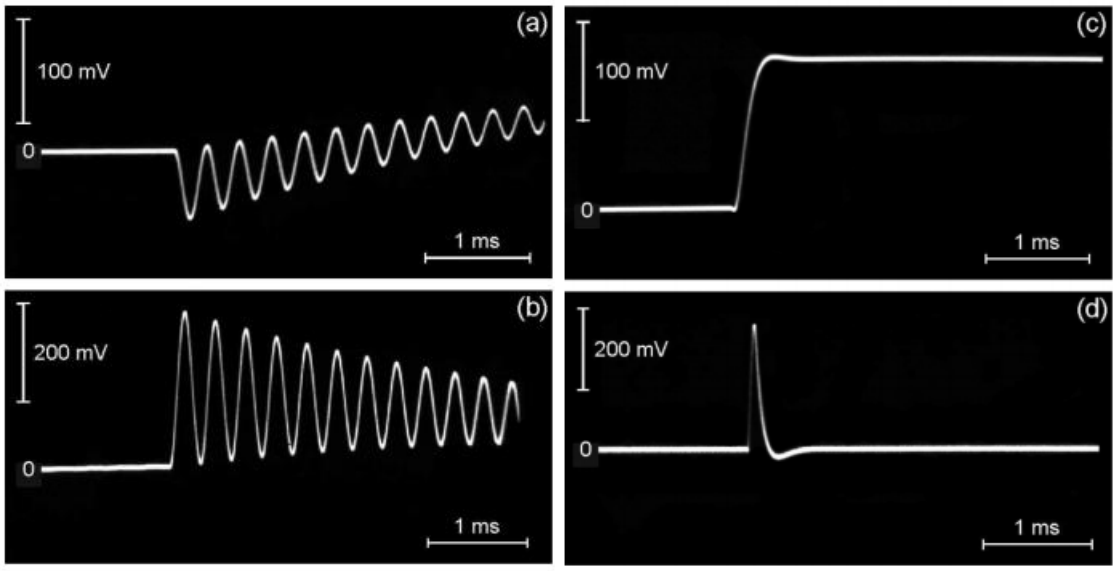

FIG. 3.19. Stabilizing the saddle in the DH oscillator. Perturbation $V^* = 15$ V; $p = -(R_2/R_4)(V^*/V_b) = -0.3$. (a, b) Simple UFC method, $C_0 = 175$ nF ($\omega = \sqrt{LC}/(R_0 C_0) = 0.06$), $k_{01} = 1$, $k_{02} = 2$, $k_{03} = 2.5$, $k = k_{02}k_{03} = 5$. (c, d) Synergetic UFDC method, $C_0 = 16$ nF ($\omega = 0.6$), $C_d = 330$ pF ($R_d C_d \approx 3.10^{-6} << \sqrt{LC} \approx 10^{-4} s$), $k_{01} = 1$, $k_{02} = 10$, $k_{03} = 30$, $k_{04} = 1$, $k = k_{02}k_{04} = 10$, $(R_d C_d/\sqrt{LC})k_{03} \approx 1$. (a, c) Output signals V_x, (b, d) Control signals V_{contr}.

Comparison between UFC, UFC||SFC, CFC, and UFDC. There are three main advantages of the UFDC method over the UFC technique. First, in the case of the UFC method at the optimal control gain $k = k_{opt} = 5$ the $\mathrm{Re}\lambda_{max} = -0.01$ (Fig. 3.17b), while in the case of the UFDC method at $k = k_{opt} = 12.5$ the $\mathrm{Re}\lambda_{max} \approx -2$, which is about 200 times larger than for the UFC technique, resulting in extremely fast convergence to the equilibrium. Secondly, the $|\mathrm{Im}\lambda_{1,2}|$ for the UFDC method is several times smaller than for the UFC method. Finally, in the case of the UFDC method there is no negative drop of the $x(t)$ at the time moment when the perturbation is applied.

To better understand the reasons for the enhanced performance of the UFDC method we replace in the 2nd equation of (3.59) $\dot{x}$ with y and $\dot{u}$ with $\omega^*(u-x)$, respectively. Then the following explicit form is obtained:

$$\begin{aligned} \dot{x} &= y, \\ \dot{y} &= x - b^* y + k^*(u - x), \\ \dot{u} &= \omega^*(u - x). \end{aligned} \tag{3.67}$$

One can see that Eq. (3.67) for the UFDC method has exactly the same form as Eq. (3.58) for the UFC method, but with the effective parameters:

$$b^* = b + k, \quad k^* = (1 + \omega^*)k, \quad \omega^* = (k - 1)\omega.$$

The most important issue is, that the effective damping coefficient b^* is increased considerably due to the sum of b and k. Therefore the cut-off frequency of the filter can be increased significantly. This is the main reason of the faster performance of the UFDC method.

In conclusion, we have proposed a synergetic UFDC method for stabilizing *a priori* unknown saddle equilibrium states of dynamical systems. The controller is model independent and reference-free. It requires neither the mathematical model nor the coordinates of the equilibrium state, but automatically tracks and stabilizes the state. The numerical and the experimental results have been presented for the DH oscillator only. However, the general form of a saddle given by Eq. (3.59) indicates that the UFDC technique can be applied to many other dynamical systems as well. The suggested UFDC controller is essentially faster than the simple UFC version

[Pyragas *et al.*, 2004]. Moreover, it is suitable to stabilize saddle equilibrium states also in dynamical system with zero ($b = 0$) and negative ($b < 0$) damping. In contrast to the simple UFC technique the cut-off frequency of the UFDC controller ω can be set relatively high and is independent of the damping of the dynamical system; the effective frequency is further increased by a factor of ($k-1$) in Eq. (3.57). The UFDC controller exhibits robust performance in the presence of external unknown forces, which change the coordinates of the equilibrium state in the phase space.

In the CFC method, described in Section 3.3, for stabilizing saddle equilibrium states, the enhancement is noticeable. Though the transients in weakly damped systems become shorter (≈ 1 ms in the experiment), the main variables and the control signals still exhibit ringing effects. In contrast, the UFDC method ensures very short transient (≈ 0.2 ms), which is close to the intrinsic response time of the oscillator $\sqrt{LC} \approx 0.1$ ms, and practically no ringing is observed. From a mathematical point of view, an additional filter in the CFC increases dimension of the overall system from three to four, thus making analysis of the 4×4 Hurwitz matrix and its four diagonal minors extremely complicated. Whereas for the UFDC method in the case of weak damping the stability criterion (3.66) is easy to derive. It has a simple form:

$$\omega < \frac{k}{k-1}, \quad k > 1. \tag{3.68}$$

All control methods described in Chapter 3 are summarized in Table 2.

TABLE 2. Real part of maximal eigenvalue λ_{max} at optimal gain k_{opt} for different control methods stabilizing saddles in conservative and weekly dissipative systems ($0 \le b \le 0.1$).

Method	**Reλ_{max}**	**Figure (page)**
UFC	+0.01 (b=0) –0.003 (b=0.01) –0.025 (b=0.1)	3.4a (p.51) 3.7a (p.58) 3.9b (p.63)
UFC||SFC	–0.5	3.4c (p.51)
CFC	–1.0	3.12b (p.67)
UFDC	–2.0	3.18a (p.74)

CHAPTER 4

STEPWISE FEEDBACK METHODS FOR STABILIZING EQUILIBRIUM

4.1. Stabilizing saddles with partially unknown dynamics [7]

Simple zeroth order stable proportional feedback technique can be used, which employs either artificially created or natural stable equilibrium (SEQ) to find unknown coordinates of the unstable equilibrium (UEQ).

1st order linear system. To illustrate the idea, we start with the extremely simple mathematical example. A dynamical system given by

$$\dot{x} = ax - c$$

has a single UEQ $x_0=c/a$, which can be easily stabilized by means of a simple proportional feedback:

$$\dot{x} = ax - c + k(x_0 - x),$$

provided $k>a$. Note, that the control term $k(x_0-x)$ vanishes, when the goal equilibrium $x\to x_0$ is achieved. However, when the system's dynamics is not fully defined, e.g. is described by

$$\dot{x} = ax - \xi \tag{4.1}$$

with ξ as an unknown term, the corresponding UEQ, $x_0=\xi/a$ is also unknown and therefore the simple proportional feedback cannot be applied directly. Nevertheless, we demonstrate that this unknown UEQ can be still stabilized by a two-step proportional feedback. In the first step we apply proportional feedback with an arbitrarily chosen reference point r_1:

$$\dot{x} = ax - \xi + k(r_1 - x), \tag{4.2}$$

where r_1 is any real, either positive or negative (zero value is also applicable) constant. For $k>a$ the feedback creates an artificial SEQ:

$$x_1 = \frac{kr_1 - \xi}{k - a}. \tag{4.3}$$

Note, that the control term $k(r_1-x)$ in Eq. (4.2), in general, does not vanish, because the r_1 is not a natural UEQ of the original Eq. (4.1). An exception is a "resonant" value $r_1=x_0$. It means that we are lucky to guess the right reference

point x_0 and the procedure is accomplished in one step. Otherwise the unknown term ξ should be derived from formula (4.3):

$$\xi = ax_1 + k(r_1 - x_1). \tag{4.4}$$

In the second step we simply replace r_1 in Eq. (4.2) with the goal UEQ $x_0=\xi/a$, where ξ is already defined and is given by formula (4.4):

$$\dot{x} = ax - \xi + k(\xi/a - x)$$

and readily stabilize the initially unknown UEQ $x_0=\xi/a$.

1st order nonlinear system. If a dynamical system has two equilibrium states, specifically an UEQ and a SEQ, the latter can be employed to find the position of the first one. In this case stabilization can be achieved in one step only, without creating an artificial SEQ. The following nonlinear equation is an example:

$$\dot{x} = ax - x^2 - \xi. \tag{4.5}$$

For $\xi<a^2/4$ it has two real equilibrium states:

$$x_{01,02} = a/2 \mp \sqrt{a^2/4 - \xi}.$$

Here the x_{01} is an UEQ, whereas the x_{02} is a SEQ. Note an important feature (independent on ξ): $x_{01} + x_{02} = a$. Thus, the natural SEQ, x_{02} (an observable) can be immediately used to find the UEQ: $x_{01}=a-x_{02}$ and inserted in the feedback term:

$$\dot{x} = ax - x^2 - \xi + k(x_{01} - x),$$

where $\xi = ax_{02} - x_{02}^2$, found from the steady-state solution of Eq. (4.5).

Now we can generalize the above specific examples in the form:

$$\dot{x} = F(x) - \xi\,, \tag{4.6}$$

where $F(x)$ is either linear or nonlinear function. Depending on $F(x)$ Eq. (4.6) can have several equilibrium points, which satisfy the steady-state equation $F(x_{0i})=\xi$. The equilibrium states are either UEQ or SEQ depending on the derivative $dF(x)/dx \equiv F'(x)$ at $x=x_{0i}$. If $F'(x)|_{x0i} >0$ the x_{0i} is an UEQ. If $F'(x)|_{x0i} <0$ the x_{0i} is a SEQ. We recall here that all the equilibrium points are unknown

because of the unknown term ξ. Let us consider an UEQ and apply the two-step procedure. The first step is given by

$$\dot{x} = F(x) - \xi + k(r_1 - x). \tag{4.7}$$

The first step yields an artificial SEQ x_1. The unknown term ξ is found from equilibrium case of Eq. (4.7):

$$\xi = F(x_1) + k(r_1 - x_1)$$

and then is inserted into Eq. (4.6) for the uncontrolled system. Its steady-state equation reads:

$$F(x_0) - F(x_1) - k(r_1 - x_1) = 0. \tag{4.8}$$

If the $F(x)$ is well defined the Eq. (4.8) can be solved with respect to x_0 and, finally, the second step is applied:

$$\dot{x} = F(x) - \xi + k(x_0 - x).$$

Mechanical pendulum. The first physical example is a mechanical pendulum:

$$\ddot{\varphi} + \beta\dot{\varphi} + \sin\varphi = \xi. \tag{4.9}$$

In Eq. (4.9) φ is the angle between the downward vertical and the rod, β is the damping coefficient, and ξ is a constant, but generally unknown torque. For small torque ξ<1, the system has two equilibrium points $(\varphi_{01,02}, \dot{\varphi}_{01,02}) = (\varphi_{01,02}, 0)$ with $\varphi_{01} = \arcsin\xi$, $\varphi_{02} = \pi - \arcsin\xi$. The φ_{01} is a SEQ (lower position of the pendulum), the φ_{02} is a saddle UEQ (upper position of the pendulum). Independently on ξ the sum of the two angles is a constant value: $\varphi_{01} + \varphi_{02} = \pi$. Thus, we can apply a simplified one-step procedure, similarly to the first-order nonlinear mathematical example given by Eq. (4.5). Here we exploit the existing natural SEQ of the pendulum to determine the position of the UEQ, without creating any artificial SEQ. The coordinate of the unknown UEQ is readily obtained from the coordinate φ_{01} of the known (observed) SEQ: φ_{02}= $\pi - \varphi_{01}$. Then we apply the proportional feedback:

$$\ddot{\varphi} + \beta\dot{\varphi} + \sin\varphi = \xi + k(\varphi_{02} - \varphi), \tag{4.10}$$

where ξ=$\sin\varphi_{01}$.

Linearization of Eq. (4.10) around φ_{02} gives the characteristic equation:

$$\lambda^2 + \beta\lambda + k + \cos(\pi - \varphi_{01}) = 0.$$

For small ξ the angle $\varphi_{01}<<\pi$, thus $\lambda_{1,2} = -\beta/2 \pm \sqrt{\beta^2/4 - (k-1)}$. The threshold value of the feedback coefficient is $k_{th}=1$, for which the largest eigenvalue λ_1 crosses zero from positive to negative values. The optimal value of the feedback coefficient $k_{opt}=1+\beta^2/4$; the eigenvalues are both negative and equal to each other, $\lambda_1=\lambda_2=-\beta/2$. Further increase of k makes the eigenvalues complex, but does not change their real parts. So, for higher feedback coefficients the convergence rate saturates with k and is fully determined by the damping coefficient β. Result of numerical integration of Eq. (4.10) is shown in Fig. 4.1.

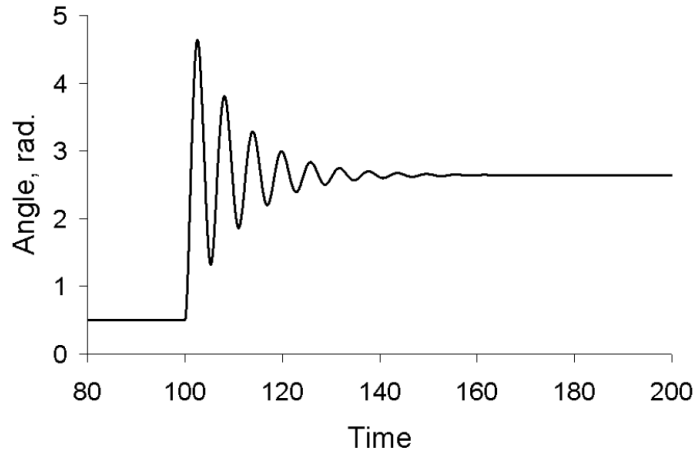

FIG. 4.1. One-step stabilization of the upper position, UEQ of mechanical pendulum given by Eq. (4.10). The control is switched on at t=100. The parameters are β=0.2, k=2. The SEQ angle observed before switching the control φ_{01}=0.5, the extracted unknown term $\xi=\sin\varphi_{01}$=0.47943, stabilized UEQ is 2.64. Angle calculated from the relationship $\varphi_{02}=\pi-\varphi_{01}$=2.64.

Duffing–Holmes (DH) oscillator. The second physical example is the DH nonlinear damped oscillator, which, in contrast to the classical DH system [Ott, 1993], lacks external periodic driving force, but includes an unknown term ξ:

$$\ddot{x} + b\dot{x} - x + x^3 = \xi. \qquad (4.11)$$

Here b is the damping coefficient. For $|\xi| < 2/\sqrt{27}$ Eq. (4.11) has three equilibrium points: $(x_{01,02,03}, \dot{x}_{01,02,03}) = (x_{01,02,03}, 0)$. The two side points are SEQ, while the middle one is a saddle UEQ. Their coordinates, in general, are rather cumbersome:

$$x_{01} = -\frac{2}{\sqrt{3}}\cos\frac{\pi-\theta}{3}, x_{02} = -\frac{2}{\sqrt{3}}\cos\frac{\pi+\theta}{3}, x_{03} = \frac{2}{\sqrt{3}}\cos\frac{\theta}{3}, \qquad (4.12)$$

where the formal parameter θ is given by

$$\theta = \arccos\frac{\xi\sqrt{27}}{2}. \qquad (4.13)$$

For ξ=0 they become: x_{01}=−1, x_{02}=0, x_{03}=1. There is a simple relationship between the three coordinates:

$$x_{01} + x_{02} + x_{03} = 0,$$

which is valid for the non-zero ξ as well. Therefore one can think about the one-step algorithm (x_{02}=−x_{01}−x_{03}), similarly to the case of the pendulum. From a practical point of view the procedure is not convenient, since one needs to find (to observe) two remote SEQ points, separated by an UEQ. So, if a system is located at one of the SEQ, say x_{01}, we have to switch it to another SEQ (x_{03}) by applying some rather strong external force. Formally, we can use only one SEQ, either x_{01} or x_{03}. From the corresponding formulas (4.12), (4.13) we can extract ξ and use it for finding x_{02}, again from the formulas (4.12), (4.13). However, this formal way requires rather long and complicated calculations.

There is a shorter way. The SEQ x_{01} satisfies the steady-state equation:

$$x_{01}^3 - x_{01} - \xi = 0.$$

From here the unknown term ξ is readily derived as $\xi = x_{01}^3 - x_{01}$ and is used to calculate x_{02} from the appropriate formulas (4.12), (4.13). Finally, this coordinate is employed in the proportional feedback:

$$\ddot{x} + b\dot{x} - x + x^3 = \xi + k(x_{02} - x). \qquad (4.14)$$

Linearization of Eq. (4.14) around x_{02} yields the characteristic equation:

$$\lambda^2 + \beta\lambda + k - 1 + 3x_{02}^2 = 0.$$

Its eigenvalues are given by $\lambda_{1,2} = -b/2 \pm \sqrt{b^2/4 - (k-1+3x_{02}^2)}$. For small ξ the coordinate of the UEQ $|x_{02}| << 1$. Then stabilization parameters are the same as that for the pendulum: the threshold coefficient k_{th}=1, the optimal value k_{opt}=1+b^2/4, and the best pair of the real negative eigenvalues $\lambda_{1,2}$=−b/2. Numerical result for the DH oscillator is presented in Fig. 4.2.

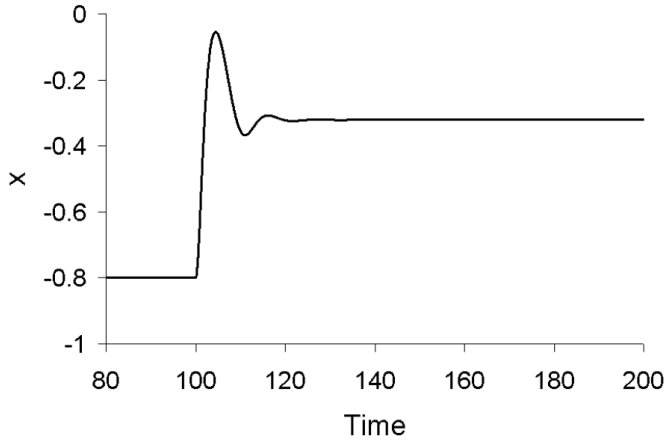

FIG. 4.2. One-step stabilization of the UEQ of the DH oscillator from Eq. (4.14). The control is switched on at t=100. b=0.5, k=1.1. SEQ observed before switching the control x_{01}=−0.8, the extracted term $\xi = x_{01}^3 - x_{01} = 0.288$, stabilized UEQ is −0.321. UEQ calculated from (4.12–4.13) x_{02}=−0.321.

Van der Pol oscillator. The next physical example is the well-known van der Pol oscillator, but with an additionally applied unknown force ξ:

$$\ddot{x} - \mu(1-x^2)\dot{x} + x = \xi. \qquad (4.15)$$

Eq. (4.15) can be presented in the form of two coupled the 1st order equations:

$$\dot{x} = -y + \mu(x - x^3/3),$$
$$\dot{y} = x - \xi.$$

The van der Pol oscillator for any μ>0 and $|\xi|$<1 has a single UEQ (x_0,y_0):

$$x_0 = \xi, \quad y_0 = \mu(\xi - x_0^3/3), \qquad (4.16)$$

which is either a spiral, if $\mu(1-\xi^2)$<2, or a node, if $\mu(1-\xi^2)$>2; however the both coordinates are unknown because of the unknown force ξ. In contrast to the two previous examples, there are no SEQ states. Therefore, we need to apply the two-step stabilization technique:

$$\begin{aligned} \dot{x} &= -y + \mu(x - x^3/3) + k_1(r_1 - x), \\ \dot{y} &= x - \xi. \end{aligned} \tag{4.17}$$

The proportional feedback with $k_1 > \mu(1-\xi^2)$ creates an artificial SEQ (x_1, y_1):

$$x_1 = \xi, \quad y_1 = \mu(x - x^3/3) + k_1(r_1 - x_1).$$

The second coordinate y_1 is not important in this specific case, since the unknown parameter ξ is found immediately from the first coordinate x_1: $\xi = x_1$. Then, in the second step we simply replace the auxiliary reference point r_1 with the ξ, found in the first step:

$$\begin{aligned} \dot{x} &= -y + \mu(x - x^3/3) + k_2(\xi - x), \\ \dot{y} &= x - \xi. \end{aligned} \tag{4.18}$$

and stabilize the natural UEQ (x_0, y_0), given by (4.16). Linearization around equilibrium point (x_0, y_0) yields the characteristic equation:

$$\lambda^2 + [k_2 - \mu(1 - x_0^2)]\lambda + 1 = 0.$$

For $x_0^2 << 1$ the $\lambda_{1,2} = -(k_2 - \mu)/2 \pm \sqrt{(k_2 - \mu)^2/4 - 1}$. Thus, the threshold coefficient $k_{2th} = \mu$ (Re λ_1 becomes negative). The optimal value is $k_{2opt} = \mu + 2$, when the both eigenvalues are negative and equal to each other, $\lambda_1 = \lambda_2 = -1$.

The two-step technique applied to the van der Pol oscillator to stabilize the unknown UEQ is illustrated by numerical results in Fig. 4.3.

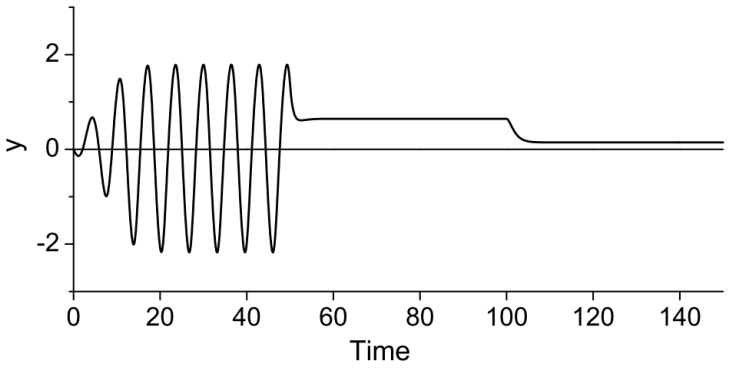

FIG. 4.3. Two-step stabilization of the UEQ of the van der Pol oscillator from Eq. (4.17) and Eq. (4.18). The first step is switched on at t=50, the second step is applied at t=100. μ=0.5, $k_1 = k_2$=2.5, r_1=0.5. The x-coordinate of the artificial SEQ is x_1=0.3, the extracted unknown force is ξ=0.3, the stabilized UEQ (x_0, y_0)=(0.3, 0.1455).

Lorenz system. Finally we consider the famous Lorenz system [Lorenz, 1963], which for certain sets of the parameters exhibits chaotic behaviour. The system is given by three coupled differential equations:

$$\begin{aligned} \dot{x} &= -\sigma x + \sigma y, \\ \dot{y} &= \rho x - y - xz, \\ \dot{z} &= xy - \beta z. \end{aligned} \tag{4.19}$$

Two parameters are usually fixed at σ=10 and β=8/3, while the third parameter ρ is considered as a control parameter to observe various kinds of bifurcations. For ρ<1 the system has a single SEQ at the origin (x_{01},y_{01},z_{01})=(0,0,0). For ρ>1 this SEQ loses its stability and two additional SEQ ($x_{02,03}$,$y_{02,03}$,$z_{02,03}$) appear at

$$(\pm\sqrt{\beta(\rho-1)},\pm\sqrt{\beta(\rho-1)},\rho-1).$$

Linearization of Eq. (4.19) around these equilibrium points leads to the following characteristic equation:

$$\lambda^3 + (\sigma+\beta+1)\lambda^2 + \beta(\sigma+\rho)\lambda + 2\sigma\beta(\rho-1) = 0. \tag{4.20}$$

Using the Routh–Hurwitz criterion we find that this pair becomes unstable for

$$\rho > \sigma\frac{\sigma+\beta+3}{\sigma-\beta-1} \approx 24.74,$$

yielding chaotic oscillations, e.g. at ρ=28, which is the most popular parameter value used in literature [Lorenz, 1963; Ott, 1993; Pyragas *et al.*, 2004].

Now we assume that the value of the parameter ρ is unknown, i.e. ρ=ξ. Consequently, the coordinates of the equilibrium points are also unknown:

$$(\pm\sqrt{\beta(\xi-1)},\pm\sqrt{\beta(\xi-1)},\xi-1). \tag{4.21}$$

Therefore, to stabilize the UEQ states we apply the two-step procedure:

$$\begin{aligned} \dot{x} &= -\sigma x + \sigma y, \\ \dot{y} &= \xi x - y - xz + k_1(r_1 - y), \\ \dot{z} &= xy - \beta z. \end{aligned} \tag{4.22}$$

For simplicity we set r_1=0. The feedback term $-k_1y$ creates a pair of artificial SEQ states ($x_{12,13}$, $y_{12,13}$, $z_{12,13}$):

$$(\pm\sqrt{\beta(\xi-k_1-1)},\pm\sqrt{\beta(\xi-k_1-1)},\xi-k_1-1).$$

We can extract the unknown parameter ξ from any coordinate of the artificial SEQ, most conveniently from the z_{12}: ξ=z_{12}+k_1+1. Then z_{02}=z_{03}=ξ–1=z_{12}+k_1.

Two other coordinates of the UEQ are: $(x_{02,03}, y_{02,03}) = (\pm\sqrt{\beta z_{02}}, \pm\sqrt{\beta z_{02}})$. The $y_{02,03}$ are inserted into Eq. (4.22) instead of the reference point r_1:

$$\begin{aligned} \dot{x} &= -\sigma x + \sigma y, \\ \dot{y} &= \xi x - y - xz + k_2(y_{02,03} - y), \\ \dot{z} &= xy - \beta z \end{aligned} \tag{4.23}$$

to stabilize the UEQ ($x_{02,03}$, $y_{02,03}$, $z_{02,03}$). Linearizing Eq. (4.23) about the equilibrium we obtain the corresponding characteristic equation:

$$\lambda^3 + (\sigma + \beta + 1 + k_2)\lambda^2 + [\beta(\sigma + \xi) + k_2(\sigma + \beta)]\lambda + 2\sigma\beta(\xi - 1) + k_2\sigma\beta = 0,$$

which for k_2=0 and $\xi=\rho$ coincides with Eq. (4.20), as expected. The Routh–Hurwitz criterion provides the following necessary and sufficient condition of stability of the UEQ:

$$\xi(k_2 - \sigma + \beta + 1) + \sigma(\sigma + \beta + 3) + k_2\left(\frac{\sigma^2}{\beta} + 2\sigma + \frac{\sigma}{\beta} + \beta + 1\right) + k_2^2\left(\frac{\sigma}{\beta} + 1\right) > 0. \tag{4.24}$$

Let us consider the 1st term only in the inequality (4.24), since it contains a negative component '$-\sigma$'. If

$$k_2 > \sigma - \beta - 1 \approx 6.33, \tag{4.25}$$

then the equilibrium is stable for all ξ>0. This is a very rough estimation (upper limit) of the stabilization threshold. However, the threshold is conveniently independent on ξ. Taking into account the 2nd term in the inequality (4.24), we find that depending on ξ the stabilization can be achieved at essentially lower feedback coefficients

$$k_2 > \sigma - \beta - 1 - \sigma\frac{\sigma + \beta + 3}{\xi} \approx 0.73$$

at ξ=28. For very large ξ the threshold approaches the value given by condition (4.25). The 3rd term in the inequality (4.24) further diminishes the stabilization threshold, e.g. to $k_2\approx0.22$ at ξ=28. The 4th term, which is quadratic with respect to k, for small k makes only very small correction.

The two-step stabilization of the UEQ (x_{02},y_{02},z_{02}) in the Lorenz system is demonstrated in Fig. 4.4 for two slightly different initial conditions. Similar results are obtained for another UEQ (x_{03},y_{03},z_{03}).

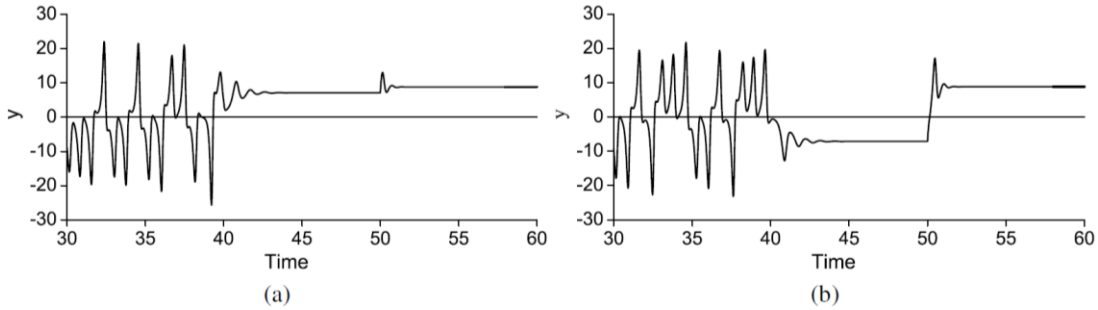

FIG. 4.4. Two-step stabilization of the spiral UEQ in the Lorenz system from Eq. (4.22) and Eq. (4.23) with ξ=30. The 1st step is switched on at t=40, the 2nd step is applied at t=50. σ=10, β=8/3, k_1=k_2=10, r_1=0. The z-coordinate of the artificial SEQ z_{12}=z_{13}=19, the extracted unknown parameter ξ=z_{12}+k_1+1=30. Stabilized UEQ is (8.79; 8.79; 29.0). Initial conditions are $y(0) = z(0) = 0$; (a) $x(0)$=0.10, (b) $x(0)$=0.11.

The same two-step method can be used to stabilize the saddle UEQ at the origin (0,0,0). The coordinates of the UEQ are known (they do not depend on ξ) in this specific case. One may think that the proportional feedback method can be applied directly. However, the feedback coefficient k, required to stabilize the UEQ, essentially depends on the unknown parameter ξ. Linearizing Eq. (4.23) around the origin we obtain one negative eigenvalue immediately, $\lambda_3 = -\beta$, independent on k_2. Two other eigenvalues are found from the quadratic characteristic equation $\lambda^2 + (\sigma + k_2 + 1)\lambda + \sigma(k_2 + 1 - \xi) = 0$:

$$\lambda_{1,2} = -(\sigma + k_2 + 1)/2 \pm \sqrt{(\sigma + k_2 + 1)^2/4 - \sigma(k_2 + 1 - \xi)}.$$

The both eigenvalues $\lambda_{1,2}$ are negative if

$$k_2 > \xi - 1. \qquad (4.26)$$

Here the parameter ξ is unknown. Therefore, it should be found from the first step, given by Eq. (4.22), and then used in condition (4.26) and in Eq. (4.23) with a modified control term: '$-k_2 y$' (since the reference point is 0) to stabilize the UEQ (x_{01},y_{01},z_{01})=(0,0,0).

Numerical results of stabilizing the saddle UEQ are presented in Fig. 4.5, again for two slightly different initial conditions.

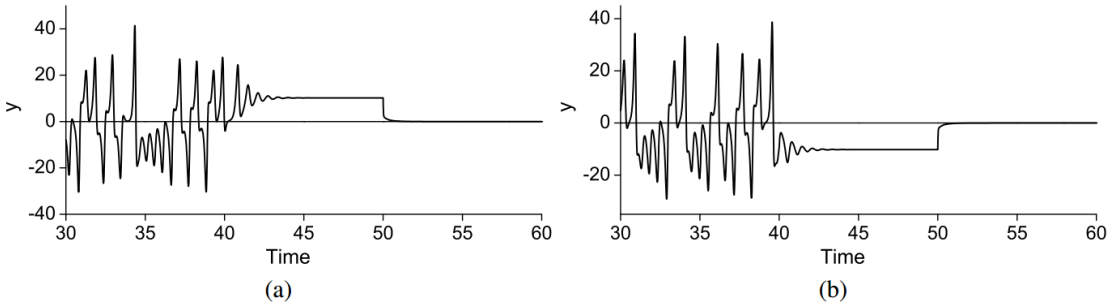

FIG. 4.5. Two-step stabilization of the saddle UEQ in the Lorenz system from Eq. (4.22) and Eq. (4.23) with ξ=50. The 1st step is switched on at t=40, the 2nd step is applied at t=50. σ=10, β=8/3, k_1=10, r_1=0. The z-coordinate of the artificial SEQ $z_{12}=z_{13}$=39, the extracted unknown parameter $\xi=z_{12}+k_1+1$=50, k_2=60. Stabilized UEQ is (0; 0; 0). Initial conditions are $y(0) = z(0) = 0$; (a) $x(0)$=0.10, (b) $x(0)$=0.11.

4.2. Three-step technique for stabilizing saddles [20]

In this section, a multistep feedback technique is suggested. In the 1st and the 2nd steps two different artificial SEQ states are created and are exploited to find the unknown coordinates of the saddle UEQ. In the final 3rd step these coordinates are used to stabilize an *a priori* unknown UEQ.

1st order system. To demonstrate the idea we start with an extremely simple one-dimensional example

$$\dot{x} = F(x, \xi). \tag{4.27}$$

Here $F(x,\xi)$ is a nonlinear function of variable x, while ξ is a set of parameters. The equilibrium states x_0 are found from an algebraic equation $F(x_0,\xi)$=0. If the derivative of $F'(x,\xi)\big|_{x0} > 0$, we deal with an UEQ. The UEQ can be stabilized by means of proportional feedback

$$\dot{x} = F(x, \xi) + k(x_0 - x). \tag{4.28}$$

If either the structure of the function $F(x,\xi)$ is unknown or it contains some unknown parameter, then x_0 is also unknown. Therefore the proportional feedback cannot be applied directly. However, we demonstrate that this UEQ can be still stabilized by multistep proportional feedback. Stabilization is achieved in three steps. In the 1st and the 2nd steps we apply proportional feedback with an arbitrarily chosen reference points $r_{1,2}$:

$$\dot{x} = F(x,\xi) + k(r_{1,2} - x), \tag{4.29}$$

where $r_{1,2}$ are any real constants, either positive or negative (zero value is also applicable). For sufficiently large k the feedback creates artificial SEQ states, $x_{1,2}$, which satisfy the steady-state equations $F(x_{1,2},\xi)+k(r_{1,2}-x_1)=0$. Note, that the control terms $k(r_{1,2}-x_1)$, in general, do not vanish, because $r_{1,2}$ are not the natural UEQ states of the original Eq. (4.27). Assuming, that the chosen reference points $r_{1,2}$ are not too far from x_0, we formally linearize the nonlinear functions $F(x_{1,2},\xi)$ around x_0: $F(x_{1,2},\xi) = F(x_0,\xi) + F'(x,\xi)|_{x0}(x_{1,2} - x_0)$. Here $F(x_0,\xi)=0$ by definition. Then the nonlinear steady-state equations read

$$F'(x,\xi)(x_{1,2} - x_0) + k(r_{1,2} - x_{1,2}) = 0. \tag{4.30}$$

These two linear equations have two unknowns, namely $F'(x,\xi)$ and x_0. Any of them or both can be easily derived. Specifically for x_0, Eq. (4.30) yields:

$$x_0 = \frac{r_1 x_2 - r_2 x_1}{(r_1 - x_1) - (r_2 - x_2)}. \tag{4.31}$$

Eventually, we use the derived value of x_0 in the final 3rd step of stabilization, given by Eq. (4.28).

As a specific mathematical example we consider Eq. (4.27) with $F(x,\xi)=ax-\xi$, where ξ is an *a priori* unknown parameter. It has a single UEQ: $x_0=\xi/a$. However, it is unknown because of ξ. Two preparatory steps with r_1 and r_2 give $x_1=(kr_1-\xi)/(k-a)$ and $x_2=(kr_2-\xi)/(k-a)$, respectively. Finally, the intrinsic UEQ x_0 is obtained from formula (4.31). One can check, that x_0 from (4.31) coincides with the expected value $x_0=\xi/a$.

2nd order system. The technique is applicable to higher order systems as well, e.g. the 2nd order dynamical system

$$\dot{x} = y, \quad \dot{y} = F(x,y). \tag{4.32}$$

The equilibrium has two coordinates. One of them is trivial: $y_0=0$. The x_0 is found from $F(x_0,0)=0$. If either $F'_x(x,y)|_{x0,y0}>0$ or $F'_y(x,y)|_{x0,y0}>0$, or both derivatives are positive, the equilibrium is an UEQ. Depending on the structure of $F(x,y)$ and the inherent parameters the UEQ might be either a node, a spiral or a saddle. Any of them can be stabilized using the proportional feedback:

$$\dot{x} = y, \quad \dot{y} = F(x,y) + k_1(r_{1,2} - x) - k_2 y. \tag{4.33}$$

Here, in the second control term with coefficient k_2 we employed the fact that y_0=0. Since the y-coordinates of the artificial equilibrium states $y_{1,2}$=0, the $x_{1,2}$ are found from the steady-state equations: $F(x_{1,2},0)+k_1(r_{1,2}-x_{1,2})=0$. After linearization $F(x_{1,2},0) = F(x_0,0) + F'(x,y)|_{x0,y0}(x_{1,2}-x_0) = F'(x,y)|_{x0,y0}(x_{1,2}-x_0)$ we come to a set of two linear equations, similar to the one-dimensional example and finally to the expression for x_0, exactly the same as formula (4.31).

Mechanical pendulum. To be specific we consider the set of equations

$$\begin{aligned} \dot{x} &= y, \\ \dot{y} &= -by - \sin x + \xi. \end{aligned} \tag{4.34}$$

Here x is the angle between the downward vertical and the rod, y is the angular velocity, b is the damping coefficient, and ξ is a constant, but generally unknown torque. For small torque ξ<1, the system has two equilibrium states $(x_{01,02},y_{01,02})=(x_{01,02},0)$, where $x_{01}=\arcsin\xi$, $x_{02}=\pi-\arcsin\xi$. The x_{01} corresponds to the SEQ, while the x_{02} is the x-coordinate of the saddle UEQ. The controlled pendulum is described by

$$\begin{aligned} \dot{x} &= y, \\ \dot{y} &= -by - \sin x + \xi + k_1(x_{02} - x) - k_2 y. \end{aligned} \tag{4.35}$$

The procedure of finding the coordinate x_{02} of the UEQ is the same as for the 2nd order system described in the previous subsection. Linearization of Eq. (4.35) around x_{02} gives the characteristic equation

$$\lambda^2 + (b + k_2)\lambda + k_1 + \cos x_{02} = 0.$$

For small ξ the angle $x_{02}\approx\pi$, thus $\lambda_{1,2}= -(b+k_2)/2\pm[(b+k_2)^2/4-k_1+1)]^{1/2}$. The threshold value of the feedback coefficient is k_{1th}=1, for which the largest eigenvalue λ_1 crosses zero from positive to negative values. The optimal value of the feedback coefficient $k_{1opt}=1+(b+k_2)^2/4$; the eigenvalues are both negative and equal to each other, $\lambda_1=\lambda_2= -(b+k_2)/2$. Further increase of k_1 makes the eigenvalues complex, but does not change their real parts. Therefore, for higher feedback coefficients the convergence rate saturates with k_1 and is fully determined by $(b+k_2)$. In the case of weak damping ($b\ll1$) a reasonable pair of

the feedback coefficients is k_1=2 and k_2=2, yielding Re$\lambda_{1,2}\approx-1$. Numerical results are shown in Fig. 4.6.

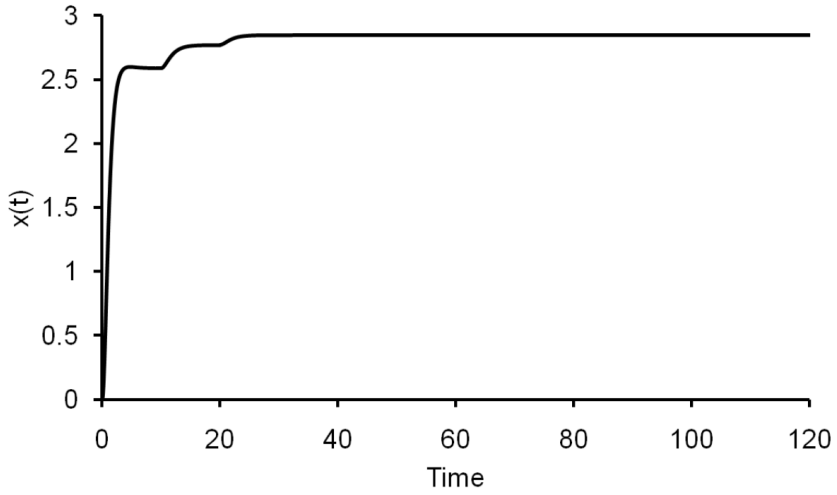

FIG. 4.6. Stabilization of the UEQ of a mechanical pendulum from Eq. (4.35). b=0.1, ξ=0.3, r_1=2.7, r_2=2.8, k_1=k_2=2. Initial conditions $x(0)$=$y(0)$=0. The control is switched on at t=0. The value stabilized in the 1st step x_1=2.5867, the value stabilized in the 2nd step x_2=2.7670, the reference point calculated from formula (4.31) x_{02}=2.8411, the value stabilized in the 3rd step x_3=2.8449, the remaining difference in the 3rd step $\delta=x_{02}-x_3=-0.0038$, $|\delta|/x_{02}\approx 0.1\%$, the analytical value of the UEQ calculated from formula $x_0=\pi-\arcsin\xi=2.8369$.

Duffing–Lindberg chaotic oscillator. The oscillator is described by a set of three differential equations [Lindberg *et al*. 2009; Tamaševičius *et al*. 2009a]:

$$\begin{aligned} \dot{x} &= y, \\ \dot{y} &= x - x^3 + by - cz + \xi, \\ \dot{z} &= \omega_0 (y - z). \end{aligned} \tag{4.36}$$

For $|\xi| < 2/\sqrt{27}$ the system has three equilibrium states $(x_0,y_0,z_0)=(x_0,0,0)$. The x-coordinates are found from a cubic steady-state equation $x_0^3 - x_0 - \xi = 0$. For ξ=0 the solution is simple: x_{01}=−1, x_{02}=0, x_{03}=1, the same as for the DH oscillator. For non-zero ξ the expressions are:

$$\begin{aligned} &x_{01} = -h\cos\frac{\pi-\theta}{3}, \quad x_{02} = -h\cos\frac{\pi+\theta}{3}, \\ &x_{03} = h\cos\frac{\theta}{3}, \quad h = \frac{2}{\sqrt{3}}, \quad \theta = \arccos\frac{3\xi}{h}. \end{aligned} \tag{4.37}$$

All the equilibrium states are unstable. The side states, x_{01} and x_{03} are either unstable nodes or unstable spirals. The most complicated is the middle one, x_{02} in the sense that it is a saddle. Similarly to the previous examples we apply proportional feedback in the form of $k_1(x_0-x)-k_2y$:

$$\begin{aligned}\dot{x} &= y,\\ \dot{y} &= x - x^3 + by - cz + \xi + k_1(x_{02} - x) - k_2 y,\\ \dot{z} &= \omega_0(y - z).\end{aligned} \tag{4.38}$$

The coordinate x_{02} of the UEQ can be found from (4.31). We note, that in equation for variable y it is possible to use one more feedback term, namely $-k_3z$. However, two terms are sufficient for stabilization. Linearization of Eq. (4.38) around x_{02} leads to a cubic characteristic equation $\lambda^3+a_3\lambda^2+a_2\lambda+a_1=0$, where

$$\begin{aligned}a_1 &= \omega_0(k_1 - 1),\\ a_2 &= k_1 + \omega_0(k_2 + c - b) - 1,\\ a_3 &= k_2 + \omega_0 - b.\end{aligned} \tag{4.39}$$

When deriving expressions (4.39) we assumed for simplicity that $3x_{02}^2 << 1$. The 3rd-order system (4.38) is stable, if the eigenvalues $\mathrm{Re}\lambda_{1,2,3}$ of the characteristic equation are all negative. $\mathrm{Re}\lambda_{1,2,3}<0$, if the all following inequalities are fulfilled:

$$a_3 > 0, \quad a_3a_2 - a_1 > 0, \quad a_1 > 0. \tag{4.40}$$

Inequalities (4.40) are derived using Ruth–Hurwitz criterion similarly to inequalities (2.7) in Chapter 2. The $a_1>0$, if $k_1>1$. Once $k_1>1$, the second inequality is easily fulfilled for the given parameters c and b (even for $k_2=0$). Finally, $a_3>0$ holds for the given parameters ω_0 and b (even for $k_2=0$). However, $k_2>0$ makes the transients shorter. Numerical results are presented in Fig. 4.7.

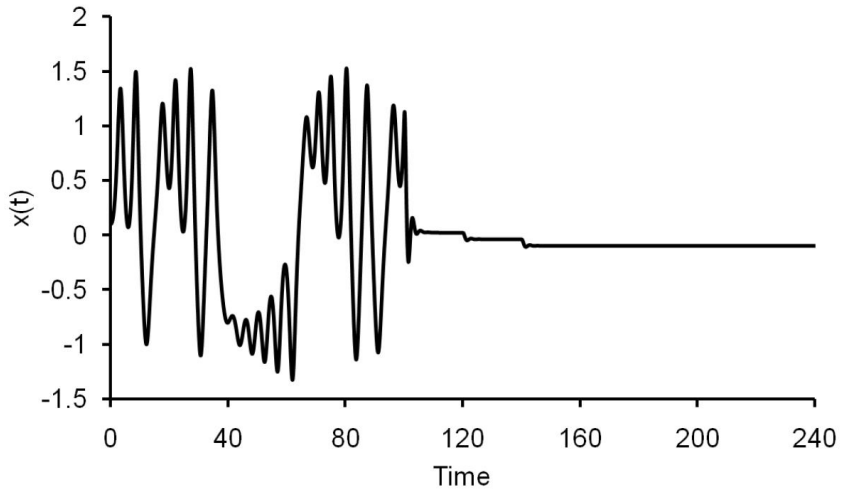

FIG. 4.7. Stabilization of the UEQ of the Duffing–Lindberg oscillator from Eq. (4.38). b=0.35, c=1.6, ω_0=0.5, ξ=0.1, r_1=0, r_2=−0.05, k_1=6, k_2=2. Initial conditions $x(0)$=0.1, $y(0)$=$z(0)$=0. Control is switched on at t=100. The value stabilized in the 1st step x_1=0.0200, the value stabilized in the 2nd step x_2=−0.0400, the reference point calculated from formula (4.31) x_{02}=−0.1, the value stabilized in the 3rd step x_3=−0.0998, the remaining difference in the 3rd step δ=x_{02}−x_3=−0.0002, $|\delta|/|x_{02}|$≈0.2%, the analytical value of the UEQ calculated from formula (4.37) x_{02}=−0.1010.

4.3. Nonlinear controller for stabilizing saddles [12]

In this Section, we describe an adaptive feedback technique, employing a nonlinear controller (the nonlinearity is a piecewise constant step function). To illustrate the idea, we start with a one-dimensional mathematical example

$$\dot{x} = x - a. \tag{4.41}$$

It has a single UEQ, x_0=a. Fluctuations grow up exponentially with an exponent λ=+1. The UEQ can be stabilized by means of proportional feedback

$$\dot{x} = x - a + k(x_0 - x), \tag{4.42}$$

provided the feedback gain k>k_{th}=1. Now the exponent λ=1−k is negative. Note that the control term $k(x_0-x)$ vanishes, when the goal equilibrium $x\to x_0$ is achieved. However, when the equation contains an unknown parameter, e.g., an unpredictable perturbation p

$$\dot{x} = x - p \tag{4.43}$$

the equilibrium x_0=p is also undefined, and therefore, the proportional feedback procedure cannot be applied directly. In this case, an adaptive technique, e.g.,

an auxiliary unstable filter, should be used in the feedback loop. In contrast to the linear controllers, described in [Pyragas *et al*., 2002, 2004], here we introduce a nonlinear controller (see also Fig. 4.8):

$$\begin{aligned} \dot{x} &= x - p + k(r - x), \\ \dot{r} &= v\,\mathrm{sgn}(r - x)H(|r - x| - \varepsilon / k). \end{aligned} \tag{4.44}$$

Here r is a variable reference point, the sgn(u) is the sign function, i.e., sgn(u>0)=1, sgn(u<0)= −1, the H is the Heaviside function, i.e., $H(u\le 0)=0$, $H(u>0)=1$, the 2ε is a pre-set small tolerance gap, and v is a constant "velocity", to be discussed later. The nonlinear function H actually is a piecewise constant function. This feature essentially simplifies the analysis.

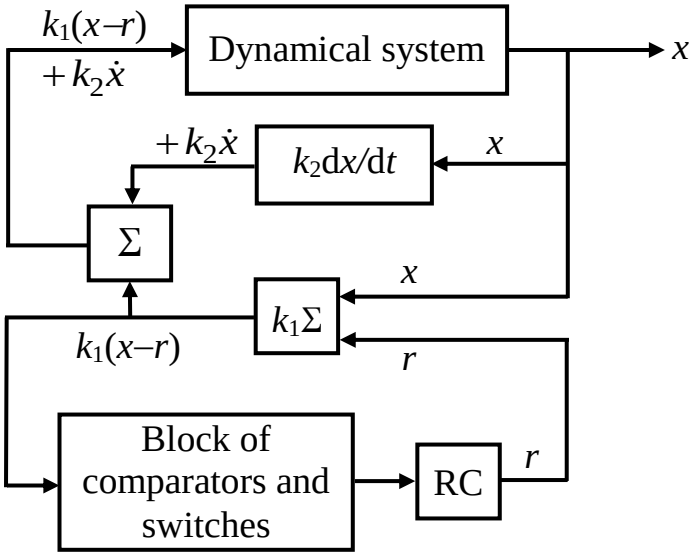

FIG. 4.8. Block diagram of stabilizing saddle state by means of the nonlinear controller.

***Case* 1: $|r-x|\le \varepsilon/k \ll 1$**. In this case, the $\dot{r}=0$. Consequently r=const. It can be formally found from the upper limit $|r-x_0|=\varepsilon/k$ or $r=x_0\pm\varepsilon/k$. Then Eq. (4.44) reads:

$$\dot{x} = x - p + k(x_0 \pm \varepsilon / k - x). \tag{4.45}$$

Eq. (4.45) has a stable equilibrium solution $x_0=p\pm\varepsilon$ or $x_0\approx p$ (with a small error of ε), as expected. However, this solution is a very formal one, since it still contains unknown parameter p. Practically, we have to start with r=0 in the control term of Eq. (4.44):

$$\dot{x} = x - p + kx = (1-k)x - p. \tag{4.46}$$

Now we can consider analytically evolution of the variable $x(t)$ also of the difference $(r-x)$ under a step perturbation p, e.g., from zero value to its nominal value p. Using the method of variation of constants and assuming the initial condition $x(0)=0$, we obtain

$$x(t) = -\frac{p}{k-1}[1-\exp(1-k)t]. \tag{4.47}$$

For a short time interval $(t<<1)$, formula (4.47) reads: $x(t)\approx -pt$. The formula gives somewhat puzzling result. Though the final value of $x(t)=x_0=p>0$ from Eq. (4.43), the transient value $x(t)$ exhibits negative sign: $x(t)\propto -p$. However, this feature coincides very well with the negative drop of $x(t)$, observed previously in Chapter 3 both numerically and experimentally.

Since $r=0$, the difference $(r-x)= -x$ is given by the same formula as (4.47), but with an opposite sign. Correspondingly, $(r-x)\approx pt$. Formula (4.47) is valid until $|r-x|=\leq \varepsilon/k$. Thus, the time moment t_1, when the difference $(r-x)$ reaches ε/k, is $t_1=\varepsilon/(pk)$.

***Case* 2: $|r-x| > \varepsilon/k$.** In this case, the $\dot{r} = v\,\mathrm{sgn}(r-x)$ and $r = vt\,\mathrm{sgn}(r-x)+r_0$. For $(r-x)>0$ (result from *Case* 1) and $r_0=0$, the variable reference point r is simply $r= +vt$. Thus, Eq. (4.44) reads

$$\dot{x} = (1-k)x - p + kvt. \tag{4.48}$$

Applying the method of variation of constants and using the initial condition $x(t_1)= -\varepsilon/k$, we find at $t\geq t_1$

$$x(t) = -\frac{p}{k-1}[1-\exp(1-k)(t-t_1)] + \frac{kv}{(k-1)^2}[(k-1)(t-t_1)-1]$$
$$+\left[\frac{kv}{(k-1)^2} - \frac{\varepsilon}{k}\right]\exp(1-k)(t-t_1).$$

The formula for $x(t)$ is very cumbersome. It becomes essentially simpler for $t>>1$: $x(t)=(kvt-p)/(k-1)$. From this simplified expression, we can easily find the time moment t_2, when the variable $x(t)$ from its negative value $(x\propto -p)$ crosses zero and becomes positive: $t_2=p/(kv)$. The difference $(r-x)=vt-x = (p-vt)/(k-1)$. The above formulas for $x(t)$ and $(r-x)$ are valid until $(r-x)$

reduces to ε/k. The corresponding time moment, when $(r-x)$ reaches ε/k, is $t_3 \approx p/v$. The value of variable $x(t_3) \approx p$, as expected.

The analytical results are compared with the results of direct numerical integration of Eq. (4.44) in Fig. 4.9. The transient behaviour reflects all the analytical estimations, including the negative drop of $x(t)$ at $0<t<t_2$. The time intervals $t_2 \approx 33$ and $t_3 \approx 167$ agree very well with the values, found from the corresponding formulas $t_2=p/(kv)$ and $t_3=p/v$. The transient time $t_{tr}=t_1+t_3$ is governed by its largest summand $t_3=p/v$. The larger is the "velocity" v, the shorter is the transient. However, v cannot be set too large. The point is that the time duration of crossing the tolerance gap 2ε, estimated as $t_\varepsilon \approx 2\varepsilon/(kv)$, should not be shorter than the characteristic time constant of the controlled system $t^* \approx (k-1)^{-1}$. Otherwise, autonomous periodic up- and down-crossings of the tolerance gap would arise. This intuitive requirement gives an estimate for the "velocity": $v<v_{\max}=2\varepsilon(k-1)/k$. The selection of the parameters in Fig. 4.9 is motivated by the following. The threshold gain $k_{\text{th}}=1$. Therefore, the gain parameter is taken large enough ($k=5$) to ensure small value of t_2, consequently small negative drop of the variable $x(t)$. The value of ε is set small ($\varepsilon=0.005$) to obtain narrow tolerance gap ($2\varepsilon=0.01$), compared to the amplitude of the main variable, $x(t>t_3)=p=1$. According to the formula for $v_{\max}$, the permissible "velocity" $v_{\max}=0.008$. The actual "velocity" is set somewhat lower: $v=0.006$.
The plots (a) and (b) in Fig. 4.9, for the simplified analytical and "exact" numerical integration results, respectively, look nearly identical. However, we intentionally present both of them in order to demonstrate that the simplifying assumptions made in the analytical treatment (*Case*1 and *Case* 2) are valid.

Duffing–Holmes (DH) oscillator. Let us consider now two-dimensional physical example, namely the damped DH oscillator, given either by

$$\ddot{x} + b\dot{x} - x + x^3 = 0 \tag{4.49}$$

or by

$$\begin{aligned} \dot{x} &= y, \\ \dot{y} &= x - x^3 - by. \end{aligned} \tag{4.50}$$

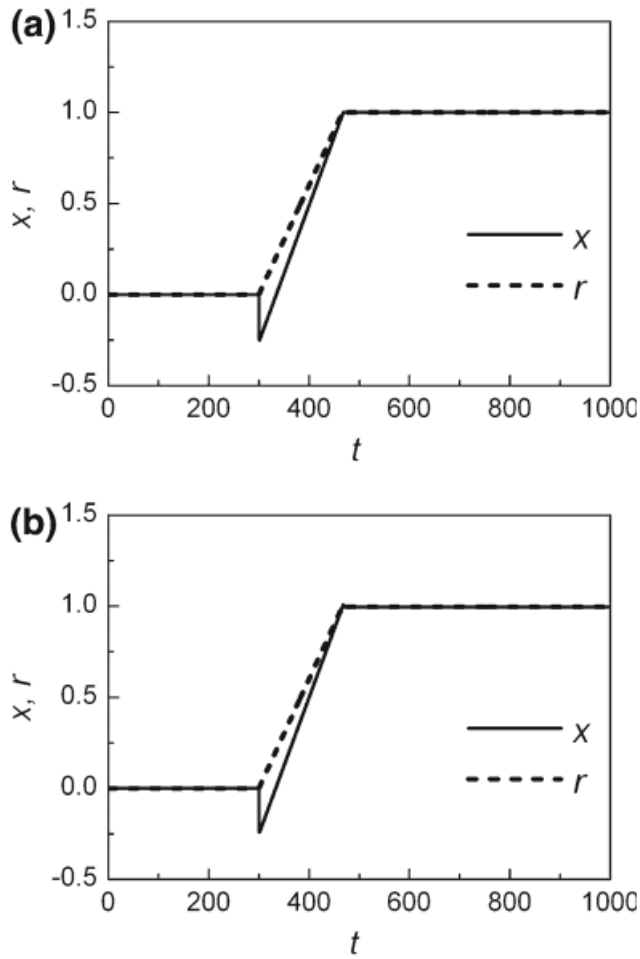

FIG. 4.9. Evolution of variables $x(t)$ and $r(t)$. (a) Analytical results, here time is shifted by 300 units. (b) Numerical results from Eq. (4.44). p=1, k=5, ε=0.005, v=0.006, $x(0)$=0.01, $r(0)$=0, the p is switched on at t =300.

In Eq. 4.49) and Eq. (4.50) b is the damping coefficient. The physical meaning of the variables are explained in [Moon, 1987; Ott, 1993]. The DH oscillator has three equilibrium states: two stable states $(x_0,y_0)=(\pm 1,0)$ and one unstable equilibrium (a saddle) at the origin $(x_0,y_0)=(0,0)$. We shall stabilize the saddle by means of a nonlinear controller:

$$\begin{aligned} \dot{x} &= y, \\ \dot{y} &= x - x^3 - by - p + k_1(r - x) - k_2\dot{x}, \\ \dot{r} &= v\,\mathrm{sgn}(r - x)H(|r - x| - \varepsilon / k). \end{aligned} \tag{4.51}$$

Here p is an *a priori* unknown perturbation. It changes the x-coordinates of all the equilibrium states. The positions of the perturbed equilibrium states are:

$$x_{01} = -\frac{2}{\sqrt{3}}\cos\frac{\pi-\theta}{3}, \quad x_{03} = \frac{2}{\sqrt{3}}\cos\frac{\theta}{3},$$
$$x_{02} = -\frac{2}{\sqrt{3}}\cos\frac{\pi+\theta}{3}, \quad \theta = \arccos\left(-\frac{3\sqrt{3}}{2}p\right).$$

Here $x_{01,03}$ correspond to the stable spirals, and x_{02} is a coordinate of the saddle. For small p, the $\theta \approx \pi/2 + 3\sqrt{3}p/2$ and the $x_{02} \approx p$. In Eq. (4.51), along with the proportional term $k_1(r-x)$, there is an additional derivative term '$-k_2\dot{x}$'. The latter term, itself, is not able to stabilize a saddle. However, it improves considerably the performance of the controller, especially for small damping coefficient b.

We analyse the stability of the system (4.51), when the difference $k|r-x|$ is within the tolerance gap, i.e., $|r-x|<\varepsilon/k$, the perturbation p is set to zero for simplicity (without the loss of generality), and the reference point $r=x_{02}=0$. The linearized Eq. (4.51) read

$$\begin{aligned} \dot{x} &= y, \\ \dot{y} &= x - by - k_1 x - k_2 y. \end{aligned} \tag{4.52}$$

The corresponding characteristic equation is a simple quadratic equation

$$\lambda^2 + (b + k_2)\lambda + (k_1 - 1) = 0,$$

which can be solved analytically:

$$\lambda_{1,2} = -\frac{b+k_2}{2} \pm \sqrt{\frac{(b+k_2)^2}{4} - (k_1 - 1)}.$$

The real parts of the eigenvalues $\mathrm{Re}\lambda_{1,2}$ are both negative (ensuring the stability of the system) if $k_1 > k_{th} = 1$. The optimal value of the feedback gain is $k_1 = 1 + (b+k_2)^2/4$, providing the best pair, i.e., the both values are negative and equal to each other, $\lambda_{1,2} = -(b+k_2)/2$. Further increase in k_1 makes the eigenvalues complex, but does not change the $\mathrm{Re}\lambda_{1,2}$.

Numerical results are shown in Fig. 4.10. The new stabilized saddle equilibrium $x(t) \to x_{02} \approx 0.2$ is in an agreement with the analytical prediction ($x_{02} \approx p = 0.2$). In numerical simulation, the damping parameter b was intentionally chosen small ($b = 0.01$) to illustrate the performance of the method

in the case of a weakly damped system. In Chapter 3, we demonstrated that stabilization of saddles in weakly damped systems required rather complicated controllers, e.g., containing both unstable and stable filters. The feedback gain was adjusted to k_1=5 in order to reach the optimal negative eigenvalues $\lambda_{1,2}$.

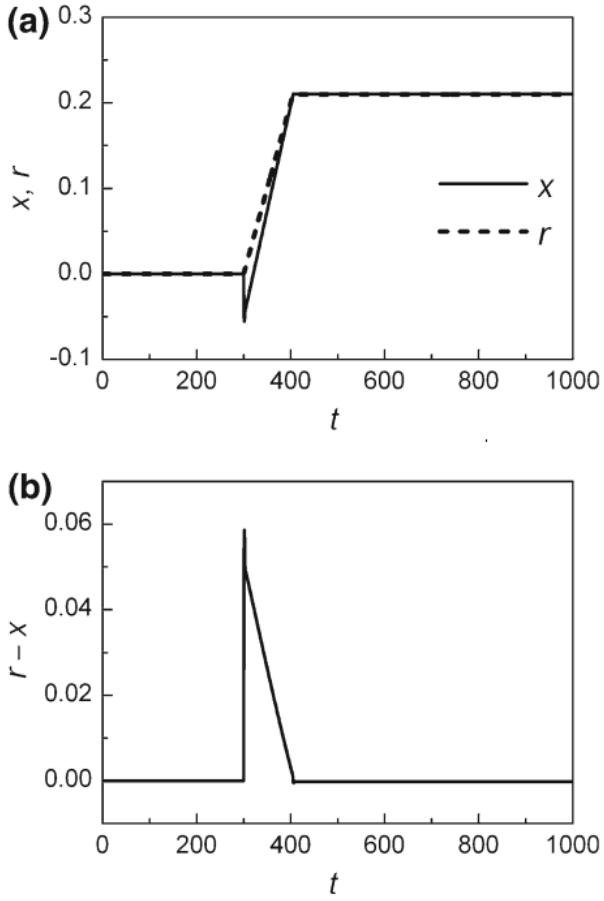

FIG. 4.10. Stabilization of a saddle equilibrium in the damped DH system from Eq. (4.51). (a) Evolution of the variables $x(t)$ and $r(t)$. (b) Evolution of the difference $r(t)$–$x(t)$. b=0.01, p=0.2, k_1=5, k_2=2, ε=0.005, v=0.002, $x(0)=10^{-4}$, $r(0)$=0, the perturbation p is switched on at t =300.

Lorenz system. The second example is the Lorenz system [Lorenz, 1963]:

$$\begin{aligned} \dot{x} &= -\sigma x + \sigma y, \\ \dot{y} &= -xz + \rho x - y, \\ \dot{z} &= xy - bz. \end{aligned} \tag{4.53}$$

The physical meaning of the variables and the coefficients are discussed in [Moon, 1987; Ott, 1993]. For ρ>1, there are three equilibrium states, namely a saddle (x_0,y_0,z_0) at the origin and two symmetrical spirals $(x_{1,2},y_{1,2},z_{1,2})$:

$$(0,0,0), \quad (\pm\sqrt{b(\rho-1)},\pm\sqrt{b(\rho-1)},\rho-1).$$

If $\rho>\rho_{th}=\sigma(\sigma+b+3)/(\sigma-b-1)$, both spirals become unstable, yielding chaotic oscillations. For conventional parameter values $\sigma=10$ and $b=8/3$, most often used for the Lorenz system, the $\rho_{th}\approx 24.74$.

If an unknown perturbation p is applied to the system, say via variable z:

$$\begin{aligned} \dot{x} &= -\sigma x + \sigma y, \\ \dot{y} &= -xz + \rho x - y, \\ \dot{z} &= xy - bz + p, \end{aligned} \tag{4.54}$$

the coordinates of the equilibrium states and the threshold parameter ρ_{th} change in the following way:

$$(x_0, y_0, z_0) = (0,0, p/b), \quad (x_{1,2}, y_{1,2}, z_{1,2}) = (\pm Q, \pm Q, \rho - 1 - p/b),$$
$$Q = \sqrt{b(\rho-1)-p}, \quad \rho_{th} = \sigma(\sigma+b+3)/(\sigma-b-1) + p/b.$$

We will focus on stabilizing the saddle (x_0,y_0,z_0) by means of a nonlinear controller, discussed in the previous sections:

$$\begin{aligned} \dot{x} &= -\sigma x + \sigma y, \\ \dot{y} &= -xz + \rho x - y + k(r-y), \\ \dot{z} &= xy - bz + p, \\ \dot{r} &= v\,\mathrm{sgn}(r-y) H(|r-y| - \varepsilon/k). \end{aligned} \tag{4.55}$$

For simplicity, we analyze stabilization of the saddle equilibrium in the absence of the perturbation ($p = 0$) that at the origin (0,0,0), similarly as in the case of the Duffing system. We assume that the difference $k|r–y|$ is in the tolerance gap, so that the reference point r is constant and is set to zero. Eq. (4.55) linearized around the saddle equilibrium point, read:

$$\begin{aligned} \dot{x} &= -\sigma x + \sigma y, \\ \dot{y} &= \rho x - (k+1) y, \\ \dot{z} &= -bz. \end{aligned} \tag{4.56}$$

There are three exponents related to the linearized equations. The first and the second exponents are found from a quadratic characteristic equation

$$\lambda^2 + (\sigma + k + 1)\lambda + \sigma(k + 1 - \rho) = 0.$$

$$\lambda_{1,2} = -(\sigma + k + 1)/2 \pm \sqrt{(\sigma + k + 1)^2/4 - \sigma(k + 1 - \rho)}.$$

The both eigenvalues $\lambda_{1,2}<0$, if $k>\rho-1$. The third exponent is always negative, $\lambda_3=-b<0$. The three negative eigenvalues ensure stabilization of the saddle. According to the formula for the saddle coordinates $(x_0,y_0,z_0)=(0,0,p/b)$, the perturbation p does not influence the x- and the y-coordinates. If the saddle is stabilized before the perturbation p is applied, the $x_0=y_0=0$. Thus the dynamics of the z-coordinate under the influence of perturbation is described by an uncoupled equation:

$$\dot{z} = -bz + p, \tag{4.57}$$

which has a simple relaxation solution $z(t)=p/b[1-\exp(-bt)]$. The variables x and y remain zeros, the r and the $(r-y)$ are nearly zeros as well, despite the fact that perturbation p changes many parameters of the Lorenz system, e.g. all the coordinates of the spirals and the threshold value ρ_{th} of the onset of chaos. The rate of convergence to the perturbed saddle state $(0,0,p/b)$ depends neither on the feedback gain k nor on the "velocity" v of the controller, but on the damping coefficient of the Lorenz system b only.

If a perturbation p is applied to the Lorenz system via the equation for variable y:

$$\begin{aligned} \dot{x} &= -\sigma x + \sigma y, \\ \dot{y} &= -xz + \rho x - y - p, \\ \dot{z} &= xy - bz, \end{aligned} \tag{4.58}$$

the (x_0,y_0,z_0), where $y_0=x_0$ and $z_0 = x_0^2/b$, have three different x_0-coordinates:

$$x_{01} = -h\cos\frac{\pi-\alpha}{3}, \quad x_{03} = h\cos\frac{\alpha}{3}, \quad x_{02} = -h\cos\frac{\pi+\alpha}{3}, \quad h = 2\sqrt{\frac{b(\rho-1)}{3}},$$

$$\alpha = \arccos\left(-\frac{4bp}{h^3}\right) = \pi - \arccos\left(\frac{4bp}{h^3}\right).$$

Similarly to the DH oscillator, the $x_{01,03}$ correspond to the spirals and x_{02} is a coordinate of the saddle. The only difference is that the spirals in the Lorenz system at $\rho>\rho_{th}$ are unstable states. For small p, the $\alpha\approx\pi/2+4bp/h^3$ and the $x_{02}\approx p/(\rho-1)$.

Let us consider stabilization of the saddle by means of the nonlinear controller (numerical results are shown in Fig. 4.11):

$$\begin{aligned}
\dot{x} &= -\sigma x + \sigma y, \\
\dot{y} &= -xz + \rho x - y - p + k_1(r - x) + k_2(r - y), \\
\dot{z} &= xy - bz, \\
\dot{r} &= v\,\mathrm{sgn}(r - y)H(|r - y| - \varepsilon / k_2).
\end{aligned} \tag{4.59}$$

The equations are similar to Eq. (4.55), except the fact, that the system is perturbed via the equation for the y-variable, and the feedback contains and additional term $k_1(r-x)$. Since $x_{02}=y_{02}$, the both control terms $k_1(r-x)$ and $k_2(r-y)$ vanish, when the stabilization is achieved, $x(t)\to x_{02}$ and $y(t)\to y_{02}$. For small p the saddle coordinates are close to the origin ($x_{02}\approx 0$, $y_{02}\approx 0$, $z_{02}\approx 0$). Then the linearized equations read

$$\begin{aligned}
\dot{x} &= -\sigma x + \sigma y, \\
\dot{y} &= (\rho - k_1)x - (k_2 + 1)y, \\
\dot{z} &= -bz.
\end{aligned} \tag{4.60}$$

The last equation in Eq. (4.60) appears to be uncoupled. The corresponding characteristic equation and its solution are

$$\lambda^2 + (\sigma + k_2 + 1)\lambda + \sigma(k_1 + k_2 + 1 - \rho) = 0.$$

$$\lambda_{1.2} = -(\sigma + k_2 + 1)/2 \pm \sqrt{(\sigma + k_2 + 1)^2/4 - \sigma(k_1 + k_2 + 1 - \rho)}.$$

Two eigenvalues are negative, $\mathrm{Re}\lambda_{1,2}<0$, if $k_1+k_2>\rho-1$. The third eigenvalue can be found directly from $\dot{z} = -bz : \lambda_3 = -b < 0$.

An important result of this analysis is that the saddle equilibrium of the Lorenz system can be stabilized in three ways, i.e., with (1) $k_1=0$, $k_2>\rho-1$, (2) $k_1>\rho-1$, $k_2=0$ and (3) $k_1+k_2>\rho-1$. It means that the single control term, either $k_2(r-y)$ or $k_1(r-x)$, is sufficient. Whereas using both of them exhibits better performance in the sense, that the negative $\mathrm{Re}\lambda_{1,2}$ can have larger values.

The value of the stabilized z-coordinate in Fig. 4.11b is in a good agreement with the result from the analytical solution, $z_0 = p/b \approx 9.4$. The control term $r-y$ in Fig. 4.11b remains zero even at $t\geq 10$, when the perturbation is switched on, as predicted analytically. The stabilized value of y_0 in Fig. 4.11c well coincides with the analytical value $y_0=x_0=p/(\rho-1)=0.27$. The control term

r–*y* in Fig. 4.11d, in contrast to *r*–*y* in Fig. 4.11b, exhibits narrow spike during the transient process (10< *t* <13) and vanishes at *t* >13, as expected.

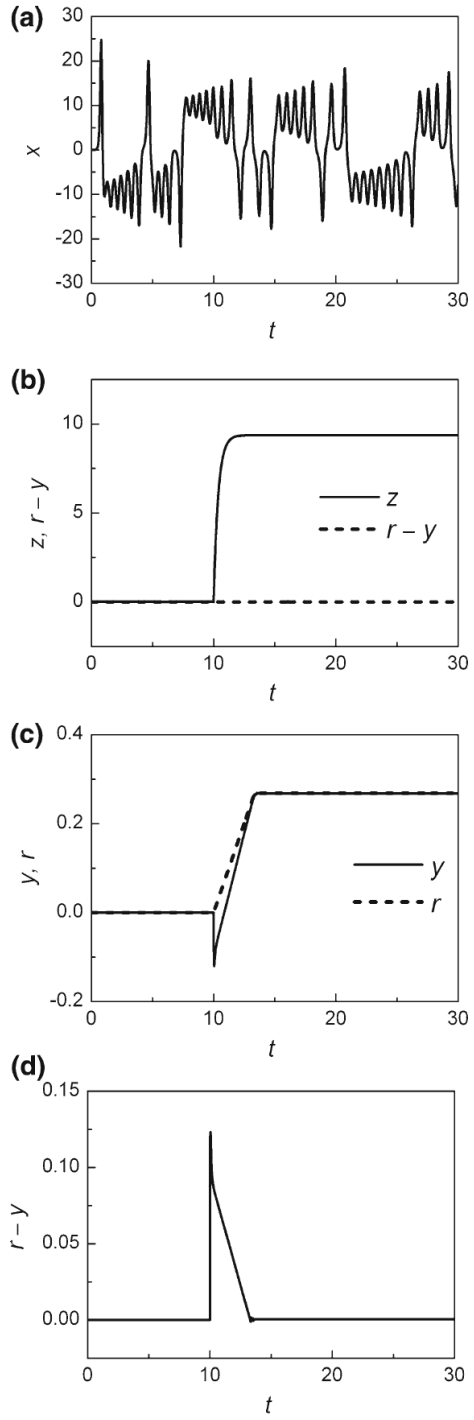

FIG. 4.11. (a) Chaotic oscillations from the uncontrolled and unperturbed Lorenz system from Eq. (4.53). (b) Stabilizing saddle from Eq. (4.55), $p = 25$, $k = 50$, $\varepsilon = 0.05$, $v = 0.05$. (c), (d) Stabilizing saddle from Eq. (4.59), $p = 10$, $k_1 = 70$, $k_2 = 70$, $\varepsilon = 0.05$, $v = 0.08$. In the all plots are $\sigma = 10$, $\rho = 38$, $b = 8/3$. The perturbation p is switched on at $t = 10$.

Analogue experiments. The DH damped oscillator and the Lorenz oscillator are sketched in *Appendix* 1 and *Appendix* 2, respectively. All signals have been recorded by means of a digital storage oscilloscope Tektronix TDS2014B. Experimental results are displayed in Fig. 4.12 and Fig. 4.13.

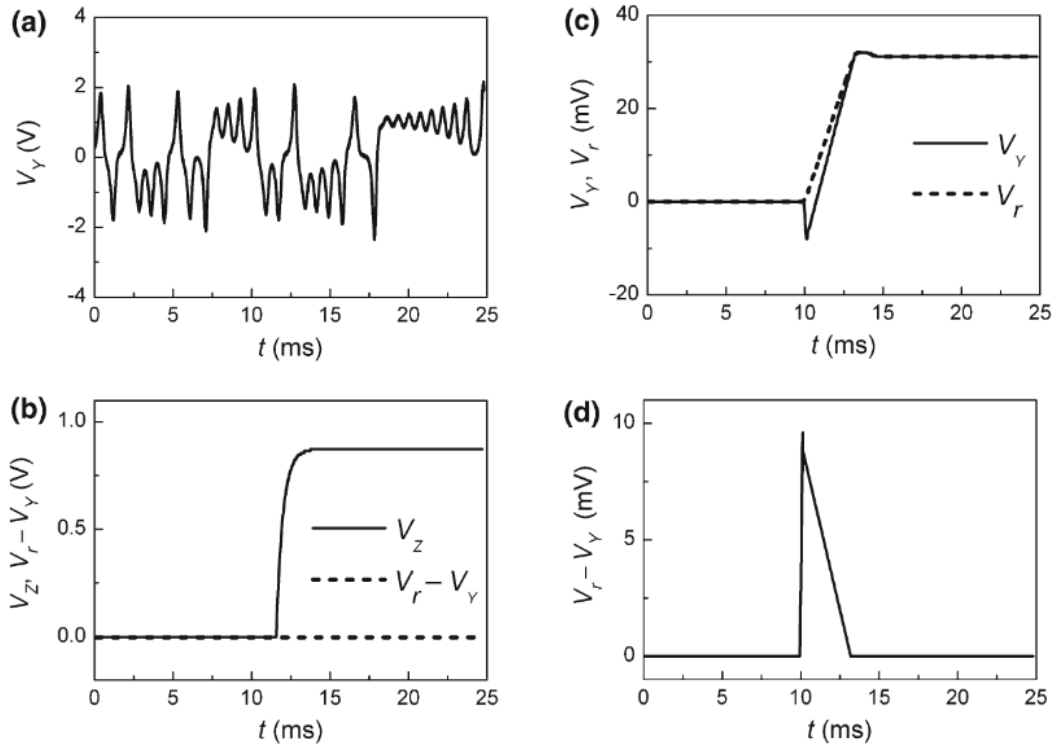

FIG. 4.12. (a) Oscillations from the uncontrolled and unperturbed Lorenz oscillator. (b) Stabilizing saddle, when $\bar{p}$ is applied to the z-variable at t = 11.6 ms, $\bar{p}$ = 0.25, $\bar{k}$ =k_0=5, $\bar{\varepsilon}$ =0.0025, $\bar{v}$ =7.10^{-4}. (c,d) Stabilizing saddle, when $\bar{p}$ is applied to the y-variable at t=10 ms, $\bar{p}$ =0.1, $\bar{k}$ =k_0R/R_2=15 (here R_2=2.5 kΩ), $\bar{\varepsilon}$ = 0.0025, $\bar{v}$ = 7.10^{-4}. Parameters of the Lorenz oscillator $\bar{\rho}$ = 3.8, $\bar{b}$ = 0.27.

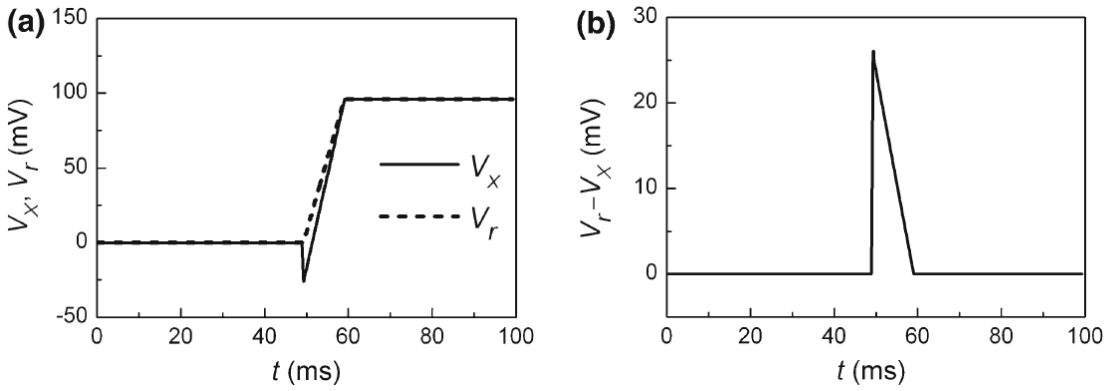

FIG. 4.13. Stabilization of a saddle in the DH oscillator. (a) $V_x(t)$ and $V_r(t)$. (b) Difference $V_r(t)-V_x(t)$. $b = R/Z$ = 0.01, V^* = 10 V (p = 0.2), $k_1 = k_0 = 5$, $k_2 = 1$, ε = 0.005, v = 0.001, p is switched on at t = 49 ms.

CHAPTER 5

CONTROLLING EQUILIBRIUM AND SYNCHRONY OF THE FITZHUGH–NAGUMO OSCILLATORS

5.1. Stabilizing equilibrium of a single FitzHugh–Nagumo oscillator [3]

In this section the FitzHugh–Nagumo (FHN) type model, which will be further used as a building block for composing arrays of oscillators, is described.

Mathematical model. We consider the following set of equations:

$$\begin{aligned} \dot{x} &= ax - f(x) - y - \xi, \\ \dot{y} &= x - by, \end{aligned} \tag{5.1}$$

$$f(x) = \begin{cases} d(x+1), & x < -1 \\ 0, & -1 \le x \le 1 \\ g(x-1), & x > 1. \end{cases} \tag{5.2}$$

All the coefficients in (5.1) and (5.2) are positive and constant, except the parameter ξ, which, in general, is unknown and/or slowly varies with time. Though the coefficients d and g are somewhat arbitrary (the only requirement is $d,g>a$), we consider the case of strong asymmetry $d \gg g$. The model can be treated as *asymmetric* FHN model, where the classical activation term $x-x^3$ [FitzHugh, 1961] is replaced with an asymmetric function $ax-f(x)$. It has different slopes at negative ($x<-1$) and positive ($x>1$) values of x. For

$$ab<1, \quad |\xi| < 1/b - a. \tag{5.3}$$

Eq. (5.1) has a single UEQ

$$x_0 = -b\xi/(1-ab), \quad y_0 = x_0/b, \tag{5.4}$$

and no SEQ. Due to the second inequality in (5.3) the $|x_0|<1$. For $\xi > 0$ the UEQ is in the negative quadrant ($x_0<0, y_0<0$). Linearization of Eq. (5.1) around (x_0,y_0) yields the characteristic equation

$$\lambda^2 - (a-b)\lambda + 1 - ab = 0, \tag{5.5}$$

which has two solutions that are independent on ξ:

$$\lambda_{1.2} = (a-b)/2 \pm \sqrt{(a+b)^2/4 - 1}. \tag{5.6}$$

For $a > b$, the real parts of $\lambda_{1,2}$ are positive, confirming that the equilibrium is unstable (either a spiral or a node). When $a > b$ and $a+b > 2$ both eigenvalues are positive and real (no imaginary part). In this case, the UEQ is an unstable node.

Now we add to Eq. (5.1) the third equation, describing a stable filter, and couple it to the FHN equations:

$$\begin{aligned} \dot{x} &= ax - f(x) - y - \xi + k(v - x), \\ \dot{y} &= x - by, \\ v &= \omega_f (x - v). \end{aligned} \tag{5.7}$$

Here k is the coupling coefficient and ω_f is the normalized threshold frequency of the filter. The system has the same equilibrium as the free-running system:

$$x_0 = v_0 = -b\xi/(1-ab), \quad y_0 = x_0/b, \tag{5.8}$$

which implies that the filter does not influence the position of the equilibrium (x_0, y_0) of the FHN system, but can change its stability properties.

The corresponding characteristic equation of the linearized system is

$$\lambda^3 + h_3\lambda^2 + h_2\lambda + h_1 = 0, \tag{5.9}$$

$$h_3 = -a + b + k + \omega_f, \; h_2 = 1 - ab + bk - (a-b)\omega_f, \; h_1 = (1-ab)\omega_f. \tag{5.10}$$

The system (5.7) is stable if the real parts of all three eigenvalues $\mathrm{Re}\lambda_{1,2,3}$ are negative. The results of the numerical solution of Eq. (5.9) are shown in Fig. 5.1.

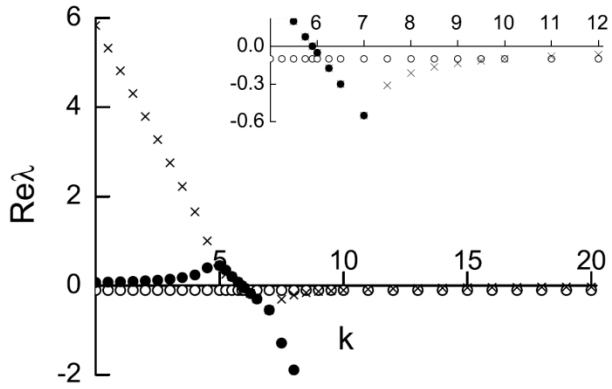

FIG. 5.1. Dependence of the Reλ on the coupling coefficient k from Eq. (5.9). $a = 6$, $b = 0.1$, $\omega_f = 0.1$. The insert is a zoomed view of the Reλ.

The largest eigenvalues Reλ cross zero and become negative at k = 5.9. The optimal values of the coupling coefficient k, providing the highest rate (λ=−0.1) of convergence to the SEQ, range from 6.5 to 10.

The necessary and sufficient conditions for stabilization can be found using the Hurwitz matrix

$$H = \begin{pmatrix} h_3 & h_1 & 0 \\ 1 & h_2 & 0 \\ 0 & h_3 & h_1 \end{pmatrix}. \qquad (5.11)$$

According to the Routh–Hurwitz stability criterion the eigenvalues Re$\lambda_{1,2,3}$ are all negative if the diagonal minors of the H matrix are all positive

$$\Delta_1 = h_3 > 0, \quad \Delta_2 = h_3 h_2 - h_1 > 0, \quad \Delta_3 = h_1 \Delta_2 > 0. \qquad (5.11)$$

Since Δ_2 should be positive according to the second inequality, the third inequality for Δ_3 can be replaced simply with h_1>0. This can be further simplified to (1−ab)>0 since ω_f >0 by definition. We note that, due to the first inequality in (5.3), the h_1>0 is always satisfied. Consequently, we should analyze Δ_1 and Δ_2. We estimate the threshold coupling coefficient k_{th} by requiring that for $k > k_{th}$ the two minors $\Delta_{1,2}$ are positive. The result is k_{th}=5.9 (for the used parameter values). It is in a good agreement with the corresponding threshold from Reλ(k) in Fig. 5.1.

Results of the numerical integration of Eq. (5.1) and Eq. (5.7) are shown in Fig. 5.2, Fig. 5.3, and Fig. 5.4.

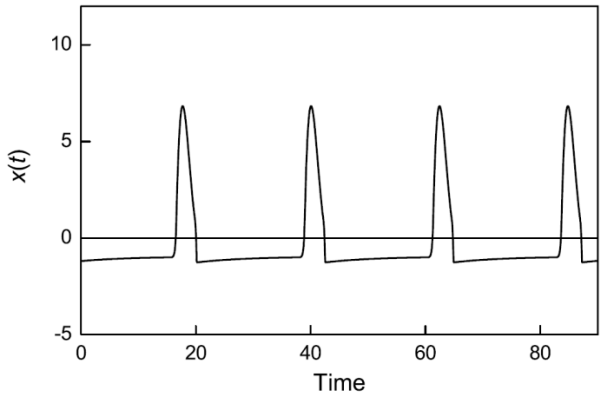

FIG. 5.2. Spikes $x(t)$ from Eq. (5.1). a = 6, b = 0.1, ξ = 1.7, d = 60, g = 7.

The waveform in Fig. 5.2 generated by the FHN model more closely resembles the behaviour of the spiking neurons in the Hodgkin−Huxley model than that of the classical FHN model with symmetric activation function $x-x^3$.

When the control ($k>k_{th}$) is turned on, the spikes are totally suppressed and the system is stabilized on non-zero equilibrium x_0, whereas the control signal $x-v$ vanishes.

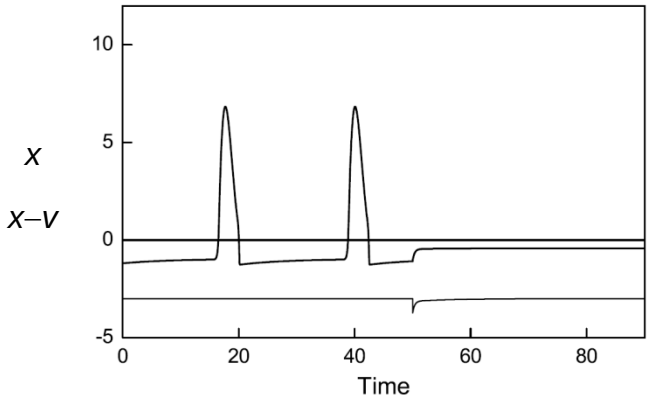

FIG. 5.3. Variable $x(t)$ (top trace) and control term $x-v$ (bottom trace). Control is switched on between two spikes. The control term display is lowered for the sake of clarity. $a = 6$, $b = 0.1$, $\xi = 1.7$, $d = 60$, $g = 7$, $\omega_f = 0.1$, $k = 9$.

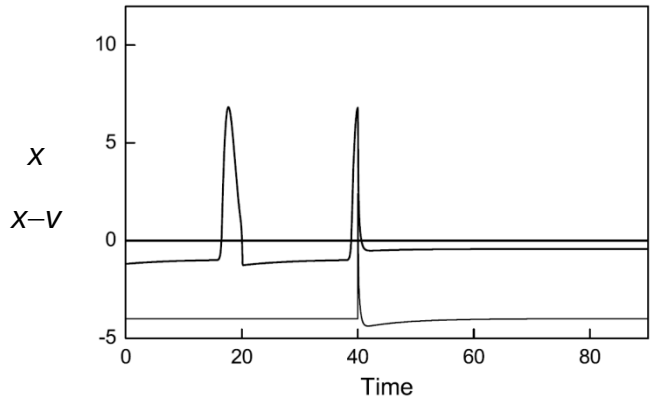

FIG. 5.4. Variable $x(t)$ (top trace) and control term $x-v$ (bottom trace). Control is switched on during a spike. Parameters the same as in Fig. 5.3.

Analogue experiments. The electrical circuit imitating the dynamics of the FHN model is sketched *Appendix* 4. Experimental results are shown in Fig. 5.6, Fig. 5.7, and Fig. 5.8. The spike train (Fig. 5.7) and the controlled dynamics (Figs. 5.8, Fig. 5.9) all are in a good agreement with the numerical results, presented in the previous subsection.

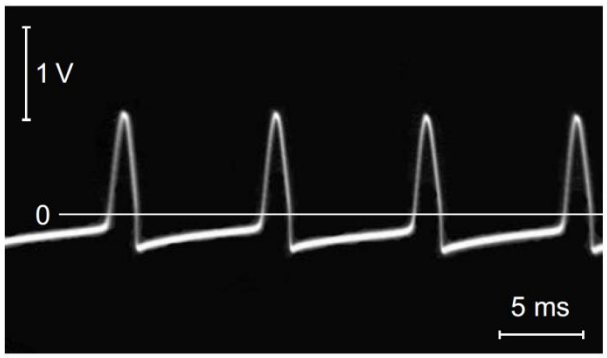

FIG. 5.7. Typical train of spikes $V_C(t)$ from the analogue circuit without control.

FIG. 5.8. Output voltage $V_C(t)$ (top trace) and control signal V_{R^*} (bottom trace) when control is switched on between two spikes. The control signal display is lowered for the sake of clarity.

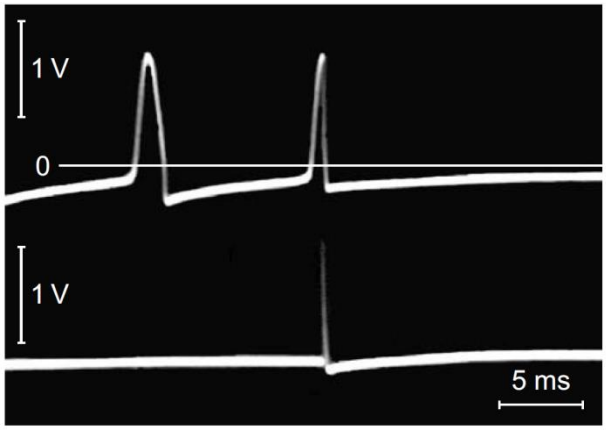

FIG. 5.9. Output voltage $V_C(t)$ (top trace) and control signal V_{R^*} (bottom trace) when control is switched on during a spike. The control signal display is lowered for the sake of clarity.

5.2. Synchrony in array of coupled FHN oscillators [5]

Mathematical model. The array is described by a set of 2*N* linearly coupled ordinary nonlinear differential equations:

$$\begin{aligned} \frac{dx_i}{dt} &= ax_i - f(x_i) - y_i - c_i + k(x_m - x_i), \\ \frac{dy_i}{dt} &= x_i - by_i, \quad i = 1, 2, \ldots, N. \end{aligned} \tag{5.12}$$

Here k is the coupling coefficient, N is the number of cells, the $f(x_i)$, similarly to Section (5.1), is given by a piece-wise linear approximation:

$$f(x_i) = \begin{cases} d(x_i + 1), & x_i < -1 \\ 0, & -1 \le x_i \le 1 \\ g(x_i - 1), & x_i > 1. \end{cases} \tag{5.13}$$

In Eq. (5.12) x_m is the mean value of the variables x_i:

$$x_m = \frac{1}{N} \sum_{i=1}^{N} x_i \ . \tag{5.14}$$

The constant bias c_i in Eq. (5.12) is intentionally set different for every individual oscillator to make them non-identical units.

Numerical simulation. Numerical results for $N = 30$, $a = 3.4$, $b = 0.15$, $c_i = 3 - 0.05(i-1)$, $d = 60$, $g = 3.4$ are presented in Fig. 5.10 and Fig. 5.11.

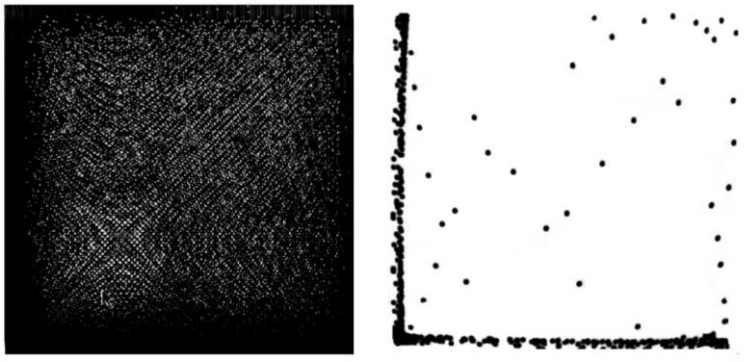

FIG. 5.10. Nonsynchronized case ($k = 0$). (Left) phase portrait $x_i(t)$ *vs.* $x_j(t)$, $i \neq j$. (Right) Poincaré section, $x_i(t)$ *vs.* $x_j(t)$ at $x_l(t) = 1$, $dx_l(t)/dt < 0$, $i \neq j \neq l$.

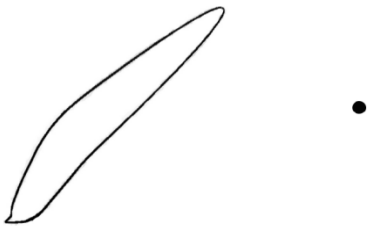

FIG. 5.11. Synchronized case, k=0.7. (Ellipse) phase portrait $x_i(t)$ *vs.* $x_j(t)$, $i \neq j$. (Dot) Poincaré section $x_i(t)$ *vs.* $x_j(t)$ at $x_l(t)$=1, $dx_l(t)/dt<0$, $i \neq j \neq l$.

Analogue electrical circuit. An array of N (i =1,2,…, N) mean-field coupled (star configuration) FHN oscillators is sketched in Fig. 5.12.

General view of the hardware analogue circuit is shown in Fig. 5.13. The construction contains four floors. The electronic oscillators are arranged on the three floors (10 oscillators on each floor), whereas the all coupling resistors R^* are placed on one floor. Typical output waveform from an individual oscillator, incorporated in an array, is presented in Fig. 5.14.

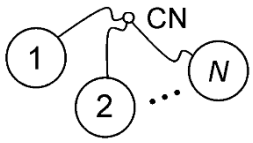

FIG. 5.12. Block diagram of FHN oscillators coupled via resistors R^* to the coupling node CN. Coupling resistor R^* is shown in the circuit diagram of a single oscillator in *Appendix* 4.

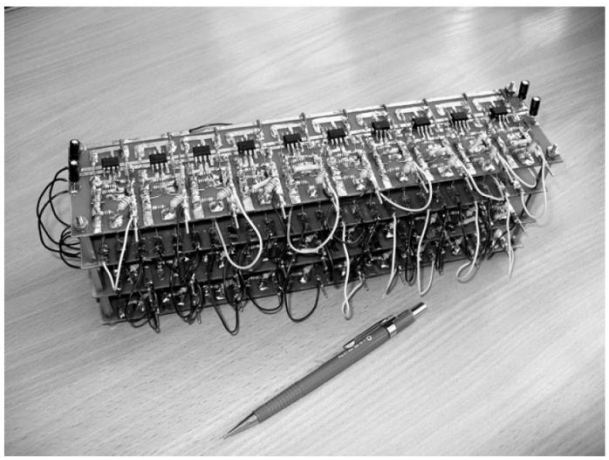

FIG. 5.13. Hardware of the array of 30 FHN oscillators. Dimensions W×H×D= 270 mm × 85 mm × 65 mm.

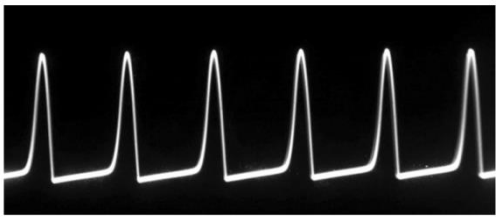

FIG. 5.14. Output waveform from an individual FHN oscillator in an array $V_i(t)$. Spike amplitude ≈3 V, inter-spike interval ≈80 μs, frequency ≈12 kHz.

Phase portraits and Poincaré sections. In the case of weak coupling (large R^*), the oscillators are spiking independently at their individual frequencies. The intricate phase portrait and multi-dot Poincaré section (Fig. 5.15) do confirm this statement. In all analogue simulations the exposure time of the camera was fixed at 1/8 s. For the spiking frequency ≈12 kHz this yielded about 1500 snapped periods of the waveforms in the phase portraits and about 1500 snapped dots in the Poincaré sections.

For strong coupling (small R^*) oscillators become fully synchronized, i.e. phase-locked, as is evident from the phase portrait, displaying a simple ellipse and a single dot in the Poincaré section (Fig. 5.16).

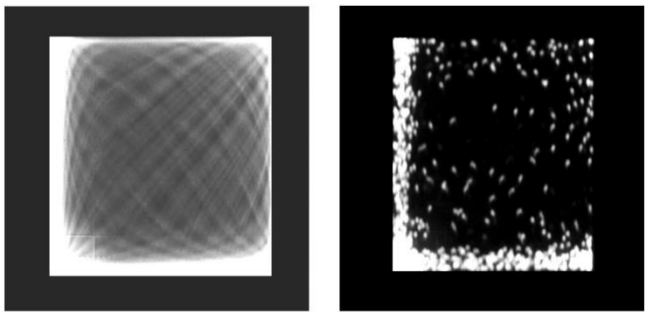

FIG. 5.15. Nonsynchronized case. (Left) phase portrait $V_i(t)$ *vs.* $V_j(t)$, $i \neq j$. (Right) Poincaré section, $V_i(t)$ *vs.* $V_j(t)$ at $V_l(t)$=1 V, $dV_l(t)/dt<0$, $i \neq j \neq l$.

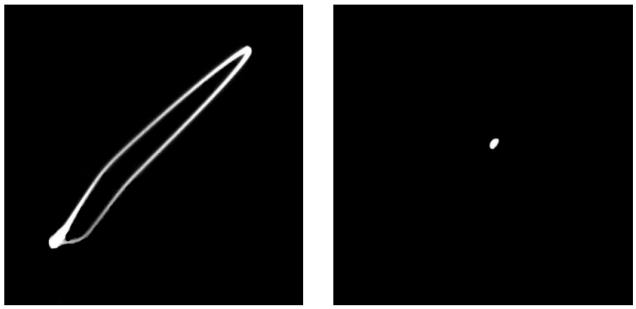

FIG. 5.16. Synchronized case. (Left) phase portrait $V_i(t)$ *vs.* $V_j(t)$, $i \neq j$. (Right) Poincaré section, $V_i(t)$ *vs.* $V_j(t)$ at $V_l(t)$=1 V, $dV_l(t)/dt<0$, $i \neq j \neq l$.

We note that in order to display analogue simulation results, presented in Fig. 5.15 and Fig. 5.16 from the hardware circuit in Fig. 5.13, one needs some special electronic equipment. Namely, an oscilloscope with an X input (horizontal channel) and an Y input (vertical channel) is required to take the phase portraits. An X/Y channelled oscilloscope with an additional feature of external beam modulation ("Z input") is necessary (along with an external pulse generator) to plot the Poincaré sections. However, this equipment may not be available in a standard laboratory.

Multi-channel method. The problem can be partially got around, using a standard at least 2-channel oscilloscope for displaying the waveforms $V_i(t)$ and $V_j(t)$ from the pairs of oscillators, $i \neq j$, as shown in Fig. 5.17 and Fig. 5.18. The internal horizontal sweep saw-tooth generator of the oscilloscope should be synchronized with one of the waveform, either with $V_i(t)$ or with $V_j(t)$. The waveforms can be inspected visually on the screen of the oscilloscope and snapshots can be taken photographically or by means of a camera, if necessary.

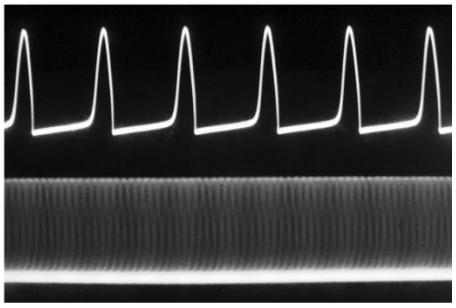

FIG. 5.17. Non-synchronized case: $V_i(t)$ (top) and $Vj(t)$ (bottom), $i \neq j$. Oscilloscope is synchronized internally with $V_i(t)$.

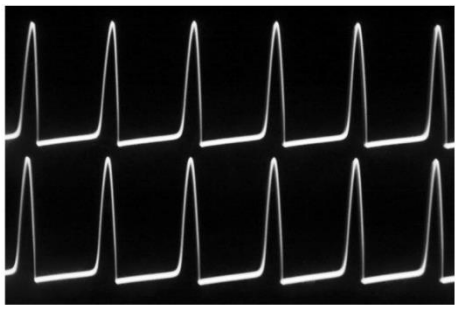

FIG. 5.18. Synchronized case: $V_i(t)$ (top) and $V_j(t)$ (bottom), $i \neq j$. Oscilloscope is synchronized internally with $V_i(t)$.

However, this method (also the previously described phase portraits and the Poincaré sections techniques) requires checking the state of all different pairs of the oscillators, $i \neq j$. It may be time consuming procedure, since there is a lot of different pairs in the network of N oscillators, given by the number of combinations:

$$C_N^2 = \frac{N!}{2!(N-2)!} = \frac{N(N-1)}{2}. \qquad (5.15)$$

In the case of $N = 30$ there are 435 pairs.

Mean voltage method. Therefore we propose one more simple alternative technique for checking the network, whether it is in either nonsynchronized or synchronized state. One needs a simple single-channel oscilloscope only. Instead of checking all the 435 pairs, the method makes use of a single measurement only. Examples are shown in Fig. 5.19 and Fig. 5.20. In the non-synchronized case the mean-field voltage $V_m(t)$ taken from the node CN (Fig. 5.12) has relatively low amplitude (<1 V). Moreover, the oscilloscope cannot be synchronized with $V_m(t)$ (Fig. 5.19). In contrast, the synchronized $V_m(t)$ has relatively high amplitude (>10 V), exhibits simple spiking periodic waveform, similar to that of an individual oscillator (Fig. 5.14). Therefore $V_m(t)$ is easily synchronized on the screen of the oscilloscope (Fig. 5.20).

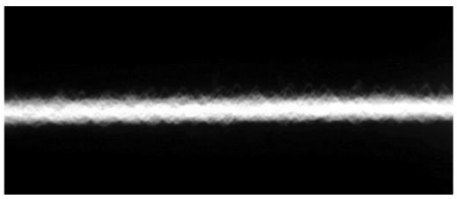

FIG. 5.19. Nonsynchronized case: mean voltage $V_m(t)$. Oscilloscope is unable to synchronize with the non-periodic waveform.

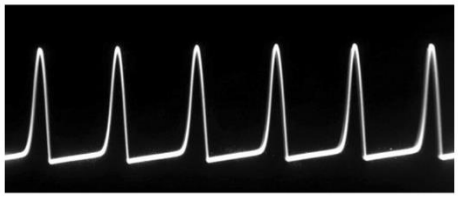

FIG. 5.20. Synchronized case: mean voltage $V_m(t)$. Oscilloscope easily synchronizes with this simple periodic waveform.

5.3. Desynchronization of coupled FHN oscillators using mean field nullifying and repulsive coupling [6,11]

In this Section two techniques are discussed, which can destroy synchrony in an array of coupled oscillators. To achieve the goal, the mean field is either artificially *nullified* or fed back into the array with a *negative sign*.

To be specific, we investigate an array of the mean-field coupled FHN oscillators (Fig. 5.21), which imitate the dynamics of spiking neurons. The considered feedback methods require neither the knowledge of dynamics of the individual oscillators, nor the access to their individual variables x_i and parameters.

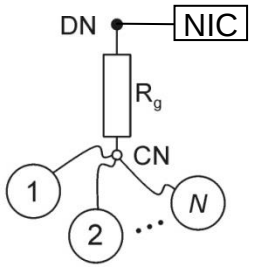

FIG. 5.21. Array of the mean-field coupled oscillators 1,2,…, *N*. NIC is the negative impedance converter. We assume, that the CN is not accessible directly from the outside, but via some passive resistance network, represented here for simplicity by an equivalent resistance R_g. DN is an accessible damping node. The feedback controller NIC is coupled to DN.

An array of the mean-field coupled FHN (*symmetric version*) non-identical oscillators is given by

$$\begin{aligned} \dot{x}_i &= x_i - x_i^3/3 - y_i + c_i + k(x_m - x_i), \\ \dot{y}_i &= \varepsilon(x_i - by_i), \quad i = 1,2,...,N. \end{aligned} \tag{5.16}$$

Variables x_i and y_i correspond to the membrane potential and the recovery variable [FitzHugh, 1961], respectively (in the original paper by FitzHugh the equations have slightly different form), k is the coupling coefficient. Note that the parameter c_i is different for each individual oscillator, thus making them non-identical units. In Eq. (5.16), the x_m is the mean value

$$x_m = \frac{1}{N}\sum_{i=1}^{N} x_i. \tag{5.17}$$

Therefore, the set of oscillators given by Eq. (5.16) is called mean-field coupled array. This type of coupling is widely known to give the synchronization effect. Following the paper by Tsimring *et al.* (2005), we call the non-identical oscillators synchronized or phase-locked, if they have fixed (not necessarily zero) phase differences. There are many other coupling possibilities, described in literature, yielding synchronous behaviour of periodic and chaotic oscillators, including the FHN systems. We just mention here synchronization of two weakly coupled chaotic FHN oscillators [Aqil *et al.* 2012] (chaotic oscillations can appear in the FHN system due to the periodic driving force), where synchrony is achieved by means of applying appropriate external input(s).

Here we demonstrate that using the feedback control of the mean field it is possible either to destroy the synchronized state of the individual oscillators, and/or to diminish essentially their mean field. To achieve the goal, we replace in Eq. (5.16) the x_m with the controlled mean x_m^*, which is found from an algebraic equation which follows from the Kirchhoff's law:

$$k\sum_{i=1}^{N}(x_i - x_m^*) - \Gamma x_m^* = 0, \tag{5.18}$$

where $\Gamma = R_3/(R_g + R_{Ctrl})$ is a parameter of the external control, R_3 is the feedback resistor of FHN oscillator (see Fig. A7 in *Appendix* A4) R_{Ctrl} is the input resistance of the NIC ($R_{Ctrl} < 0$). It follows from Eq. (5.18) that

$$x_m^* = \frac{kN}{kN + \Gamma} x_m. \tag{5.19}$$

Without the control (NIC is disconnected from DN; formally $R_{Ctrl} \to \infty$, $\Gamma = 0$), the $x_m^* = x_m$, as expected. There are two special and important cases of control.

***Case 1, mean field nullifying*:** if $R_{Ctrl} = -R_g$, then $|\Gamma| >> kN$. Thus, the controlled mean $x_m^* \approx 0$, i.e., coupling is nullified. We note the difference between the uncoupled oscillators ($k = 0$) and the nullified coupling ($x_m^* = 0$): the presence of terms $-kx_i$ in the latter case. However, for $k < 1$, these terms involve only small local damping and do not cause any synchronization of the array.

Case 2, repulsive coupling. If $\Gamma < -kN$, then the controlled mean x_m^* becomes negative. Specifically, at $\Gamma = -2kN$ the $x_m^* \approx -x_m$. This special case of $x_m^* \approx -x_m$ is called the repulsive coupling. It has been considered analytically and numerically for the array of simple one-dimensional phase oscillators (the Kuramoto model) [Tsimring *et al*., 2005, Hong *et al*., 2011]. Below, we present the results, both numerical and experimental, for a more complicated model, namely, array of two-dimensional FHN oscillators.

Numerical simulation. Results, obtained from the Eq. (5.16) with $x_m \to x_m^*$, are shown in Fig. 5.22. The individual parameters c_i range from –5.0 to –4.5 with the increment $c_{i+1}=c_i+0.05$, where $c_1=-5$.

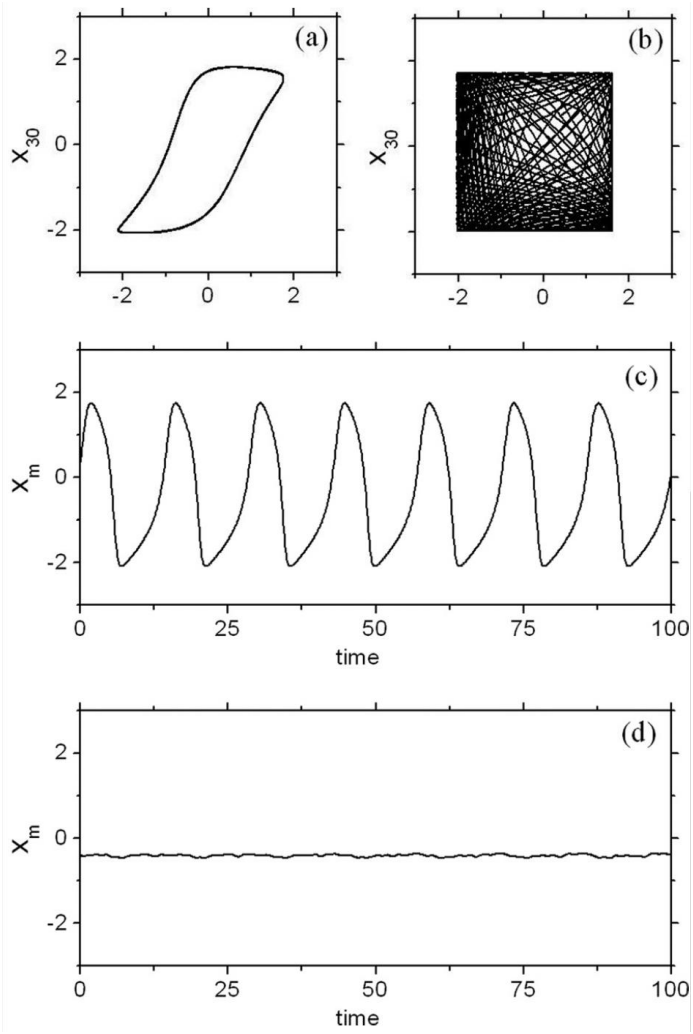

FIG. 5.22. Array of coupled FHN oscillators, $N = 30$, $\varepsilon = 0.3$, $b = 0.1$, $k = 0.1$. (a) and (b) phase portraits, x_{30} *vs.* x_1. (c) and (d) waveforms $x_m(t)$. (a) and (c) uncontrolled array, $\Gamma = 0$. (b) and (d) controlled array, $\Gamma = -2kN = -6$.

Phase portrait (x_1, x_{30}) in Fig. 5.22a and all other phase portraits x_i, $x_{j\neq i}$ (not plotted in Fig. 5.22) demonstrate synchronization effect of the all oscillators in the uncontrolled array ($k \neq 0$, $x_m>0$). The complicated phase portrait shown in Fig. 5.22b, evidences that the controlled oscillators ($k\neq0$, $x_m^* \approx -x_m$) are not phase synchronized. The high amplitude of the mean-field variable x_m (Fig. 5.22c), observed in the case of the synchronized oscillators ($\Gamma= 0$), decreases drastically, by a factor of more than 10 (Fig. 5.22d), when control is applied ($\Gamma= -2kN$).

Qualitatively similar numerical results obtained using the ELECTRONICS WORKBENCH PROFESSIONAL software from the *asymmetric* FHN model introduced in Sec. 5.1 and Sec. 5.2. Moreover, qualitative results do not depend on the number of the oscillators coupled in the array (Fig. 5.23).

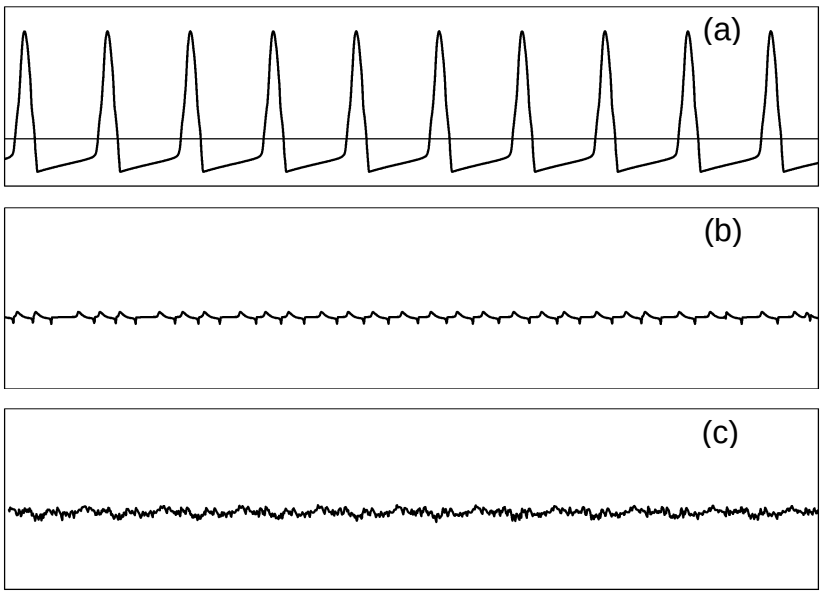

FIG. 5.23. Typical waveforms obtained from the CN. (a) Synchronized oscillators ($N = 3$ and $N = 30$), amplitude about 1.5V. (b) Desynchronized oscillators ($N = 3$), amplitude about 3 mV. (c) Desynchronized oscillators ($N = 30$), amplitude about 3 mV.

In addition, we investigated the dependence of voltage at the CN on the resistance R_{Ctrl} of the controller NIC (Fig. 5.24). Desynchronization can be achieved in a relatively large range of R_N.

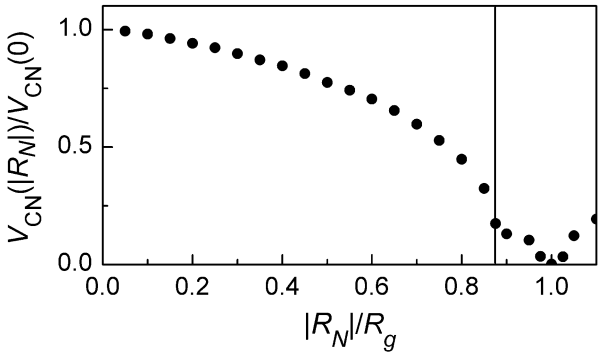

FIG. 5.24. Voltage at the CN as a function of resistor $R_N \equiv R_{\text{Ctrl}}$ of the controller ($R_{\text{Ctrl}} < 0$), $N = 3$. Vertical line at 0.875 divides the synchronized mode (on the left) and the desynchronized mode (on the right) of oscillations. The normalized mean voltage observed at the resonance value $|R_N|=R_g$ is about 0.002 in agreement with the amplitude 3 mV in Fig. 5.23b and Fig. 5.23c.

Experimental results. Experiments with the hardware array (Fig. 5.25) of coupled oscillators confirm the main features demonstrated by means of numerical simulations. Single loop in the phase portrait (Fig. 5.25a) shows that the oscillators are synchronized in the uncontrolled array ($\Gamma = 0$). The multi-loop phase portrait (Fig. 5.25b), in contrast, indicates that the oscillators are not in synchrony in the controlled array ($\Gamma = -6$). Also, the high/low amplitudes of the mean-field voltage V_m are typical characteristics of the uncontrolled/controlled arrays, (Fig. 5.25c and Fig. 5.25d), respectively.

Also, the high/low amplitudes of the mean-field voltage V_m are typical for the uncontrolled/controlled arrays (Fig. 5.25c and Fig. 5.25d, respectively). The control parameter $\Gamma = -6$, introduced by the controller, corresponds to $\Gamma = -2kN$ and provides $x_m^* \approx -x_m$, i.e., implements experimentally the repulsive coupling technique, considered theoretically in [Tsimring *et al.*, 2005].

The results for the case of the nullified mean ($|\Gamma| >> kN$, $x_m^* \to 0$), look the same as for $\Gamma = -6$ (Fig. 5.25b and Fig. 5.25d).

Spectral analysis. Using an analogue spectrum analyser, we have taken the power spectra of the mean-field voltage V_m at four different values of the control parameter Γ (Fig. 5.26). Depending on Γ, several different situations are observed.

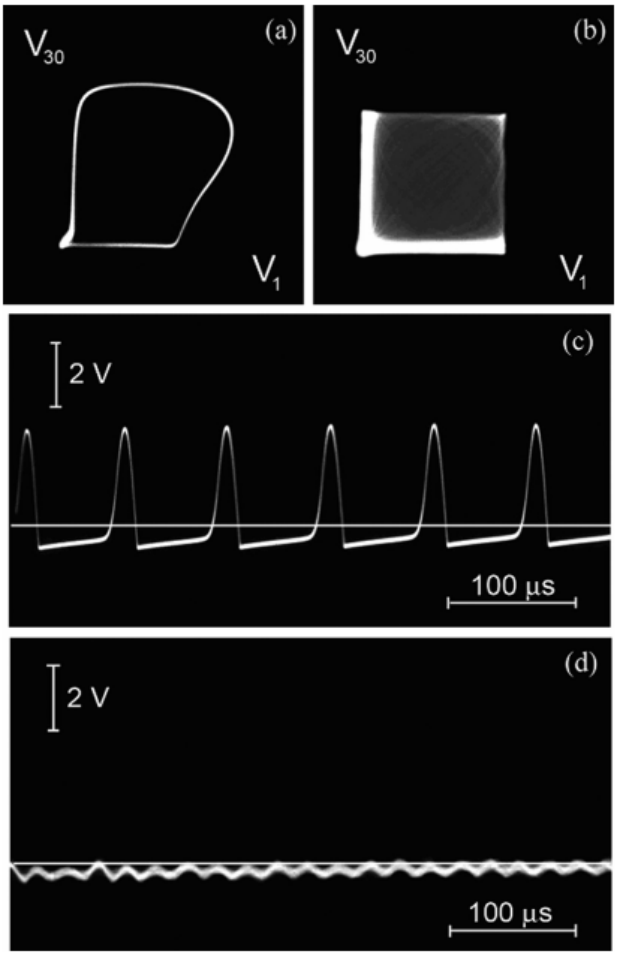

FIG. 5.25. Experimental results from the circuit in Fig. 5.21. (a), (b) phase portraits, V_{30} *vs.* V_1. (c), (d) waveforms of the mean voltage V_m. (a), (c) uncontrolled array, $\Gamma = 0$. (b), (d) controlled array, $\Gamma = -6$. For the circuit element values, used in the experiment, the coupling coefficient $k \approx 0.1$; for $N=30$, $kN=3$.

Situation 1: $\Gamma=0$ (no control), all the cells are synchronized due to the positive (attractive) mean field V_m and oscillate, as expected, at the same frequency f_m=12 kHz, which is indicated by a single discrete line in Fig. 5.26a. Here, the 2nd harmonic $2f_m$ = 24 kHz and the higher harmonics of the f_m are out of the spectral range 11 to 16 kHz.

Situation 2: $|\Gamma| >> kN$ (nullified mean field, $V_m^* \approx 0$), all the cells are desynchronized and oscillate at their natural frequencies, discretely distributed from 12.3 to 13.8 kHz in the narrow band of approximately 1.5 kHz. In Fig. 5.26b, not all the 30 lines are distinguishable, because some cells oscillate at frequencies separated by only 1 or 2 Hz, i.e., less than the spectral resolution of the analyser (3 Hz). The mean-field voltage V_m is low, like in Fig. 5.25d.

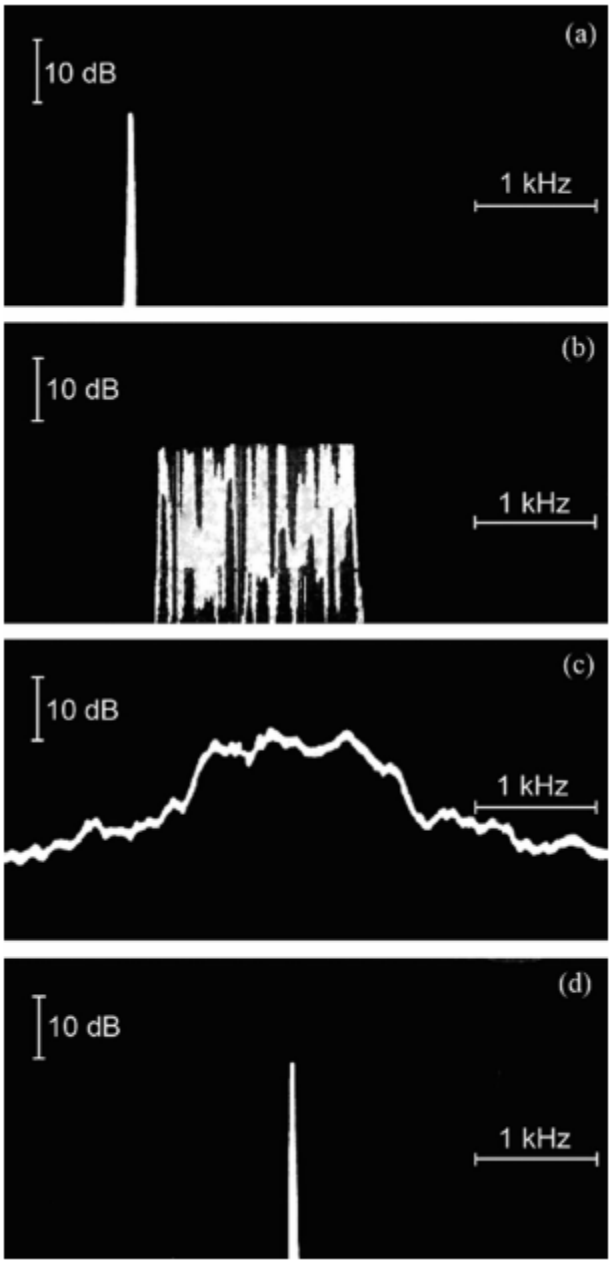

FIG. 5.26. Experimental power spectra of the mean-field voltage V_m in the range of 11–16 kHz with spectral resolution of 3 Hz at different control parameters Γ. (a) uncontrolled, Γ= 0, f_m = 12.0 kHz (since the mean-field V_m is high, the signal has been attenuated by 30 dB), (b)–(d) controlled array; (b) nullified mean-field voltage V_m^*, $|\Gamma| \to \infty$, f_m = 12.3… 13.8 kHz, (c) and (d) repulsive control; (c) Γ= –6, (d) Γ= –5, f_m =13.3 kHz.

Situation 3: $\Gamma < -kN$, e.g., at $\Gamma = -6$, the individual oscillators are also desynchronized, however, their frequencies are continuously spread in the "broadband" spectrum (Fig. 5.26c), typical to chaotic signals. The V_m is low (Fig. 5.25d).

Situation 4: $-5 \le \Gamma < -3$, the cells become synchronized again as evidenced by a single spectral line in Fig. 5.26d. The spectral line is shifted towards slightly higher frequencies, compared with the case of the uncontrolled array (Fig. 5.26a). However, in contrast to the uncontrolled array, the mean-field voltage V_m remains low, like in Fig. 5.25d. This indicates that the oscillators are in antiphase states. More precisely, the phases are distributed on the interval between 0 and 2π.

5.4. Inhibition of spikes in an array of FHN oscillators by means of external periodic forcing [14]

External periodic forcing can inhibit spikes in an array of coupled oscillators. To be specific, an array of the mean-field coupled electronic FHN oscillators [Ratas & Pyragas, 2012; Ratas, 2015], also known in literature as the Bonhoeffer–van der Pol oscillators [Rabinovitch *et al.*, 1994; 2015], is considered. The corresponding diagram is presented in Fig. 5.27, where CN is a coupling node. It is assumed, that the CN is not accessible directly from the outside, but via some passive resistance network, represented here for simplicity by an equivalent resistance R_g. DN is an accessible damping node.

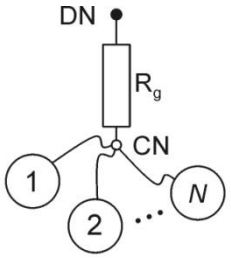

FIG. 5.27. Circuit diagrams: array of mean-field coupled oscillators. CN is a coupling node, DN is a damping node.

Experimental results. In the experiments we employed a hardware array with N=30, described in details (without any external control) in Section 5.2. The external inhibitory AC current $I_{inh}(t)=I_A\sin(2\pi ft)$ was injected from an external sine wave generator via the damping node DN. For the best performance it is necessary to choose an appropriate drive amplitude I_A and frequency f. The f should be much higher than the natural frequency f_0 of the spiking oscillators

(f_0≈12 kHz). The experimental results are shown in Fig. 5.28 and Fig. 5.29, by the waveforms and the phase portraits (in classical electronics called the Lissajous figures). Here the $<V_C>$ is the mean-field voltage of the voltages V_{Ci} from the individual oscillators (i=1,2…, 30). The threshold amplitude of the inhibitory current is I^*_A=50 mA, the optimal frequency is f ≈150 kHz, providing the lowest threshold. The time average of the high frequency non-spiking voltage $<V_C>$ (right hand side of the bottom plot), taken over the period (T=1/f) of the external current, is $\overline{U}_C \approx -0.18$ V. It is non-zero value because of the DC bias V_0= –15 V (Fig. A7). The $\overline{U}_C$ is noticeably different from the natural equilibrium $<V_{0C}>$= –0.27 V, measured in a non-oscillatory mode (all coils L are short-circuited).

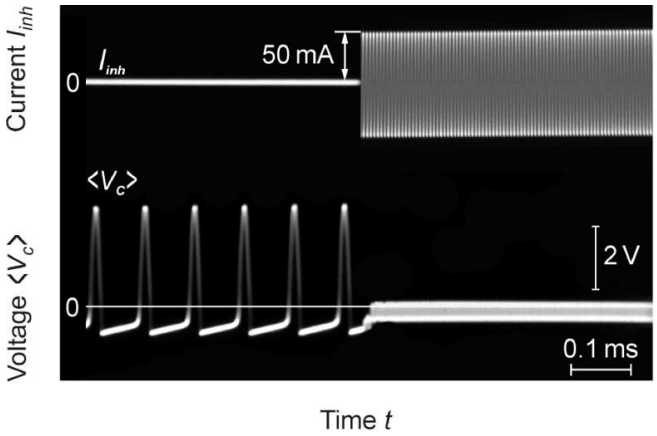

FIG. 5.28. Experimental waveforms of the external periodic current I_{inh} and the mean-field voltage of the array $<V_C>$. f =150 kHz.

Evidently, the self-sustained low frequency (f_0≈12 kHz) spikes of about 4 V height are totally suppressed, when the inhibitory current $I_A \geq I_A^*$=50 mA is injected. However, we have a finite (≈10%) higher frequency artefact. The voltage oscillates around the time average $\overline{U}_C$ with the amplitude of about 0.4 V at the external drive frequency f.

Fine diagonals in Fig. 5.29, $[V_{C30},<V_C>]$ indicate, that the individual oscillator No.30 is strongly synchronized with the mean-field of the array. Other oscillators, No.1 to No.29 were also checked experimentally by means of the phase portraits $[V_{Ci},<V_C>]$ and gave similar result.

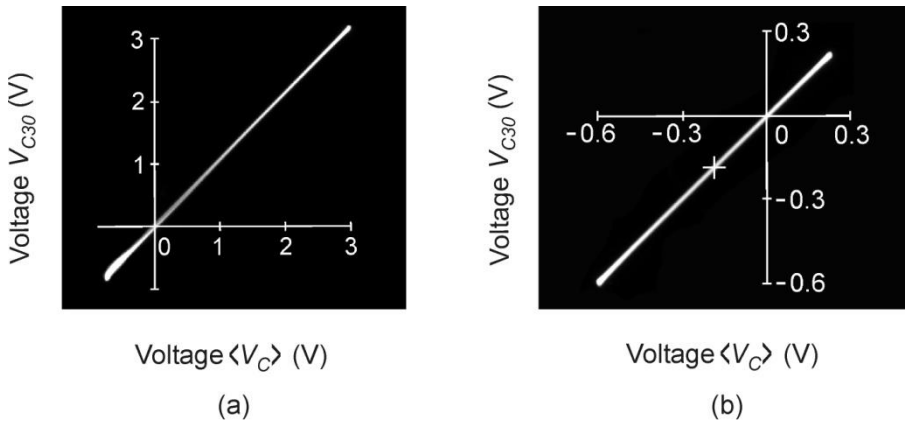

FIG. 5.29. Phase portraits [V_{C30},<V_C>]. (a) spiking oscillators (no control, I_A=0), (b) non-spiking oscillators, I_A=50 mA, f=150 kHz. Small cross in (b) marks the averages of the voltages [$\overline{U}_{C30}$,$\overline{U}_C$] taken over the period of the external inhibitory current $I_{inh}(t)$. They are at about [–0.18 V,–0.18 V]. Note different position of the diagonal also different horizontal and vertical scales in (b), compared to (a).

Moreover, the artefact voltage continues to change (Fig. 5.30), when the external drive amplitude I_A is increased above the threshold value I^*_A (the amplitude I_A should be somewhat higher than the threshold to guarantee robust inhibition). For example, at a double drive amplitude, I_A/I_A^*=2 the average voltage changes its sign. Similar behaviour was observed, but not emphasized, earlier in the numerically simulated bifurcation diagram for the Hodgkin –Huxley single neuron model [Pyragas *et.al.* 2013].

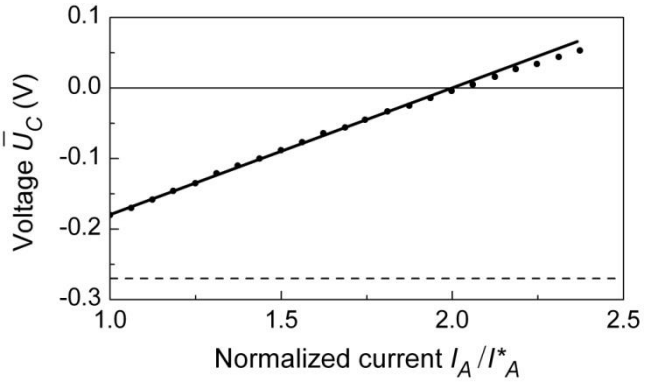

FIG. 5.30. Time average of the mean-field voltage $\overline{U}_C$, taken over the period (T=1/f) of the external inhibitory current I_{inh}, as a function of the normalized amplitude I_A/I_A^* of the external current. I_A^*=50 mA. Extrapolation to zero control (I_A=0) provides a value of $\overline{U}_C$ close to the natural equilibrium <V_{0C}>=–0.27 V (dashed line in the plot).

Mathematical model. We consider Eq. (5.12) with and additional external periodic drive:

$$\begin{aligned} \dot{x}_i &= ax_i - f(x_i) - y_i + c_i + k(x_m - x_i) + A\sin\omega t, \\ \dot{y}_i &= x_i - by_i, \quad i = 1, 2, \ldots N. \end{aligned} \tag{5.20}$$

Here x_m is given by formula (5.17). The $f(x_i)$ in (5.20) is a nonlinear function, presented by a piecewise linear function, the same as Eq. (5.13):

$$f(x_i) = \begin{cases} d(x_i + 1) & , \quad x_i < -1, \\ 0 & , \quad -1 \le x_i \le 1, \\ g(x_i - 1) & , \quad x_i > 1. \end{cases} \tag{5.21}$$

Note, that due to $d >> g$ the $f(x_i)$ is an essentially asymmetric function in contrast to the common FHN cubic parabola x^3. The DC bias parameters c_i are intentionally set different for each individual oscillator, thus making them non-identical units.

Numerical results. Integration of Eq. 5.20 has been performed using the Wolfram MATHEMATICA package. The numerical results are presented in Fig. 5.30. They are in a good agreement with the experimental plots in Fig. 5.28. The mean-field variable x_m does not converge to a constant equilibrium, but oscillates around it at the drive frequency. Strictly speaking, the non-autonomous (externally driven) dynamical systems, e.g. given by Eq. (5.20), do not possess equilibrium states at all.

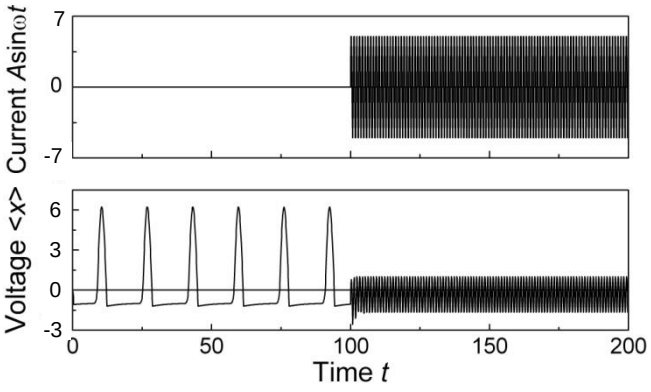

FIG. 5.31. Simulated waveforms of the inhibitory current $A\sin(\omega t)$ and the mean-field voltage $\langle x \rangle \equiv x_m$ from Eq. (5.20), $N = 30$. $A = 5.1$, $\omega = 6.28$, $a = 3.4$, $b = 0.16$, $c_i = -44/(24+i)$, $i = 1,2,\ldots, 30$, $d = 60$, $g = 3.4$, $k = 3.4$. The external inhibitory term $A\sin(\omega t)$ is activated at $t = 100$.

Only in the case of high frequency ($f >> f_0$) drive we can introduce the average values, taken over the external period. These averages more or less are related to the equilibrium states.

Mean-field approach. Linear analysis of Eq. (5.20) is essentially simplified, if we consider the mean-field variables only, obtained by direct averaging the x_i, y_i, $f(x_i)$, and c_i in Eq. (5.20). The coupling term $k\langle(x_m - x_i)\rangle = k(\langle x_m\rangle - \langle x_i\rangle) = k(x_m - x_m) = 0$ in Eq. (5.20) is nullified independently on the value of k. Thus, we obtain differential equations, which do not describe full dynamics of the mean field, but provide its equilibrium. The steady-state equations read:

$$\begin{aligned} 0 &= a\langle x_0\rangle - \langle f(x_{0i})\rangle - \langle y_0\rangle + \langle c\rangle + A\sin\omega t, \\ 0 &= \langle x_0\rangle - b\langle y_0\rangle. \end{aligned} \tag{5.22}$$

We assume, that $-1 \le x_{0i} \le 1$. According to (5.21) this leads to $f(x_{0i}) = 0$ and $\langle f(x_{0i})\rangle = 0$. In the absence of the external drive ($A = 0$) and for $ab < 1$, $|c_i| \le 1/b - a$) the equilibrium coordinates:

$$\langle x_0\rangle = b\langle c\rangle/(1-ab), \quad \langle y_0\rangle = \langle x_0\rangle/b. \tag{5.23}$$

Stability analysis (similar to the case of a single oscillator in Sec. 5.1) shows, that for and $a > b$ the equilibrium (5.23) is unstable (the real parts of the both eigenvalues are positive). If in addition to $a > b$ the sum $a+b > 2$, then the eigenvalues are real (no imaginary parts). Thus, the equilibrium (5.23) is an unstable node. Whereas the external periodic forcing ($A \neq 0$), similarly to the mechanical pendulum [Thomsen *et al.* 2003], can stabilize the originally unstable equilibrium.

For the set of the parameter values, employed in numerical simulations: $a = 3.4$, $b = 0.16$, and $c_i = -44/(24+i)$, the equilibrium coordinates, given by (5.23), have the following values: $\langle x_0\rangle = -0.41$, $\langle y_0\rangle = -2.57$. Using the definitions of the dimensionless variables $\langle x_0\rangle = \langle V_{0C}\rangle/V^*$ and $\langle y_0\rangle = \rho\langle I_{0L}\rangle/V^*$, where $V^* \approx 0.6$ V, we estimate the means of the FHN circuit dimensional variables: $\langle V_{0C}\rangle \approx -0.25$ V, $\langle I_{0L}\rangle \approx -1$ mA. The estimated equilibrium voltage $\langle V_{0C}\rangle$ is close to its experimental value –0.27 V.

5.5. Stabilizing an array of coupled FHN oscillators using stable filter control technique [13,15,21,22]

In this Section, an alternative method and its electronic implementation to damp the spiking FHN type oscillators, more specifically to stabilize their unstable equilibrium states, is described.

The general set-up for damping oscillations in an array is sketched in Fig. 5.32, where CN is a coupling node, in general, not accessible from outside directly, but via effective resistance R_g. The individual oscillators are coupled to the CN via resistors R^*, not shown in the diagram (for R^* see Fig. A7). DN is an accessible damping node.

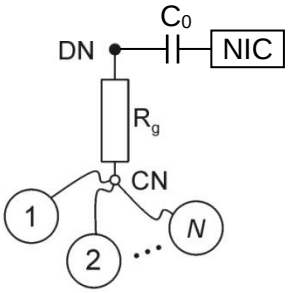

FIG. 5.32. Block diagram of coupled oscillators with negative impedance converter (NIC) applied to the array. NIC is shown in *Appendix 5*.

Equations and numerical results. An individual FHN type asymmetric oscillator is described by in Sec. 5.1. An array of N mean-field coupled FHN oscillators is discussed in Sec. 5.2:

$$\begin{aligned} \dot{x}_i &= ax_i - f(x_i) - y_i - c_i + k_i(x_m - x_i), \\ \dot{y}_i &= x_i - by_i, \quad i = 1,...N. \end{aligned} \tag{5.24}$$

Here x_m is the mean value of the variables x_i, the k_i are the coupling coefficients, further for simplicity assumed to be all equal $k_i = k$.

In the case the controller is applied to the array the equations read:

$$\begin{aligned} \dot{x}_i &= ax_i - f(x_i) - y_i - c_i + k(z - x_i), \\ \dot{y}_i &= x_i - by_i, \quad i = 1,...N, \\ \dot{z} &= \omega_f(x_m - z). \end{aligned} \tag{5.25}$$

Here z is the dimensionless voltage across the capacitor C_0 of the controller, ω_f is the cut-off frequency of the filter, composed of R^* and C_0. In the case the controller is switched off (formally, $C_0 = 0$), the $\omega_f \to \infty$ and consequently $z = x_m$,

as expected. Numerical simulation results are presented in Fig. 5.33 and Fig. 5.34.

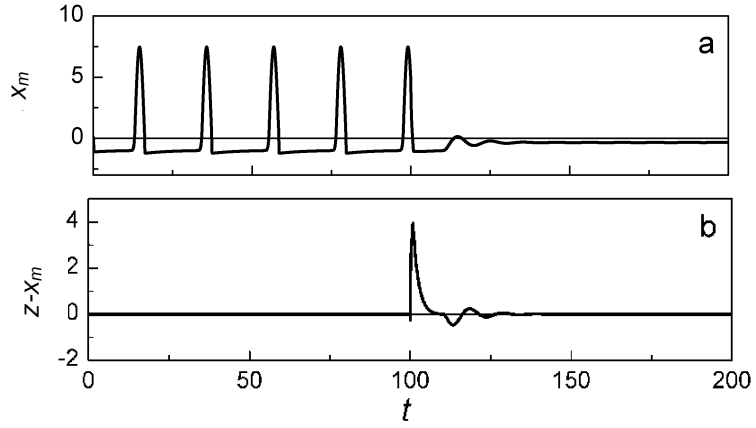

FIG. 5.33. Stabilizing unstable equilibrium in the array of coupled FHN oscillators from Eq. (5.25). $N = 3$, $a = 4$, $b = 0.1$, $c_1 = 3.4$, $c_2 = 3.2$, $c_3 = 3.0$, $d = 70$, $g = 4$, $k = 5$, $\omega_f = 0.04$. (a) Mean value x_m. (b) Control term $z–x_m$. Controller is switched on at $t = 100$.

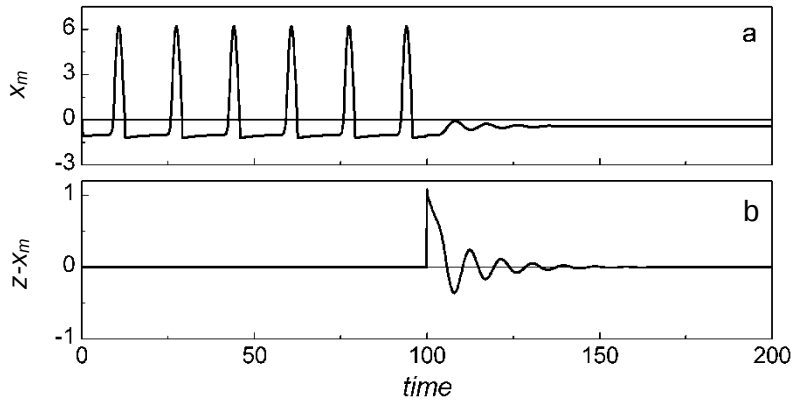

FIG. 5.34. Stabilizing unstable equilibrium in the array of coupled FHN oscillators from Eq. (5.25). $N = 24$. $a = 3.4$, $b = 0.16$, $c_i = 43.5/(24+i)$, $d = 60$, $g = 3.4$, $k = 3.4$, $\omega_f = 0.15$. (a) Mean value x_m. (b) Control term $z–x_m$. Controller is switched on at $t = 100$.

In addition, the positions of equilibrium points x_{0i} of individual oscillators were calculated (Fig. 5.35).

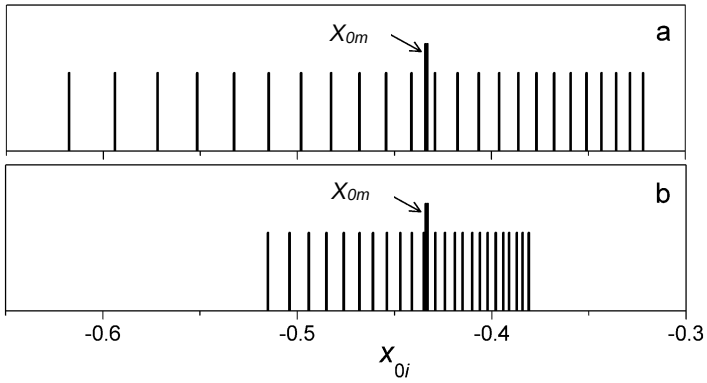

FIG. 5.35. Equilibrium point spectra x_{0i} (i = 1, 2 ,… 24). (a) nonsynchronized (uncoupled) oscillators, (b) stabilized oscillators from numerical solution of (5.25) at t = 200. Parameters are the same as in the caption of Fig. 5.34. The higher and thicker lines in the spectra indicate the mean field fixed points x_{0m}.

Experimental results. Experiments have been performed using an array, composed of N mean-field coupled electronic FHN type *asymmetric* oscillators. The snapshots of the experimental signals are shown in Fig. 5.36.

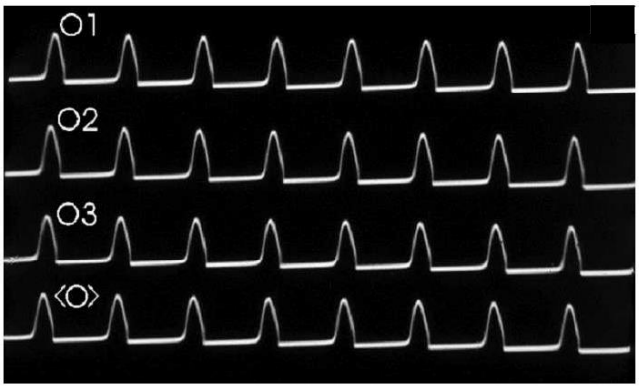

FIG. 5.36. (a) Outputs from the synchronized oscillators O1, O2, O3 (N = 3) and mean voltage <O> at the coupling node CN. Spike height ≈ 2 V, period ≈ 0.7 ms.

The signals in Fig. 5.36 and the closed loops in the phase portraits (Fig. 5.37) indicate that the coupled oscillators are all phase-synchronized.

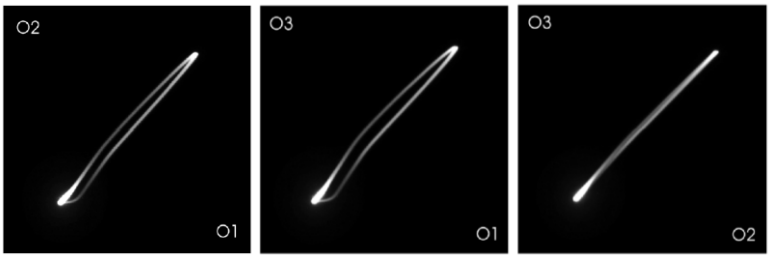

FIG. 5.37. Phase portraits from the individual oscillators. N = 3.

The stabilization experiments, shown in Fig. 5.38 and Fig. 5.39, are in a very good agreement with the numerical simulation, presented in Fig. 5.33 and Fig. 5.34.

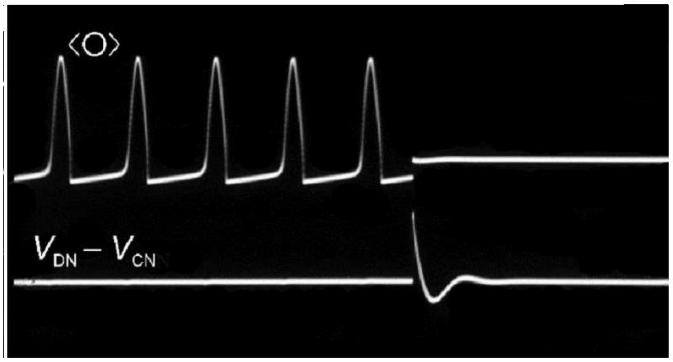

FIG. 5.38. Stabilization of the array $N = 3$. Mean-field voltage <O> and control signal $V_{DN}–V_{CN}$. Spike height ≈2 V, period ≈ 0.7 ms. $R^* = 470\ \Omega$, $R_g = 1\ k\Omega$, $R_{03} = 1\ k\Omega$ ($R_{in2} = –1\ k\Omega$; $R_g + R_{in} = 0$). $C_0 = 2.2\ \mu F$.

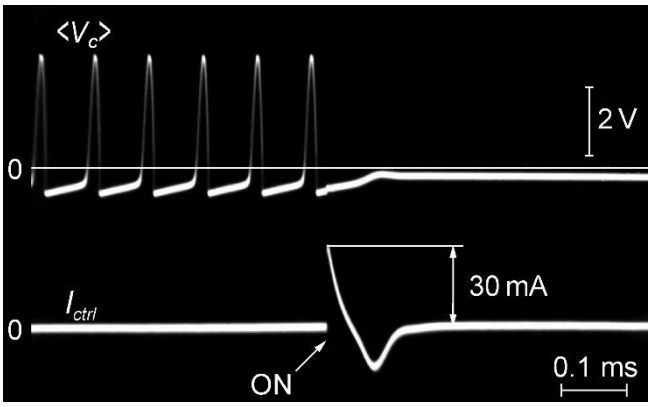

FIG. 5.39. Stabilization of the array $N = 30$. Experimental waveforms, the mean-field voltage $\langle V_C \rangle$ and the control current I_{ctrl}. The arrow indicates the time moment, when the control is switched on. $R^* = 510\ \Omega$, $R_g = 100\ \Omega$, $R_{03} = 100\ \Omega$ ($R_{in2} = –100\ \Omega$; $R_g + R_{in} = 0$). $C_0 = 2.2\ \mu F$.

Remark. Concerning possible application of the developed feedback methods of the desynchronization and stabilization (Sec.5.3 and Sec.5.5) to real neuronal systems, separate electrodes for recording signals and feedback application could be used [Pyragas *et al.*, 2007; Tukhlina *et al.*, 2007]. An alternative solution is to use act-and-wait algorithm [Ratas & Pyragas, 2014].

MAIN RESULTS AND CONCLUSIONS

1. The efficiency of the Pyragas' unstable filter control to switch the motionless dynamical systems from the stable equilibrium states, e.g. spirals or nodes, to unknown unstable equilibrium states, specifically the saddles, has been demonstrated.

2. An adaptive control technique for tracking and stabilizing unknown and slowly varying saddle equilibrium has been developed. The technique employs an unstable high-pass filter. Using high-pass filter instead of common low-pass filter makes the controller technically simpler.

3. An analogue electronic controller using the instrumentation amplifiers instead of the operational amplifiers for stabilization of equilibrium states has been designed and built. It can be easily switched between a stable and an unstable modes of operation for stabilizing either unstable spirals/nodes or saddles, respectively.

4. A synergetic control method, using unstable and stable filters operating in parallel, has been proved to stabilize unknown and slowly varying saddles of conservative and weakly damped dissipative dynamical systems.

5. Stabilization of saddles under influence of inertia in the feedback loop by means of stable and unstable filters operating in parallel has been described.

6. A synergetic method, robust to the influence of unknown external forces, for stabilizing unknown saddle equilibrium by means of linearly combined unstable and stable low-pass filter techniques, has been described.

7. A synergetic technique for stabilizing unknown saddle equilibrium by means of unstable filter control, supported by the derivative control, has been suggested.

8. Zeroth-order proportional feedback technique for stabilizing equilibrium of systems with uncertain dynamics has been proposed. The technique employs either artificially created stable equilibrium or natural stable equilibrium to find the coordinates of the unstable equilibrium.

9. Three-step adaptive proportional feedback method for stabilizing unknown saddles has been proposed. The technique makes use of the artificially created

two stable equilibrium states to find the coordinates of the inherent unstable equilibrium state.

10. An adaptive feedback method for stabilizing unknown saddle equilibrium, employing Heaviside nonlinear function has been described. The analogue electronic controller uses a comparator as a nonlinear unit.

11. The FitzHugh–Nagumo (FHN) type spiking neuron model, equipped with an asymmetric activation function has been investigated. The first-order stable filter, coupled to a system, has been demonstrated to inhibit spikes, more specifically to stabilize the unstable equilibrium.

12. An electrical network, consisting of 30 FHN oscillators, has been designed, built and investigated. Synchrony in the array of the mean-field coupled oscillators has been demonstrated.

13. An implementation of an analogue feedback controller, using negative impedance converter, for controlling synchrony of the mean-field coupled FHN oscillators has been described. If the mean field is artificially nullified, then synchrony is broken up. If the mean field is fed back with a negative sign (repulsive coupling), its value is essentially decreased.

14. Inhibition of spikes in an array of 30 mean-field coupled FHN oscillators by external periodic forcing has been studied.

15. The stable filter control technique has been developed for stabilizing unstable equilibrium in an array of mean-field coupled FHN oscillators.

About the author

Elena Adomaitienė (Tamaševičiūtė) was born in Vilnius, Lithuania, in 1987. She graduated from the Mykolas Biržiška gymnasium in 2005 and was admitted to the Faculty of physics at the Vilnius University. Elena successfully completed the bachelor program of the Physics and management of modern technology in 2009. She obtained the master's degree from the Swiss Federal Institute of Technology Zurich in 2011. Elena started her doctoral studies in physics (02P) at the Center for Physical Sciences and Technology in 2012.

PAGRINDINIAI REZULTATAI IR IŠVADOS

1. Pademonstruotas Pyrago valdymo nestabiliuoju filtru metodo efektyvumas, perjungiant nejudančią dinaminę sistemą iš stabiliosios pusiausvyros, pvz., spiralės arba mazgo, į nežinomą nestabiliąją pusiausvyrą, pvz., balną.
2. Sukurtas adaptyvusis valdiklis nežinomai ir lėtai kintančiai balno pusiausvyrai aptikti ir stabilizuoti. Valdiklis remiasi nestabiliuoju aukštųjų dažnių filtru. Naudojant aukštųjų dažnių filtrą vietoje įprasto žemųjų dažnių filtro valdiklis tampa techniškai paprastesnis.
3. Panaudojant instrumentinius stiprintuvus vietoje įprastinių operacinių stiprintuvų sukurtas ir sumontuotas analoginis elektroninis valdiklis įvairioms pusiausvyros būsenoms stabilizuoti. Valdiklį lengva perjungti iš stabiliojo režimo, skirto nestabilioms spiralėms ir mazgams stabilizuoti, į nestabilųjį režimą, tinkantį balnams stabilizuoti.
4. Aprašytas sinerginis valdymo metodas, naudojantis nestabilųjį ir stabilųjį filtrus, veikiančius lygiagrečiai. Valdiklis stabilizuoja nežinomus ir lėtai kintančius balnus konservatyviose ir silpnai slopstančiose disipatyviose dinaminėse sistemose.
5. Stabilųjį ir nestabilųjį filtrus, veikiančius lygiagrečiai, pasiūlyta balnams stabilizuoti, esant signalo inercijai grįžtamojo ryšio grandinėje.
6. Aprašytas sinerginis nežinomo balno pusiausvyros stabilizavimo metodas, atsparus išorinėms nežinomoms jėgoms, naudojantis tarpusavyje tiesiškai sujungtus stabilųjį ir nestabilųjį žemųjų dažnių filtrus.
7. Pasiūlytas sinerginis metodas, skirtas nežinomo balno pusiausvyrai stabilizuoti, naudojantis valdymą nestabiliuoju filtru kartu su išvestinės grįžtamuoju ryšiu.
8. Pasiūlytas nulinės eilės proporcinio grįžtamojo ryšio metodas, skirtas pusiausvyros būsenoms stabilizuoti sistemose su iš dalies žinoma dinamika. Nestabilios pusiausvyros koordinačių nustatymui naudojama arba dirbtinai sukurta stabilioji pusiausvyra, arba natūrali stabilioji pusiausvyra.
9. Pasiūlytas trijų pakopų adaptyvusis proporcinis grįžtamojo ryšio metodas nežinomiems balnams stabilizuoti. Nestabiliosios pusiausvyros koordinatės

apskaičiuojamos, panaudojant dvi dirbtinai sukurtas stabiliosios pusiausvyros būsenas.

10. Aprašytas adaptyvusis grįžtamojo ryšio metodas nežinomai balno pusiausvyrai stabilizuoti, naudojantis Heaviside laiptinę funkciją. Elektroniniame valdiklyje pritaikyti įtampos komparatoriai.

11. Ištirtas FitzHugh–Nagumo (FHN) neurono modelis su asimetrine aktyvacijos funkcija. Stabilusis pirmos eilės filtras, prijungtas prie sistemos, slopina impulsus, o būtent stabilizuoja nestabiliąją pusiausvyrą.

12. Suprojektuotas, sumontuotas ir ištirtas masyvas, jungiantis 30 FHN osciliatorių. Pademonstruota vidutiniu lauku susietų osciliatorių sinchronija.

13. Aprašytas analoginis grįžtamojo ryšio valdiklis, panaudojantis neigiamo impedanso keitiklį ir skirtas vidutiniu lauku susietųjų FHN osciliatorių sinchronijai valdyti. Jei vidutinis laukas dirbtinai panaikinamas (*angl*. nullified mean field), osciliatorių sinchronija išyra. Jei vidutinis laukas grąžinamas su neigiamu ženklu, t. y. įgyvendinamas atstumiantysis sujungimas (angl. repulsive coupling), vidutinio lauko dydis žymiai sumažėja.

14. Ištirtas impulsų slopinimas išorine periodine jėga 30-ies vidutiniu lauku susietų FHN osciliatorių masyve.

15. Valdymo stabiliuoju filtru metodas pritaikytas nestabiliosios pusiausvyros būsenoms stabilizuoti susietųjų FHN osciliatorių masyve.

Apie autorę

Elena Adomaitienė (Tamaševičiūtė) gimė 1987 m. Vilniuje. 2005 m. baigusi Mykolo Biržiškos gimnaziją įstojo į Vilniaus universiteto Fizikos fakultetą. 2009 m. baigė Moderniųjų technologijų fizikos ir vadybos bakalauro studijų programą. 2011 m. baigė Šveicarijos federalinio technologijos instituto Ciuriche magistrantūrą. 2012 m. priimta į Fizinių ir technologijos mokslų centro fizikos krypties (02P) doktorantūros studijas.

APPENDIXES

ELECTRONIC ANALOGS OF THE DYNAMICAL SYSTEMS AND ELECTRONIC CONTROLLERS

Introduction

Appendixes (A1 to A5) include the circuit diagrams and descriptions of the electronic analogues of the investigated dynamical systems: the Duffing–Holmes (DH) oscillator (A1), the Lorenz system (A2), the Lagrange point L2 of the Sun–Earth system (A3), the FitzHugh–Nagumo (FHN) oscillator (A4). The electronic controllers are presented in A5.

There are many examples in science and engineering where analogue electrical circuits have been used to model temporal evolution of dynamical systems. This modelling method has been applied to diverse disciplines and areas. Mackey and Glass (MG) [1977] proposed a delay differential equation to describe heamatological disorders. The MG model has a simple electronic analogue [Namajūnas *et al.*, 1995a]. An electrical circuit has been suggested to imitate the chaotic behaviour of a periodically forced mechanical system [Lai *et al.*, 2005], described by the DH ordinary differential equations. Several electrical circuits have been proposed to model the dynamics of neurons, e.g. [Binczak *et al.*, 2003]. A very interesting solution has been suggested to model mammalian cochlea using high order electrical circuit [Martignoli *et al*., 2007].

It should be emphasized that design of such electrical circuits is not for its own purpose. The analogue circuits mentioned above have been employed for testing various methods developed to control dynamics of the systems, specifically to stabilize equilibrium states [Namajūnas *et al.*, 1995a; 1997] and periodic orbits in chaotic systems [Tamaševičius *et al.*, 2007a,b]. In addition, experiments with electronic analogues can help to better understand the mechanisms behind the behaviours of complex systems, e.g. the pitch in human perception of the sound [Martignoli *et al.*, 2010]. Moreover, the electronic cochlea provides an efficient design of an artificial hearing sensor [Stoop *et al*., 2007].

One can argue that there is no difference between an analogue electrical circuit, imitating a dynamical system, and an analogue computer, solving corresponding differential equations. We note that any analogue computer is a standard collection of the following main blocks: inverting RC integrators, inverting adders, invertors, inverting and noninverting amplifiers, multipliers, and piecewise linear nonlinear units. Programming the differential equations on an analogue computer in the essence is simple wiring these units according to strictly predetermined rules. Differences between the "intrinsically" analogue electrical circuits, imitating behaviour of dynamical systems, and the conventional analogue computers were discussed by Matsumoto, Chua and Komuro more than 30 years ago [Matsumoto *et al.*, 1985]. In this regard, it makes sense to present here an excerpt from their paper: "… the circuit … is not an analogue computer in the sense that its building blocks are not integrators. They are ordinary circuit elements; namely, resistors, inductors and capacitors. Both current and voltage of each circuit element play a crucial role in the dynamics of the circuit. On the contrary, the variables in a typical analogue computer are merely node voltages of the capacitor-integrator building-block modules, where the circuit current is completely irrelevant in the circuit's dynamic operation. Hence it would be misleading to confuse our circuit as an analogue computer … "

A1. Electronic analog of the Duffing–Holmes (DH) system [1]

In this Appendix, we describe an extremely simple analogue electrical circuit dedicated for simulation the DH equation. There are three different approaches developed to process the DH equation and its solutions electrically. The first technique is a hybrid one making use of simulation the DH equation on a digital computer and digital-to-analogue conversion of the digital output for further analogue processing [Namajūnas *et al.*, 1994]. The second method employs purely analogue means based on analogue computer design. For example, analogue computer has been used to simulate the DH equation and to investigate scrambling effects of chaotic signals in linear feedback shift

registers [Namajūnas *et al.*, 2000a,b]. Later analogue computer, simulating the DH equation and displaying the electrical output voltages on the screen of an oscilloscope, has been suggested for chaos demonstration in the undergraduate student laboratories [Jones & Trefan, 2001]. Evidently, the first and the second techniques are rather general and can be applied to other differential equations as well. In contrast, the third approach is based on building some specific analogue electrical circuit for a given differential equation. Despite the limitation to specific equations, electrical circuits have an attractive advantage due to their simplicity and cheapness. Such circuits comprise only small number of discrete electrical components: resistors, capacitors, inductors, semiconductor diodes, also may include a single (sometimes several) operational amplifier.

The circuit diagram of the DH oscillator is shown in Fig. A1. It is an externally driven damped RLC oscillator with all elements linear. The nonlinearity is involved by the positive feedback loop consisting of the resistor R3 and two diodes D1-D2. The operational amplifier OA plays the role of both, the buffer for the external sinusoidal force and the amplifying stage for the positive nonlinear feedback. The electrical circuit resembles the Young–Silva oscillator [Lai *et al.*, 2005], but is essentially simpler. It includes a single operational amplifier, two diodes, and four resistors only, in contrast to the Young–Silva circuit containing four operational amplifiers, four diodes, and nine resistors.

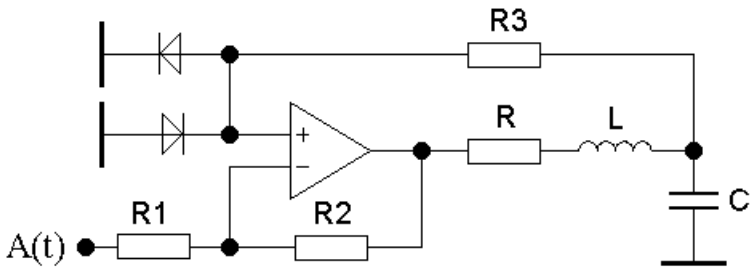

FIG. A1. Circuit diagram of the DH oscillator. In the case of a non-autonomous oscillator $A(t)=A\sin(\omega t)$. In the case of an autonomous damped oscillator $A(t) = 0$ (the corresponding node is simply grounded).

Typical chaotic output of the DH oscillator is illustrated in Fig. A2 with a waveform, a phase portrait, and a stroboscopic map (the Poincaré section).

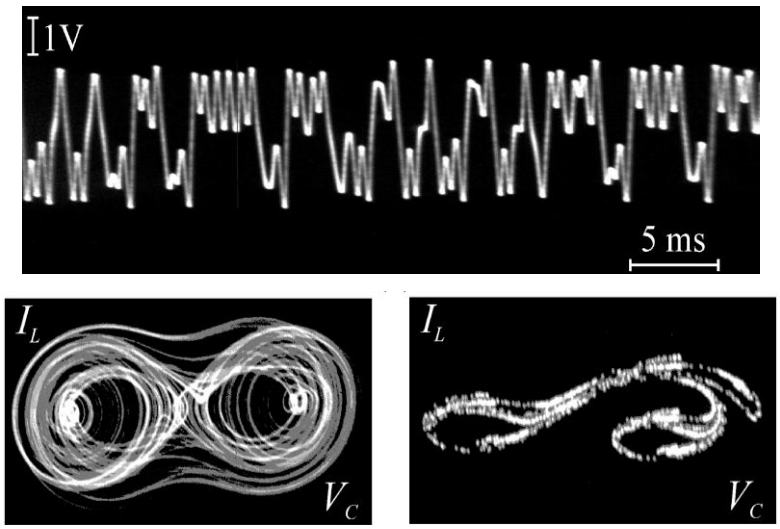

FIG. A2. Chaotic waveform $V_C(t)$ (top), phase portrait [I_L *vs.* V_C] (bottom left), stroboscopic map (Poincaré section) [I_L *vs.* V_C; $t_n=2\pi n$] (bottom right). A = 200 mV, $f = \omega/2\pi$ = 1.5 kHz.

Using the Kirchhof's laws for the circuit in Fig. A1 and introducing the dimensionless variables and parameters, we obtain dimensionless equations (which can be compared with the conventional DH equations [Ott, 1993]):

$$\begin{aligned} \dot{x} &= y, \\ \dot{y} &= F_E(x) - by + a\sin\omega\tau, \end{aligned} \tag{A1}$$

$$F_E(x) = \begin{cases} -(x+1), & x < -0{,}5 \\ x, & -0{,}5 \le x \le 0{,}5 \\ -(x-1), & x > 0{,}5. \end{cases}$$

The corresponding potential is given by the piecewise parabolic function

$$W_E(x) = -\int F_E(x)dx = \begin{cases} (x+1)^2 - 0{,}5 & x < -0{,}5 \\ -x^2, & -0{,}5 \le x \le 0{,}5 \\ (x-1)^2 - 0{,}5 & x > 0{,}5 \end{cases} \tag{A2}$$

Eq. (A1) has the same structure as the conventional DH equation [Ott, 1993]:

$$\begin{aligned} \dot{x} &= y, \\ \dot{y} &= F(x) - by + a\sin\omega\tau. \end{aligned} \tag{A3}$$

However, the nonlinear function $F(x) = x - x^3$ and the nonparabolic potential

$$W(x) = -\int F(x)dx = -\frac{x^2}{2} + \frac{x^4}{4} \qquad \text{(A4)}$$

are somewhat different from F_E and W_E. The potentials W_E and W are sketched in Fig. A3 for comparison.

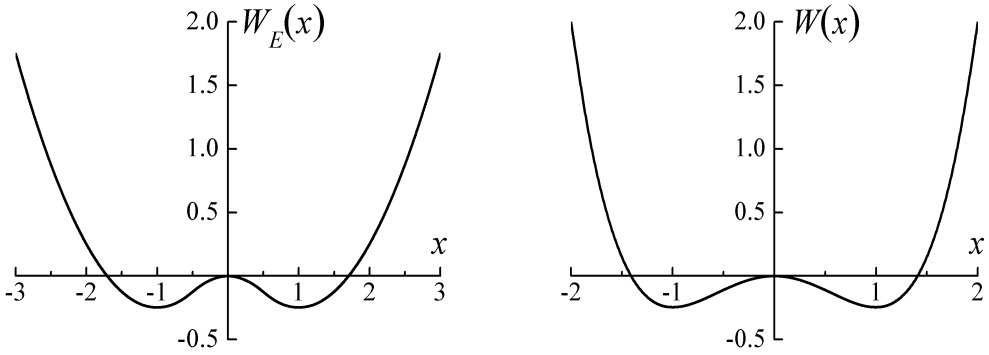

FIG. A3. Piecewise parabolic potential $W_E(x)$ from formula (A2) (left) and nonparabolic potential $W(x)$ from formula (A4) (right).

Despite some difference in the form of the potentials the electronic analogue exhibits very similar behaviour (Fig. A2) as the conventional DH oscillator illustrated in Fig. A4.

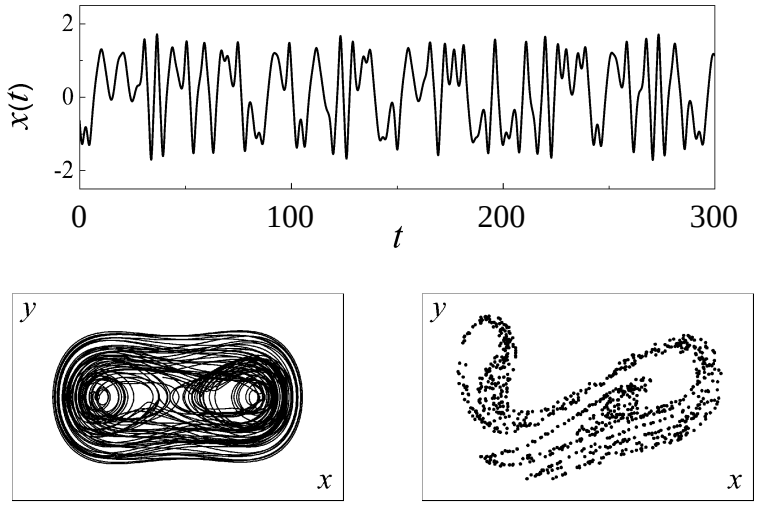

FIG. A4. Numerical results from Eq. (A3). $a = 0.3$, $b = 0.1$, $\omega = 1.3$.

More details, numerical results, experimental results, and discussion can be found in [1]. We have designed and investigated an electrical circuit, which can be treated as an electrical analogue of the DH mathematical oscillator. The circuit is extremely simple, easy to build and operate. Nevertheless, it exhibits typical behaviour of chaotic systems, including period-doubling route to chaos, narrow odd-period windows in chaotic regime, etc. We have shown that many basic qualitative characteristics, such as the waveforms, the phase portraits, and the stroboscopic maps (the Poincaré sections) can been easily taken in experiment. These characteristics coincide very well with the numerically obtained characteristics from the DH equation. This allows us to conclude that dynamical behaviour of the DH type systems is not very sensitive to the details of the nonparabolic potential. The main point is the existence of the two-well form of the potential.

A2. Electronic analog of the Lorenz system [10]

The electronic circuit of the Lorenz system has been built according to Eqs. (2.17) in Chapter 2. In contrast to the DH oscillator the structure of the Lorenz circuit is a typical example of an analogue computer, based on inverting integrators and multipliers. Similar circuits have been described in [Cuomo & Oppenheim, 1993; Cuomo *et al*., 1993].

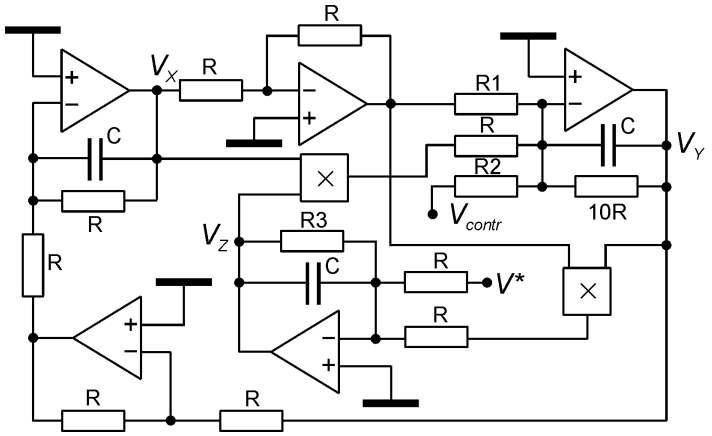

FIG. A5. Electronic analogue of the Lorenz system. C = 15 nF, R = 7.5 kΩ, R_1 = 2 kΩ, R_2 = 2.4 kΩ, R_3 = 27 kΩ, op–amps are the LM741, multipliers are the AD633 integrated circuits. The perturbation (if required) is applied to the node V^*, the signals from the controller are applied to the node V_{contr}.

A3. Electronic analog of a body at the Lagrange point L2 of the Sun–Earth system [4]

An analogue circuit, imitating dynamics of a system with a conservative saddle equilibrium, is shown in Fig. A6.

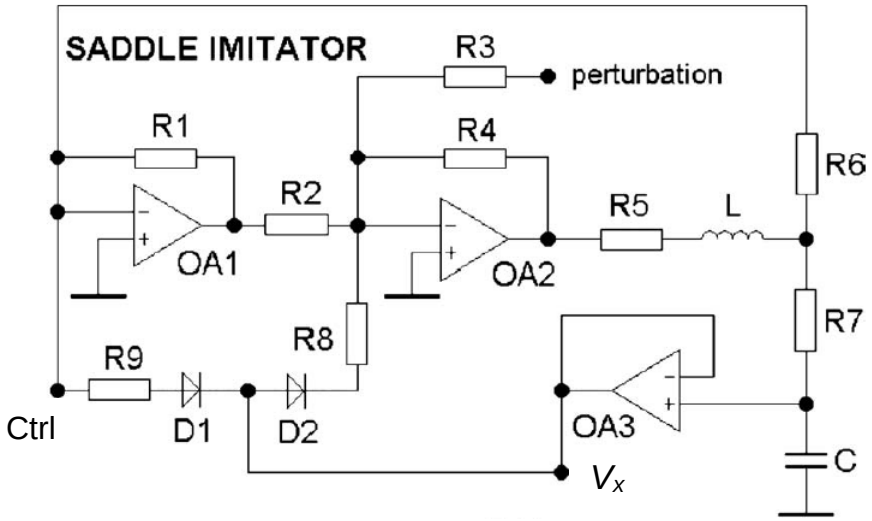

FIG. A6. Circuit diagram of a conservative saddle imitator. R_1=R_2=R_4=10 kΩ, R_3=1 MΩ, R_5=100 Ω, R_6=5 kΩ, R_7=150 Ω (adjustable), R_8=11 kΩ, R_9 =200 Ω, L=210 mH, C=4.7 μF. OA1–OA3 are LM741 integrated circuits; D1 and D2 are BAS21 type diodes. Signal is taken from the node V_x, control signal is applied to the node Ctrl.

It should be emphasized that the imitator is an essentially nonlinear circuit described by Eq. (3.2) in Chapter 3. The experimental nonlinear function $F(r)$, taken from the circuit in Fig. A6, is presented in Fig. 3.5 (Chapter 3). The system imitator is the OA1- and OA2-based circuit. The positive feedback introduced by the resistor R_6 makes the circuit unstable (the positive feedback coefficient k^+=R_1/R_6=2). The role of the additional resistor R_7, coupled in series with the capacitor C, is to compensate the losses in the load resistor R_5 and in the inherent 'ohmic' resistance R_L of the inductance coil L, also the losses in the LC tank introduced by the resistor R_6. The value of the adjustable resistor R_7 should be tuned to $R_7=(R_5+R_L+\rho^2/R_6)/(k^+-1)$ in order to make the system "conservative" (here $\rho=\sqrt{L/C}$). The nonlinear function $F(r)$ is implemented by means of the diodes D1 and D2 with the resistors R_9 and R_8 coupled in series to the diodes. The OA3 stage is a buffer.

A4. Electronic analog of the FitzHugh–Nagumo oscillator [3,5,6,11,13,14,15]

The circuit diagram of the FitzHugh–Nagumo (FHN) asymmetric oscillator is sketched in Fig. A7.

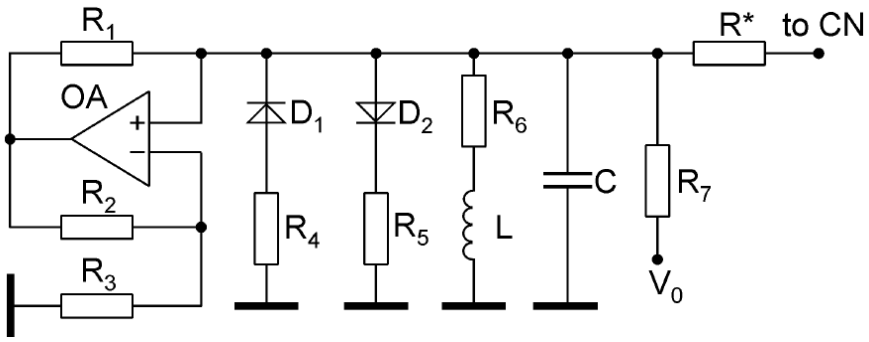

FIG. A7. FHN asymmetric (R_4<<R_5) oscillator. A7 OA is a general-purpose operational amplifier, e.g. NE5534 type device, D1 and D2 are the BAV99 type Schottky diodes, L =10 mH, C =3.3 nF, R_1 = R_2 = 1 kΩ, R_3 = 510 Ω, R_4 = 30 Ω, R_5 = 510 Ω, R_6 = 275 Ω (an external resistor R'_6 = 220 Ω in series with the coil resistance R''_6 = 55 Ω), R_7 = 24 kΩ, R* = 510 Ω, V_0 = –15 V. The circuit element values may vary in different experiments [3, 5, 6, 11, 13–15].

The FHN oscillator in Fig. A7 is a circuit with a strongly asymmetric nonlinearity (R_4<<R_5). It essentially differs from the earlier asymmetric version of the FHN type oscillator, suggested in [Binczak *et al*., 2003; Jacquir, 2006].

The output, $V_C(t)$ is illustrated in Fig. A8.

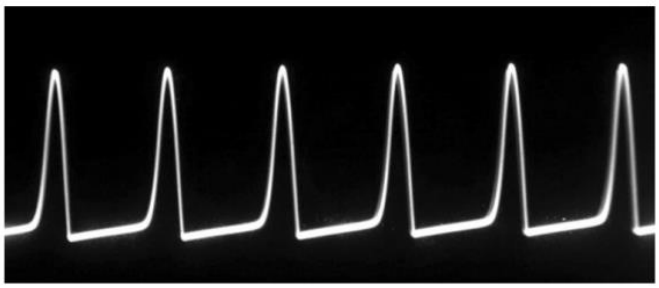

FIG. A8. Typical spiking waveform from an individual FHN type oscillator. Spike amplitude $V_C(t)$ is about 3 V (across the capacitor C) and is about 10 V from the output node of the OA. Inter-spike interval ≈80 μs (f_0≈12 kHz). The spike characteristics are given for the specific circuit element values given in the caption to Fig. A7.

A5. Electronic controllers [2-4,6,8–13,15–19,22]

A variety of electronic controllers and their modifications have been described and used in the author‘s publications on the topic of the dissertation. Moreover, the circuit element values for the same type of controller differ in specific papers, depending on the controlled dynamical system. Therefore, we do not present the all circuit diagrams in the dissertation and this appendix A5. One of the circuit diagrams is shown in Fig. 2.9 in Chapter 2. One more, specifically the negative impedance converter (NIC), is presented in Fig. A9. Other electronic controllers are summarized in Table A1 with references to filter type, filter order, active devices, and equilibrium type.

Table A1. Electronic controllers for stabilizing equilibrium and controlling synchrony in dynamical systems.

Method	**Filter type; filter order**	**Active devices**	**Equilibrium type**	**Reference**
UFC	LPF or HPF; 1st order	OA, IA	saddles	[2,10,17]
UFC||SFC	HPF; 2nd order	OA	conservative or weakly damped saddles; inertia	[4,18]
CFC	LPF; 2nd order	IA	conservative or weakly damped saddles	[8]
UFDC	LPF; 1st order	IA	conservative or weakly damped saddles	[9]
SFC	LPF; 1st order	IA, OA	spirals/nodes; spirals/nodes in an array of oscillators	[3,10,13,22]
NC	LPF; 1st order	IA, OA, COMP	saddles	[12]
MFN	zero order	OA	desynchronized array of oscillators	[6,11]
RS	zero order	OA	desynchronized array of oscillators	[6]

Abbreviations: UFC – unstable filter control, UFC||SFC – unstable filter control and stable filter control operating in parallel, CFC – combined filter control, UFDC – unstable filter control combined with derivative control, SFC – stable filter control, NC – nonlinear control, MFN – mean field nullifying, RS – repulsive synchronization, LPF – low-pass filter, HPF – high-pass filter, OA – operational amplifier, IA – instrumentation amplifier, COMP – comparator.

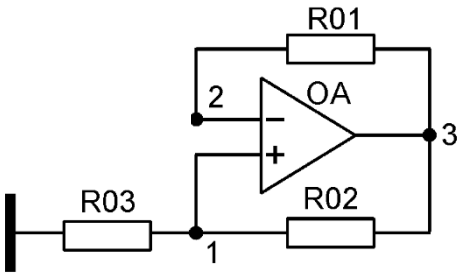

FIG. A8. Circuit diagram of the negative impedance converter NIC. OA is an operational amplifier, e.g. NE5534 type device. In case $R_{01}=R_{02}$, input resistance at node 2, $R_{in2} = -R_{03}$.

REFERENCES

A. Ahlborn and U. Parlitz, 'Chaos control using notch filter feedback,' *Phys. Rev. Lett.* **96**, 034102 (2006).

M. Aqil, K. S. Hong, and M. Y. Jeong, 'Synchronization of coupled chaotic FitzhHugh–Nagumo systems,' *Commun. Nonlinear Sci. Numer. Simul.* **17**, 1615 (2012).

S. Bielawski, M. Bouazaoui, D. Derozier, and P. Glorieux, 'Stabilization and characterization of unstable steady states in a laser,' *Phys. Rev. A* **47**, 3276 (1993).

S. Binczak, V. B. Kazantsev, V. I. Nekorkin, and J. M. Bilbaut, 'Experimental study of bifurcations in modified FitzHugh–Nagumo cell,' *Electron. Lett.* **39**, 961 (2003).

D. J. Braun, 'Adaptive steady-state stabilization for nonlinear dynamical systems,' *Phys. Rev. E* **78**, 016213 (2008).

A. Chang, J. C. Bienfang, G. M. Hall, J. R. Gardner, and D. J. Gauthier, 'Stabilizing unstable steady states using extended time-delay autosynchronization,' *Chaos* **8**, 782 (1998).

M. Ciofini, A. Labate, R. Meucci, and M. Galanti, 'Stabilization of unstable fixed points in the dynamics of a laser with feedback,' *Phys. Rev. E* **60**, 398 (1999).

K. M. Cuomo and A. V. Oppenheim, 'Circuit implementation of synchronized chaos with applications to communications,' *Phys. Rev. Lett.* **71**, 65 (1993).

K. M. Cuomo and A. V. Oppenheim, and S. H. Strogatz, 'Synchronization of Lorenz-based chaotic circuits with applications to communications,' *IEEE Trans. Circuits Syst. II: Analog and Digital Signal Processing* **40**, 626 (1993).

Y. Ding, W. Jiang, and H. Wang, 'Delayed feedback control and bifurcation analysis of Rössler chaotic system,' *Nonlin. Dyn.* **61**, 707 (2010).

R. FitzHugh, 'Impulses and physiological states in theoretical models of nerve membrane,' *Biophys. J.* **1**, 445 (1961).

A. Franci, A. Chaillet, E. Panteley, and F. Lamnabhi-Lagarrigue, 'Desynchronization and inhibition of Kuramoto oscillators by scalar mean-field feedback,' *Math. Control, Signals, Syst.* **24**, 169 (2012).

A. Gjurchinovski, T. Jungling, V. Urumov, and E. Schöll, 'Delayed feedback control of unstable steady states with high-frequency modulation of delay,' *Phys. Rev. E* **88**, 032912 (2013).

K. Höhne, H. Shirahama, Ch.-U. Choe, H. Benner, K. Pyragas, and W. Just, 'Global properties in an experimental realization of time-delayed feedback control with an unstable control loop,' *Phys. Rev. Lett.* **98**, 214102 (2007).

H. Hong and S. H. Strogatz, ‘Kuramoto model of coupled oscillators with positive and negative coupling parameters: an example of conformist and contrarian oscillators,’ *Phys. Rev. Lett.* **106**, 054102 (2011).

P. Hövel and E. Schöll, ‘Control of unstable steady states by time delayed feedback methods,’ *Phys. Rev. E* **72**, 046203 (2005).

P. Hövel, *Control of Complex Nonlinear Systems with Delay (Springer Thesis)* (Springer, Berlin, Heidelberg, 2010).

H. Huijberts, ‘Linear controllers for the stabilization of unknown steady states of chaotic systems,’ *IEEE Trans. Circuits Syst. I: Regular Papers* **53**, 2246 (2006).

S. Jacquir, S. Binczak, J. M. Bilbaut, V. B. Kazantsev, and V. I. Nekorkin, ‘Synaptic coupling between two electronic neurons,’ *Nonlin. Dyn.* **44**, 29 (2006).

G. A. Johnston and E. R. Hunt, ‘Derivative control of the steady state in Chua's circuit driven in the chaotic region,’ *IEEE Trans. Circuits Syst., I: Fundam. Theory Appl.* **40**, 833 (1993).

B. K. Jones and G. Trefan, ‘The Duffing oscillator: a precise electronic analog chaos demonstrator for the undergraduate laboratory,’ *Am. J. Phys*. **69**, 464 (2001).

B. C. Kuo, *Automatic Control Systems* (Prentice-Hall, Englewood Cliffs, New Jersey, 1995).

Y.-Ch. Lai, M. Ding, and C. Grebogi, ‘Controlling Hamiltonian chaos,’ *Phys. Rev. E* **47**, 86 (1993).

Y.-Ch. Lai, A. Kandangath, S. Krishnamoorthy, J. A. Gaudet, and A. P. S. de Moura, ‘Inducing chaos by resonant perturbations: theory and experiment,’ *Phys. Rev. Lett.* **94**, 214101 (2005).

S. Lenci and G. Rega (eds.), *Exploiting Chaotic Properties of Dynamical Systems for their Control*, Special issue of *Philos. Trans. R. Soc. London A* **364**, 2267 (2006).

E. Lindberg, E. Tamaševičiūtė, G. Mykolaitis, S. Bumelienė, T. Pyragienė, A. Tamaševičius, and R. Kirvaitis, ‘Autonomous third-order Duffing–Holmes type chaotic oscillator,**’** *Proc. Eur. Conf. Circuit Theory and Design*, 663 (IEEE, Piscataway, New Jersey, 2009), http://ieeexplore.ieee.org/stamp/stamp.jsp?tp=&arnumber=5275062

E. N. Lorenz, ‘Deterministic nonperiodic flow,’ *J. Atmos. Sci.* **20** 130 (1963).

A. Q. Luo, ‘A theory for synchronization of dynamical systems,**’** *Commun. Nonlin. Sci. Numer. Simul.* **14**, 1901 (2009).

M. Luo and J. Xu, ‘Suppression of collective synchronization in a system of neural groups with washout-filter-aided feedback,’ *Neural Networks* **24**, 538 (2011).

M. C. Mackey and L. Glass, ‘Oscillation and chaos in physiological control system,’ *Science* **197**, 287 (1977).

S. Martignoli, J. J. van der Vyver, A. Kern, Y. Uwate, and R. Stoop, ‘Analog electronic cochlea with mammalian hearing characteristics,’ *Appl. Phys. Lett.* **91**, 064108 (2007).

S. Martignoli and R. Stoop, ‘Local cochlear correlations of perceived pitch,’ *Phys. Rev. Lett.* **105**, 048101 (2010).

T. Matsumoto, L. O. Chua, and M. Komuro, ‘The double scroll,’ *IEEE Trans. Circuits Syst*., **32**, 797 (1985).

F. C. Moon, *Chaotic Vibrations: An Introduction for Applied Scientists and Engineers*, (John Wiley & Sons, New York, 1987).

A. Namajūnas, A. Tamaševičius, ‘Simple laboratory instrumentation for measuring pointwise dimensions from chaotic time series,’ *Rev. Sci. Instr*. **65**, 3032 (1994).

A. Namajūnas, K. Pyragas, and A. Tamaševičius, ‘An electronic analog of the Mackey–Glass system,’ *Phys. Lett. A* **201**, 42 (1995a).

A. Namajūnas, K. Pyragas, and A. Tamaševičius, ‘Stabilization of an unstable steady state in a Mackey–Glass system,’ *Phys. Lett. A* **204**, 255 (1995b).

A. Namajūnas, K. Pyragas, and A. Tamaševičius, ‘Analog techniques for modeling and controlling the Mackey–Glass system,’ *Int. J. Bifurcation Chaos* **7**, 957 (1997).

A. Namajūnas, A. Tamaševičius, G. Mykolaitis, and A. Čenys, ‘Spectra transformation of chaotic signals,’ *Lith. J. Phys*. **40**, 134 (2000a).

A. Namajūnas, A. Tamaševičius, G. Mykolaitis, and A. Čenys, ‘Smoothing chaotic spectrum of nonautonomous oscillator,’ *Nonlin. Phenom. Complex Syst.* **3**, 188 (2000b).

K. Ogata, *Modern Control Engineering*, (Prentice Hall, Englewood Cliffs, New Jersey (2010).

A. A. Olyaei and C. Wu, ‘Controlling chaos using a system of harmonic oscillators,’ *Phys. Rev. E* **91**, 012920 (2015).

E. Ott, *Chaos in Dynamical Systems*, (Cambridge University Press, Cambridge, 1993).

E. Ott, C. Grebogi, and J. A. Yorke, ‘Controlling chaos,’ *Phys. Rev. Lett.* **64**, 1196 (1990).

P. Parmananda, M. A. Rhode, G. A. Johnson, R. W. Rollins, H. D. Dewald, and A. J. Markworth, ‘Stabilization of unstable steady states in an electro-chemical system using derivative control**,**’ *Phys. Rev. E* **49**, 5007 (1994).

A. Pikovsky, M. Rosenblum, and J. Kurths, *Synchronization: A Universal Concept in Nonlinear Sciences*, (Cambridge University Press, Cambridge, 2003)

O. V. Popovych, C. Hauptmann, and P. A. Tass, 'Effective desynchronization by nonlinear delayed feedback,' *Phys. Rev. Lett.* **94**, 164102 (2005).

O. V. Popovych, C. Hauptmann, and P. A. Tass, 'Control of neuronal synchrony by nonlinear delayed feedback,' *Biol. Cyber.* **95**, 69 (2006).

K. Pyragas, 'Continuous control of chaos by self-controlling feedback,' *Phys. Lett. A* **170**, 421 (1992).

K. Pyragas and A. Tamaševičius, 'Experimental control of chaos by delayed self-controlling feedback,' *Phys. Lett. A* **180**, 99 (1993).

K. Pyragas, 'Control of chaos via extended delay feedback,' *Phys. Lett. A* **206**, 323 (1995).

K. Pyragas, 'Control of chaos via an unstable delayed feedback controller,' *Phys. Rev. Lett.* **86**, 2265 (2001).

K. Pyragas, V. Pyragas, I. Z. Kiss, and J. L. Hudson, 'Stabilizing and tracking unknown steady states of dynamical systems,' *Phys. Rev. Lett.* **89**, 244103 (2002).

K. Pyragas, V. Pyragas, I. Z. Kiss, and J. L. Hudson, 'Adaptive control of unknown unstable steady states of dynamical systems,' *Phys. Rev. E* **70**, 026215 (2004).

K. Pyragas, O. V. Popovych, and P. A. Tass, 'Controlling synchrony in oscillatory networks with a separate stimulation-registration setup,' *Europhys. Lett.* **80**, 40002 (2007).

K. Pyragas, V. Novičenko, and P. Tass, 'Mechanism of suppression of sustained neuronal spiking under high-frequency stimulation,' *Biol. Cyber.* **107**, 669 (2013).

V. Pyragas, *Adaptive Control of Dynamical Systems Using Unstable Degrees of Freedom in the Feedback Loop*, Doctoral dissertation, (Vilnius University, Vilnius, 2007).

V. Pyragas and K. Pyragas, 'Relation between the extended time-delayed feedback control algorithm and the method of harmonic oscillators,' *Phys. Rev. E* **92**, 022925 (2015).

K. Pyragas and P. A. Tass, 'Suppression of spontaneous oscillations in high-frequency stimulated neuron models,' *Lithuanian J. Phys.* **56**, 223 (2016).

A. Rabinovitch, R. Thieberger, and M. Friedman, 'Forced Bonhoeffer–van der Pol oscillator in its excited mode,' *Phys. Rev. E* **50**, 1572 (1994).

A. Rabinovitch, Y. Biton, D. Braunstein, M. Friedman, and I. Aviram, 'A neuron under external sinusoidal stimulation,' *Brain Stimul.* **8**, 310 (2015).

I. Ratas and K. Pyragas, 'Effect of high-frequency stimulation on nerve pulse propagation in the FitzHugh–Nagumo model,' *Nonlin. Dyn.* **67**, 2899 (2012).

I. Ratas and K. Pyragas, 'Controlling synchrony in oscillatory networks via an act-and-wait algorithm,' *Phys. Rev. E* **90**, 032914 (2014).

I. Ratas, *Algorithms for Inhibition and Desynchronization of Neural Systems*, Doctoral dissertation, (Vilnius University, Vilnius, 2015).

B. Rezaie and M.-R. J. Motlagh, 'An adaptive delayed feedback control method for stabilizing chaotic time-delayed system,' *Nonlin. Dyn.* **64**, 167 (2011).

M. Rosenblum and A. Pikovsky, 'Synchronization: from pendulum clocks to chaotic lasers and chemical oscillators,' *Contemp. Phys.* **44**, 401 (2003).

M. G. Rosenblum and A. S. Pikovsky, 'Controlling synchronization in an ensemble of globally coupled oscillators,' *Phys. Rev. Lett.* **92**, 114102 (2004).

N. F. Rulkov, L. S. Tsimring, and H. D. I. Abarbanel, 'Tracking unstable orbits in chaos using dissipative feedback control,' *Phys. Rev. E* **50**, 314 (1994).

E. Schöll and H. G. Schuster (eds.), *Handbook of Chaos Control*, (Wiley-VCH, Weinheim, 2008).

J. H. Sheeba, V. K. Chandresekar, and M. Lakshmanan, 'General coupled-nonlinear-oscillator model for event-related (de)synchronization,' *Phys. Rev. E* **84**, 036210 (2011).

A. Schenck zu Schweinsberg and U. Dressler, 'Characterization and stabilization of the unstable fixed points of a frequency doubled Nd:YAG laser,' *Phys. Rev. E* **63**, 056210 (2001).

R. Stoop, T. Jasa, Y. Uwate, and S. Martignoli, 'From hearing to listening: design and properties of an actively tunable electronic hearing sensor,' *Sensors* **7**, 3287 (2007).

A. Tamaševičius, E. Tamaševičiūtė, G. Mykolaitis, and S. Bumelienė, 'Stabilization of unstable periodic orbit in chaotic Duffing–Holmes oscillator by second order resonant negative feedback,' *Lith. J. Phys*. **47**, 235 (2007a).

A. Tamaševičius, G. Mykolaitis, V. Pyragas, and K. Pyragas, 'Delayed feedback control of periodic orbits without torsion in nonautonomous chaotic systems: theory and experiment,' *Phys. Rev*. *E* **76**, 026203 (2007b).

A. Tamaševičius, S. Bumelienė, R. Kirvaitis, G. Mykolaitis, E. Tamaševičiūtė, and E. Lindberg, 'Autonomous Duffing–Holmes type chaotic oscillator,' *Elektronika ir Elektrotechnika* **5**(93), 43 (2009a).

A. Tamaševičius, E. Tamaševičiūtė, T. Pyragienė, G. Mykolaitis, and S. Bumelienė, 'Extended resonant feedback technique for controlling unstable periodic orbits of chaotic system,' *Commun. Nonlin. Sci. Numer. Simul.* **14**, 4273 (2009b).

P. A. Tass, *Phase Resetting in Medicine and Biology: Stochastic Modelling and Data Analysis*, (Springer-Verlag, Berlin, 2007).

J. J. Thomsen, *Vibrations and Stability – Advanced Theory, Analysis and Tools*, (Springer-Verlag, Berlin, Heidelberg, New York, 2003).

L. S. Tsimring, N. F. Rulkov, M. L. Larsen, and M. Gabbay, 'Repulsive synchronization in an array of phase oscillators,' *Phys. Rev. Lett.* **95**, 014101 (2005).

N. Tukhlina, M. Rosenblum, A. Pikovsky, and J. Kurths, 'Feedback suppression of neural synchrony by vanishing stimulation,' *Phys. Rev. E* **75**, 011918 (2007).

S. Yanchuk, M. Wolfrum, P. Hövel, and E. Schöll, 'Control of unstable steady states by long delay feedback,' *Phys. Rev. E* **74**, 026201 (2006).

J. Zhou and D. Yang, 'Chaos control of a new 3D autonomous system by stability transformation method,' *Nonlin. Dyn.* **73**, 565 (2013).

W. Zou, M. Zhan, and J. Kurths, 'Revoking amplitude and oscillation deaths by low-pass filter in coupled oscillators,' *Phys. Rev. E* **95**, 062206 (2017).